Research Progress on Negative Electrodes for Practical Li-Ion Batteries: Beyond Carbonaceous Anodes

ARTICLE *in* ADVANCED ENERGY MATERIALS · APRIL 2015

Impact Factor: 16.15 · DOI: 10.1002/aenm.201402225

3 AUTHORS, INCLUDING:

Vanchiappan Aravindan

Nanyang Technological University

136 PUBLICATIONS **1,505** CITATIONS

SEE PROFILE

Y.s. Lee

Chonnam National University

200 PUBLICATIONS **2,563** CITATIONS

SEE PROFILE

ADVANCED ENERGY MATERIALS
www.advenergymat.de

Research Progress on Negative Electrodes for Practical Li-Ion Batteries: Beyond Carbonaceous Anodes

Vanchiappan Aravindan, Yun-Sung Lee,* and Srinivasan Madhavi**

Research activities related to the development of negative electrodes for construction of high-performance Li-ion batteries (LIBs) with conventional cathodes such as $LiCoO_2$, $LiFePO_4$, and $LiMn_2O_4$ are described. The anode materials are classified in to three main categories, insertion, conversion, and alloying type, based on their reactivity with Li. Although numerous materials have been proposed (i.e., for half-cell assembly), few of them have reached commercial applications, apart from graphite, $Li_4Ti_5O_{12}$, Si, and Sn-Co-C. This clearly demonstrates that full-cell studies are desperately needed rather than just characterizing materials in half-cell assemblies. Additionally, the performance of such anodes in practical Li-ion configurations (full-cell) is much more important than merely proposing materials for LIBs. Irreversible capacity loss, huge volume variation, unstable solid electrolyte interface layer formation, and poor cycleability are the main issues for conversion and alloy type anodes. This review addresses how best to circumvent the mentioned issues during the construction of Li-ion cells and the future prospects of such anodes are described in detail.

1. Introduction

Clean energy is one of the prime areas of research today because the unavoidable environmental pollutions, especially from the motor vehicles, and its associated health hazards are the main concern for the society,. Therefore, the need for research and development (R&D) in the implementation of electric vehicles (EVs) and hybrid electric vehicles (HEVs) is strongly encouraged. Lithium ion batteries (LIBs) are considered as most promising electrochemical energy storage system in this era and are anticipated to power the mentioned applications. LIBs in the "rocking-chair" configuration were introduced for consumer applications by Sony in 1990 and have dominated the entire electronic appliance market for over two decades, remaining popular at present.[1] This fascinating feature of Li-ion chemistry is bound with several beneficial and favorable factors; for instance Li is the most electropositive element (–3.04 V vs. standard hydrogen electrode) with lightest metal (equivalent weight $M = 6.94$ g mol^{-1} and specific gravity of 0.534 g cm^{-3}), it is the 25th most abundant element on the earth crust, has high theoretical capacity (≈3862 mAh g^{-1}), has high energy density in both gravimetric and volumetric point of view, has a high working potential, has less self-discharge compared to other secondary batteries, and no memory effect.[2–7] ($LiFePO_4$ based cells are experiencing memory effect issues.[8]). Unfortunately, the dendrite growth upon cycling in the presence of conventional aprotic solvents hampers the possibility of using metallic Li in practical cells.[9–11] Therefore, alternate anodes with lower working potential is desperately needed. The discovery of reversible Li-intercalation into graphite with lower working potential (<0.1 V vs. Li) via the "host-guest" concept makes the materials become most promising for LIB applications.[12,13] The same concept has been successfully translated into commercial cells along with conventional cathodes such as $LiCoO_2$ and $LiFePO_4$.[14,15] Although graphitic anodes (LiC_6) have 10 times lower theoretical capacity (≈372 mAh g^{-1}), requires smooth solid electrolyte interface (SEI) layer for the safe operation of the cell, and suffers high current operation compared to metallic Li, they remain attractive for small and medium scale applications. As a result, achieving high power capability for graphitic anode based systems is difficult. High power capability is one of the prerequisites for the power packs to be employed in EV and HEV.[16] On the other hand, electric double layer capacitors (EDLCs) and lithium-ion hybrid electrochemical capacitors (Li-HECs) are capable of delivering the high power density, but energy density remains an issue.[17,18] This clearly suggests that the development of high performance anodes is required to construct high energy and high power capability Li-ion power packs.

Generally, anodes used in LIB are broadly classified in to three main categories: intercalation, conversion (displacement), and

Dr. V. Aravindan, Prof. S. Madhavi
Energy Research Institute @ NTU (ERI@N)
Nanyang Technological University
Research Techno Plaza
50 Nanyang Drive, Singapore 637553
E-mail: aravind_van@yahoo.com; Madhavi@ntu.edu.sg
Prof. Y.-S. Lee
Faculty of Applied Chemical Engineering
Chonnam National University
Gwang-ju 500–757, Korea
E-mail: leeys@chonnam.ac.kr
Prof. S. Madhavi
School of Materials Science and Engineering
Nanyang Technological University
Singapore 639798
Prof. S. Madhavi
TUM-CREATE, 1 Create way
#10–02 CREATE Tower
Singapore 138602

DOI: 10.1002/aenm.201402225

alloy types based on the reaction mechanism with Li (**Figure 1**). A detailed analysis of the mentioned classification is described in the next sections. Insertion type materials exhibit lower reversible capacity and higher working potential than graphitic anodes (over 1.5 V vs. Li). As a result, a loss in energy density is observed, but improvement in the power density is realized within the thermodynamic stability window of the conventional carbonate based electrolytes.[19] In line with this, Toshiba Inc., recently introduced the $Li_4Ti_5O_{12}$ anode based LIB for consumer applications, preferably for the EV market.[5] However, the conversion type anodes show higher reversible capacity and power capability than insertion type anodes, which includes graphite, but higher working potential, unstable SEI formation, volume variation, and large polarization prohibit the potential usage in practical Li-ion cells.[20] Alloy based anodes are much more promising than the other two types because of their high power capability, high reversible capacity, and lower working potential and reached the commercial market; example Sn-based composites (Sn-Co-Ti-C) were introduced by Sony in Nexelion configuration and the commercialization of Si based anodes has been announced by Panasonic, although this has certain drawbacks such as unstable SEI formation, huge volume variation, and poor cycleability issues.[21] It is unfortunate that, although numerous materials with various morphological features and surface modifications are proposed for the three categories of LIB applications, limited reports are available only in the practical configuration. To study the performance with cathodes is more important than proposing the materials from anode point of view. Furthermroe, several notable reviews have been published covering the materials aspect (half-cell assembly) but none of them exclusively report the practical configuration.[2,22–25] In the half-cell configuration, metallic Li acts as a reservoir for the source of Li-ions, which can uphold the huge irreversible capacity loss (ICL) issue observed in the mentioned anodes by supplying more Li. On the other hand, in a practical cell assembly the cathode is the only source for the Li-ions and it cannot to sustain such a huge Li loss during conversion and alloying reaction (this includes the amorphous matrix element, i.e., Li_2S, Li_2O etc., formation). Excess loading of the cathode is one of the efficient ways to overcome the ICL, but too much cathode loading and the presence of partially de-lithiated material affects the energy density and stability of the cell, respectively.This article focuses entirely on the performance of such anodes in practical cells such as solid-state, flexible, and conventional configurations based on the anodes classified above. Furthermore, discussion of the pre-lithiation process and how best to overcome the ICL issues observed in conversion as well as alloy type anodes are summarized in detail. It is noteworthy that graphitic anodes have been extensively investigated for over four decades and were commercialized 25 years ago. Therefore, discussion and study of the carbonaceous materials anodes in full-cell configurations are not included in this review.

2. Intercalation

Intercalation is the reversible inclusion or insertion of guest ions or molecules into the host matrix. Upon such an intercalation process, a small deviation in the structural properties of

Vanchiappan Aravindan is currently working at the Energy Research Institute @ NTU (ERI@N), of Nanyang Technological University, Singapore. He received his PhD in 2009 at Gandhigram Rural University, Gandhigram, Tamilnadu, India. He then joined The Research Institute for Catalysis, Chonnam National University, Gwang-ju, South Korea as a post-doctoral fellow with Prof. Yun-Sung Lee in the Faculty of Applied Chemical Engineering. In 2010, he moved to his present organization. His research interests include the development of high-performance electrodes and electrolyte materials for aqueous and non-aqueous Li-ion and Na-ion batteries and supercapacitors.

Yun-Sung Lee currently works as an Associate Professor at Chonnam National University, Gwang-ju, Korea. He received his M.S. from Chonbuk National University in 1998, and his research was carried out under the guidance of Prof. Kee-Suk Nahm. He received his PhD in Applied Chemistry from Saga University, Japan under the direction of Prof. Masaki Yoshio in 2001. In the same year, he joined Professor Yuichi Sato at Kanagawa University, Japan as a doctoral researcher. He joined Chonnam National University, Korea in 2003 as an Assistant Professor. His research interests include Li-ion batteries, electrode materials, and hybrid capacitor systems.

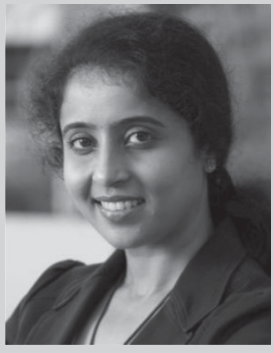

Madhavi Srinivasan is an Associate Professor at the School of Materials Science and Engineering, Nanyang Technological University (NTU), Singapore. She graduated from the Indian Institute of Technology (IIT), Chennai, India and received her PhD from the National University of Singapore. Her research interests include enhancing the performance of energy storage devices such as lithium ion batteries, supercapacitors, and advanced batteries with the help of multifunctional nanoscale materials as a means of powering printed electronics, to store energy from renewable sources, and for powering electric vehicles. Her focus is on the fabrication and investigation of nanoscale materials/architectures for electrochemical energy storage devices.

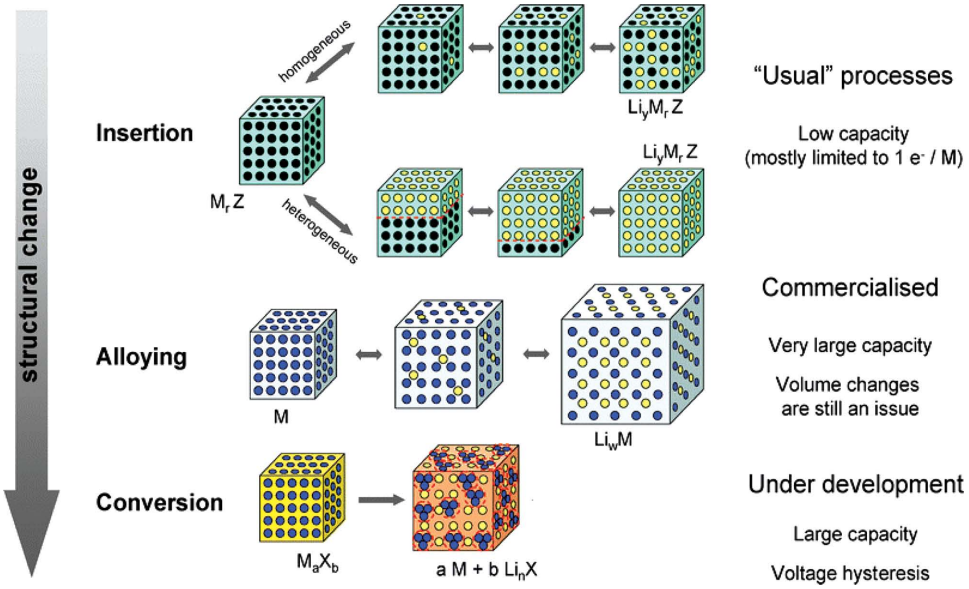

Figure 1. Schematic representation of the different reaction mechanisms observed in electrode materials for lithium batteries. Black circles: voids in the crystal structure, blue circles: metal, yellow circles: lithium. Reproduced with permission.[24] Copyright 2009, The Royal Society of Chemistry.

host matrix is observed and this process is called "topotactic reaction", which is either chemically or thermally reversible; a perfect example is Li-intercalation into a graphite matrix. Such intercalation chemistry has been successfully used in Li-ion batteries for both anode and cathode materials and has also been commercialized (i.e., $LiCoO_2/Li_xC_6$ and $LiFePO_4/Li_xC_6$).[4,5] The insertion type materials, i.e., metal oxides have several advantages over graphitic anodes when used in practical cells; these include a negligible amount of ICL, no Li-platting issues, no solvent co-intercalation, no electrolyte decomposition, no SEI required for the safe operation of the cell, it is capable of delivering high power density, and has an easy synthesis protocol. On the other hand, less reversible capacity and higher intercalation potential are the notable setbacks compared to graphite. Although numerous Li-intercalating materials are proposed as possible anodes for LIB applications, few of them have only been tested or commercialized in the "rocking-chair" configuration, for instance $Li_4Ti_5O_5$ anode. Apart from the mentioned anode, few other insertion type materials have been also evaluated in the rocking-chair configuration for LIBs. Accordingly, the next section describes the structural and electrochemical performance of various intercalation anodes evaluated in the rocking-chair configuration.

2.1. TiO_2

The existence of several polymorphs is reported for the case of TiO_2, but anatase, rutile, brookite, and bronze phases have only been reported for Li-storage.[26] Reversible insertion of one mole of Li is theoretically possible, independent of the polymorph, with a capacity of ≈335 mAh g^{-1}. However, variation in the Li-insertion potential and reaction mechanism has been observed for such polymorphs. Easy synthesis protocols, scalability, inexpensiveness, ease of tailoring the desired morphology, and eco-friendliness are other key features for utilizing TiO_2 polymorphs for the construction of Li-ion power packs.[27–29]

2.1.1. Anatase

The anatase phase is one of the widely investigated polymorphs of TiO_2 for Li-storage.[27] Theoretically, one mole of Li is possible, but practically only ≈0.5 mole Li is reversible upon cycling. Several research attempts have been carried out to improve the reversible capacity, including utilizing high energy (0 0 1) facets because of their dominant higher surface energy (0.90 J m^{-2}) compared to (1 0 0) facets (0.44 J m^{-2}) and using thermodynamically more stable (1 0 1) facets (0.53 J m^{-2}).[30,31] Although high Li-reversibility could be achieved for such (0 0 1) facets, capacity fading remains an issue upon cycling.[32] Li-diffusion co-efficient (D_{Li}) values for anatase phase are in the range of 1×10^{-17} to 4×10^{-17} cm^2 s^{-1} for Li-insertion and extraction processes, respectively.[27] In the crystal chemistry of the anatase phase, TiO_6 octahedra sharetwo adjacent edges with two other octahedral so that planar double chains are formed with tetragonal body-centered space groups ($I4_1/amd$).[27] Li-migration occurs along a reaction path connecting the octahedral interstitial sites.[33] Additionally, Li-intercalation into the anatase phase induces the phase transformation from the tetragonal ($I4_1/amd$) to the orthorhombic ($Li_{0.5}TiO_2$, space group $Pnm2_1$) phase because of the loss of symmetry in the *y* direction.[34,35] As a result, unit cell volume variation (+3.7%, 136 to 141 $Å^3$) is noted; for example, a decrease in the unit cell along the *c*-axis and an increase along the *b*-axis.[36] However, high insertion potential (≈1.75 V vs. Li) is another important issue for the commercialization of anatase-based Li-ion cells.The Li-insertion mechanism in anatase phase is found to be complicated and it occurs at higher potential via a multi-step process, i.e., first, Li-insertion results in the formation of a solid-solution (open

circuit potential of ≈1.75 V vs. Li) followed by a two-phase reaction (flat potential at ≈1.75 V vs. Li), and subsequent interfacial storage (monotonous curves <1.75 V vs. Li).[37–39] Gratzel and co-workers[40,41] first demonstrated the fabrication of ≈2 V class Li-ion cells using layered type $LiCoO_2$ and its derivatives ($LiNi_{0.5}Co_{0.5}O_2$). Substantial improvement in the same $LiCoO_2$/TiO_2 configuration was realized by Subramaniam et al. [42] utilizing nanocrystalline TiO_2. However, capacity fading remains an issue when paired with layered structured cathodes, and even $LiMn_{1/3}Ni_{1/3}Co_{1/3}O_2$ is not an exception.[43] In order to overcome such capacity fading in 2 V class Li-ion cells, spinel $LiMn_2O_4$ is used as the cathode instead of layered type cathodes. The $LiMn_2O_4$/electrospun TiO_2 displayed much better cycleability and capacity retention characteristics than layered type cathodes.[34] Recently, Aravindan et al.[44] reported the fabrication of Li-ion cells composed of all 1D electro-active materials such as $LiMn_2O_4$ nanofibers, anatase nanofibers, and polyvinylidene fluoride-*co*-hexafluoropropylene (PVdF-HFP) nanofiber membranes by electrospinning. The cell delivered exceptional performance and retained ≈90% of its initial capacity after 700 cycles, which is the best result reported for the ≈2 V class Li-ion cell fabricated with an anatase anode (**Figure 2**). Xin et al.[45] demonstrated the performance of TiO_2/graphene composites in 18 650 configuration with a $LiMn_2O_4$ cathode that retained ≈90% (after 200 cycles) and ≈80% (after 300 cycles) of initial capacities at 1 C and 5 C rates, respectively. The same all 1D concept has also been extended for the case of the high voltage $LiNi_{0.5}Mn_{1.5}O_4$ configuration by Arun et al.[46] As a result, $LiNi_{0.5}Mn_{1.5}O_4$/TiO_2 assembly delivered outstanding performance (retained ≈86% of initial capacity after 400 cycles), which is unrivaled by the previous reports by Brutti et al.[47] and Plylahan et al.[48] Similar to the 2 and 3 V class rocking-chair Li-ion cells, attempts have also been made to fabricate ≈1.4 V class Li-ion cells using olivine-type $LiFePO_4$ cathodes with long–term cycleability for small scale applications.[49–52] However, anatase nanotubes prepared by anodization of Ti sheets delivered inferior electrochemical profiles when coupled with $LiFePO_4$.[53] Among the $LiFePO_4$/TiO_2 configurations, composite with graphene nanosheets and core-shell nanofibers are found to be appealing in terms of high rate capability and long cycle life.[49,50] Recently, Ming et al.[54] attempted to maximize the capacity by cycling the anatase anodes prepared using a large amount of porous carbon for deep cycling between 0.01 and 3 V *vs.* Li. As a result, the composite composed of 70 wt% porous carbon showed a stable reversible capacity of ≈546 mAh g^{-1} in the half-cell assembly, which is much higher than the theoretical limitation of one mole of Li. The cell displayed a reversible capacity of ≈413 mAh g^{-1} without any characteristic charge-discharge profile at 1.75 V vs. Li, i.e., they showed only monotonous curves. On the other hand, the full-cell fabricated with a small amount of carbon loading (≈7 wt%) showed a characteristic plateau at ≈2.8 V with a reversible

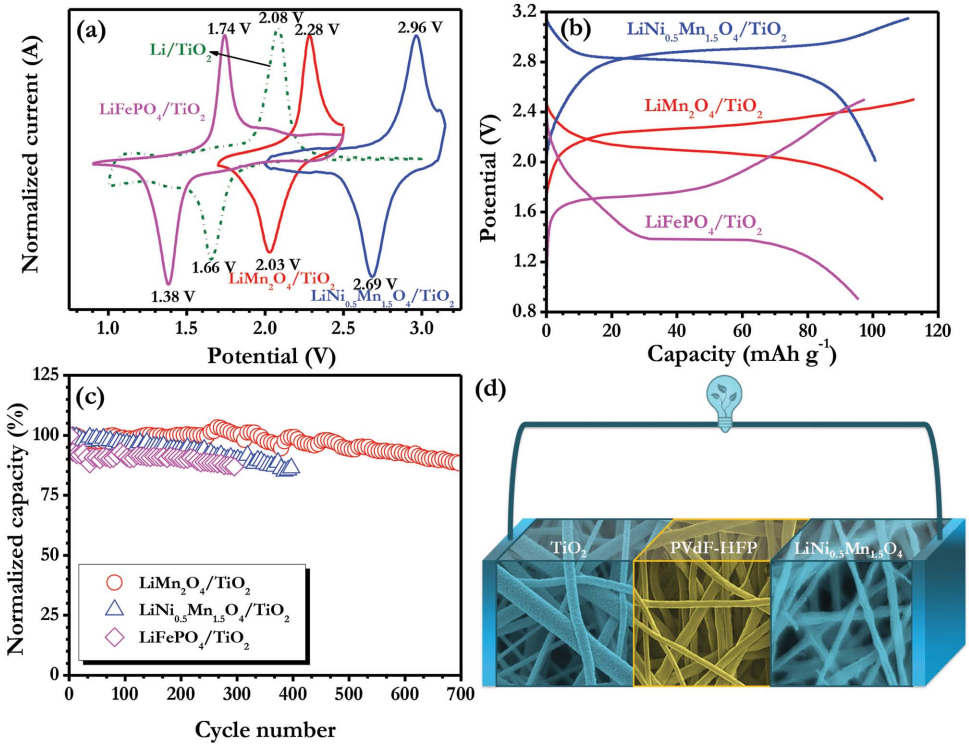

Figure 2. a) Typical cyclic voltammetry (CV) signature of anatase TiO_2 anodes in full-cell assembly with eco-friendly cathodes such as $LiMn_2O_4$, $LiNi_{0.5}Mn_{1.5}O_4$, and $LiFePO_4$ at slow scan rate of 0.1 mV s^{-1}. The performance of anatase TiO_2 in half-cell assembly (Li/TiO_2) also given for the comparison. b) Typical galvanostatic charge-discharge curves of $LiMn_2O_4$/TiO_2 (current density: 150 mA g^{-1}), $LiNi_{0.5}Mn_{1.5}O_4$/TiO_2 (current density: 15 mA g^{-1}) and $LiFePO_4$/TiO_2 (current density: 100 mA g^{-1}) cells. c) Plot of normalized reversible capacity of the above-mentioned cells. d) Schematic representation of the typical LIB composed of all 1D nanostructured components. Reproduced with permission.[26] Copyright 2015, Elsevier.

capacity of ≈240 mAh g^{-1}. In both cases the stable cycleability was noted for the reported 100 cycles with retention of ≈95 and 79% for large and small amounts of porous carbon composite, respectively.

2.1.2. Rutile

Rutile phase is one of the very stable polymorphs and not been explored much compared to its counterparts, includinganatase and bronze phases, because of its inferior electrochemical activity towards Li. In the bulk crystalline form, it is able to accommodate up to 0.1 mole Li, whereas at elevated conditions (120 °C) the intake level has been improved to 0.5 mole. It is well known that Li-diffusion in the rutile phase is highly anisotropic and proceeds through rapid diffusion along *c*-axis channels. The Li^+ diffusion coefficient along the *c*-axis is found to be ≈10^{-6} cm^2 s^{-1} whereas in the *ab*-plane it is only about 10^{-15} cm^2 s^{-1}. As a result, Li-migration and favorable filling in the octahedral sites are severely limited by the *c*-channels. Additionally, the strong repulsive Li-Li interactions in the *c*-channels, together with trapped Li-ion pairs in the *ab*-planes, block the *c*-channels and restrict insertion to well below its theoretical limit.[33] Particulate size is reduced to below 10 nm and results in the accommodation of ≈0.85 mole of Li. The Li- insertion reaction progresses through two solid-solution domains and then via the irreversible phase transformation of electroactive $LiTiO_2$ (rock-salt type) because of the expansion of the *ab*-plane.[55] As a consequence, 0.5 mole of Li is reversibly cycled with good stability, which is similar to the reversibility of bulk anatase phase. On the other hand, Hu et al.[56] suggested that the surface storage is more favorable for rutile phase compared to the bulk intercalation. However, Hassoun et al.[57] reported the fabrication of a full-cell assembly using nanostructured rutile phase as the anode and olivine phase $LiFePO_4$ as the cathode. The full-cell delivered a reversible capacity of ≈150 mAh g^{-1} with appreciable cycleability for 20 cycles under ambient conditions (**Figure 3**). In contrast, a reversible capacity of ≈75 mAh g^{-1} was obtained after 40 cycles under high temperature conditions, even using the solid polymer electrolyte ($PEO_{20}LiCF_3SO_3$+10 wt% ZrO_2).

2.1.3. Bronze

Bronze phase is one of the important polymorphs reported as an insertion anode for the construction of high powered LIBs because of its facile Li-insertion/extraction and high reversibility of both anatase and rutile phases, especially in the nanostructured form.[28,38,58–65] Apart from the high reversibility, the slightly lower insertion potential (≈1.55 V vs. Li) compared to the anatase phase (≈1.75 V vs. Li) is worth noting; this simultaneously translates to a higher energy density of the LIB. Furthermore, the observed insertion potential is almost the same as that of the well-established spinel $Li_4Ti_5O_{12}$ anode.[38,66] Unlike that of the complicated Li-insertion mechanisms noted in the anatase phase, the bronze phase undergoes a simple two-phase insertion mechanism during electrochemical cycling.[39,62] However, Kavan and co-workers[27,67] proposed pseudocapacitive Li-storage in such bronze phases. The crystal chemistry is believed

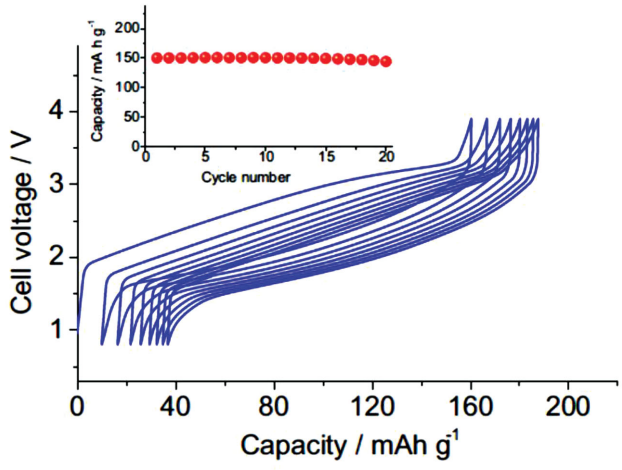

Figure 3. Voltage profile and in inset cycling behavior of the galvanostatic test performed on the $LiFePO_4/TiO_2$ lithium ion cell at C/3 rate (1C = 170 mA g^{-1}) in the 0.8–3.8 V voltage range. EC:DMC 1:1, $LiPF_6$ 1 M electrolyte. Room temperature. Reproduced with permission.[57] Copyright 2012, Elsevier.

to be the main reason for the better electrochemical performance of the bronze phase. Likewise, the monoclinic bronze phase is composed of corrugated sheets of edge and corner sharing TiO_6 octahedral units, however the sheets are joined together to form a 3D frame work parallel to the *b*-axis that sits between axial oxygens.[68,69] Bruce and co-workers [60,65] first reported the performance of the bronze phase with $LiFePO_4$ and $LiNi_{0.5}Mn_{1.5}O_4$ cathodes in the presence of polyvinilydene fluoride (PVdF)-based gel polymer electrolyte. Both $LiFePO_4$ and $LiNi_{0.5}Mn_{1.5}O_4$ cathodes with the TiO_2-B anode delivered a good cycleability (over 80% after 100 cycles) at working potentials of ≈1.9 and ≈3.1 V, respectively. Interestingly, the $LiFePO_4/TiO_2$-B configuration outperformed the $LiFePO_4/Li_4Ti_5O_{12}$ system, especially at high current rates, which confirms the high power capability of the bronze phase. Guo et al.[70] also reported a similar $LiFePO_4/TiO_2$-B system with superior performance compared to the $LiFePO_4/Li_4Ti_5O_{12}$ assembly. Recently, Aravindan et al.[38] reported the long-term cycleability of such a bronze phase with a $LiMn_2O_4$ cathode in the presence of an electrospun PVdF-HFP membrane (**Figure 4**). However, slightly inferior performance is noted for such an electrospun membrane (≈67% retention), compared to the commercial Whatman separator (≈74% retention) after 1000 cycles at a working potential of ≈2.5 V. Similarly, the long-term cycleability with a Ni-rich layered cathode ($LiNi_{0.8}Co_{0.1}Mn_{0.1}O_2$) has also been investigated with spherical-shaped micrometer-sized particles.[71] The $LiNi_{0.8}Co_{0.1}Mn_{0.1}O_2/TiO_2$-B cell retained a ≈80% capacity after 3000 cycles at a 1 C rate (1 C = 2.8 A) and at 25 °C.

2.2. VO_x

Vanadium oxides (V_2O_5, VO_2-B, V_6O_{13} and LiV_3O_8) have been widely investigated as potential electrode materials for energy storage applications.[72–83] This is mainly because of their wide range of oxidation states and they can be tuned according to the

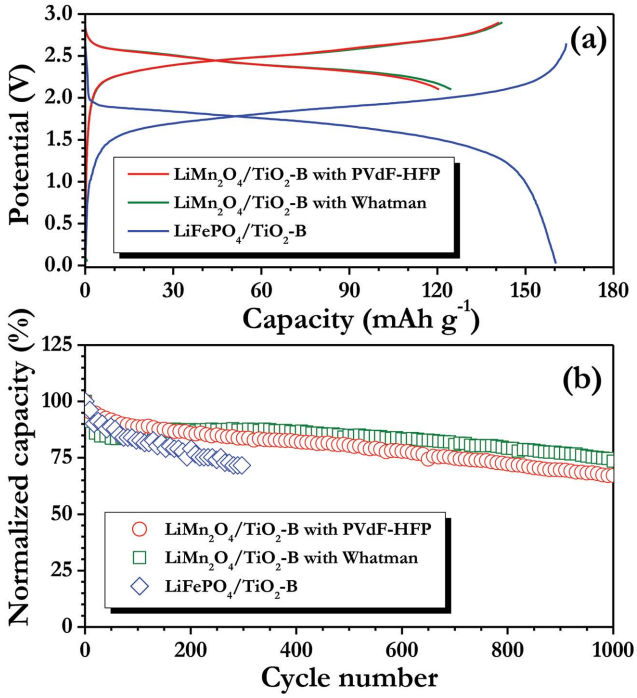

Figure 4. a) Typical charge-discharge curves of $LiMn_2O_4/TiO_2$-B cells with Whatman and PVdF-HFP separators at current density of 150 mA g^{-1} (capacity calculated based on cathode active mass) and $LiFePO_4/TiO_2$-B (capacity calculated based on anode active mass). b) Plot of normalized reversible capacity *vs.* cycle number for $LiMn_2O_4/TiO_2$-B cells at current density of 150 mA g^{-1} and $LiFePO_4/TiO_2$-B at current density of 4 A g^{-1} (for this measurement the cell was charged at battery was first charged to 2.65 V with current density of 4 A g^{-1}, and then the battery voltage was held at 2.65 V for 1 min, i.e., constant current-constant voltage mode). Reproduced with permission.[26] Copyright 2015, Elsevier.

requirements, i.e., working potential.[75] Although, vanadium is hazardous and a P-listed toxic material, several research works have been reported for energy storage applications, including supercapacitors, Li-ion capacitors, Li-ion batteries, and vanadium redox flow systems.[74–81,84–86] The structure of VO_x ($2 \leq x \leq 2.5$) is composed of both VO_5 square pyramidal and VO_4 tetrahedral units. VO_5 pyramidal units are hare edges to form the zig-zag chain along the (0 1 0) direction, which are connected by corner-shared square pyramidal and tetrahedral units.[82,87] Ding et al.[88] successfully used the hydrothermal route for preparation of the monoclinic $VO_x.nH_2O$ phase and 0.43 mole of water molecules is present in the mentioned phase. Li-insertion in to VO_2. $0.43H_2O$ (VO (F)) takes place at ≈2.6 V vs. Li and involves the formation of solid solution ($Li_{0.2}VO$ (F)), followed by a two-phase reaction ($Li_{0.5}VO$(F)). With the exception of the first cycle, the VO(F) delivered exceptional cycleability in the half-cell assembly, irrespective of the applied current rate. The same thermal stability of VO_2 (B) is anticipated for the present VO(F) phasebecause VO_2(B) exhibits better thermal stability than both mesoporous carbon microbeads (MCMBs) and $Li_4Ti_5O_{12}$ phase in the de-lithiated phase.[89] An attempt has been made to fabricate rocking-chair type Li-ion cells with $LiFePO_4$, $LiCoO_2$, and $LiNi_{0.5}Mn_{1.5}O_4$ cells with VO(F) anodes. As expected, the higher redox potential of the VO(F) anode results in the lower working potential for the rocking chair configurations, for example $LiFePO_4$/VO(F), $LiCoO_2$/VO(F) and $LiNi_{0.5}Mn_{1.5}O_4$/VO(F) assemblies exhibit net operating potentials of ≈0.7, ≈1.2 and ≈2 V, respectively. Notable cycleability is observed for all of the mentioned configurations with good capacity retention characteristics at various current rates (**Figure 5**).

2.3. $Li_4Ti_5O_{12}$

A spinel framework composed of the general formula AB_2O_4 ($Li_4Ti_5O_{12}$ can be written as $Li(Li_{1/3}Ti_{2/3})O_4$) has been extensively investigated as a promising insertion anode for Li-ion power packs and was recently commercialized by Toshiba Inc. The success story of the spinel phase $Li_4Ti_5O_{12}$ as an anode in Li-ion power packs lies on its manifold advantages, which includes a maximum of three Li could be reversibly inserted in to the spinel lattice ($Li_7Ti_5O_{12}$) with a corresponding theoretical capacity of ≈175 mAh g^{-1};[90,91] ii) no SEI formation is evident; iii) a flat operating potential at ≈1.55 V vs. Li is associated with the two-phase insertion mechanism (in space notations $Li_{(8a)}[Li_{1/3}Ti_{5/3}]_{(16d)}O_{4(32e)} + 3Li^+ + 3e^- \leftrightarrow Li_{2(16e)}[Li_{1/3}Ti_{5/3}]_{(16d)}O_{4(32e)}$);[33,92,93] iv) no volume variation is noted during Li-insertion/extraction (so called "zero-strain" insertion host);[36,93,94] v) very high reversibility, i.e., the coloumbic efficiency is >95% even at high current rates;[95] vi) easy synthesis procedures with tailored morphology; and vii) inexpensiveness and eco-friendliness. One of the primary issues for this material is its inherent electrical conductivity ($<10^{-13}$ S cm^{-1}),[96] which limits the Li-diffusion ($<10^{-6}$ cm^2 s^{-1})[97] particularly at high current operation. In order to overcome the mentioned issue, composites with carbonaceous materials have been proposed and such composites are capable of delivering appreciable capacity (≈80 mAh g^{-1}) even at a 1200 C rate (3 s charging).[95,96,98–100] The compatibility of $Li_4Ti_5O_{12}$ anodes with various cathodes including $LiCoO_2$, $Li_{1.03}Mn_{1.97}O_4$, and $Li_{1.025}Mn_{1.95}O_4$ have been studied to ensure the reversibility with a working potential of ≈2.5 V under ambient temperature conditions.[101] Short circuit reactions on the spinel $Li_4Ti_5O_{12}$ anode are three orders of magnitude lower compared to conventional carbonaceous anodes, which is evident from the internal short-circuit abuse tests. Furthermore, the $Li_4Ti_5O_{12}$ anode paired with a layered type $LiCoO_2$ cathode in a prototype cell exhibits higher energy density (66 Wh kg^{-1}) than $LiNi_{1/3}Co_{1/3}Mn_{1/3}O_2$ (64 Wh kg^{-1}) and $LiMn_2O_4$ (61 Wh kg^{-1}) cathodes.[102] Wang et al.[103] confirmed the better compatibility of the $Li_4Ti_5O_{12}$ anode with $LiCoO_2$ than with $LiMn_2O_4$. Jansen et al.[104] first reported the ultralong cycleability of the $LiCoO_2/Li_4Ti_5O_{12}$ configuration for 117 000 cycles. Similarly, Majima et al.[105] revealed the extended cycleability of over 4000 cycles with good capacity retention characteristics of the $LiCoO_2/Li_4Ti_5O_{12}$ cell, whereas poor cycleability resulted for a $LiCr_{0.1}Mn_{1.9}O_4/Li_4Ti_5O_{12}$ assembly. A dramatic improvement in the high power capability of the $LiCoO_2/Li_4Ti_5O_{12}$ cell was noted when layered type Li_2RuO_3 was incorporated as the additive on the positive side ($LiCoO_2$+Li_2RuO_3, 60%+40%).[106] Improvement in the electrochemical profiles of $LiCoO_2/Li_4Ti_5O_{12}$ systems in the presence of the ionic liquid, 1.0 M LiTFSI with SEI forming additives such as vinylene carbonate (VC) and 1,3-propane sultone, was reported by Kim et al.[107] and VC, trimethoxyboroxine (TMOBX), and lithium

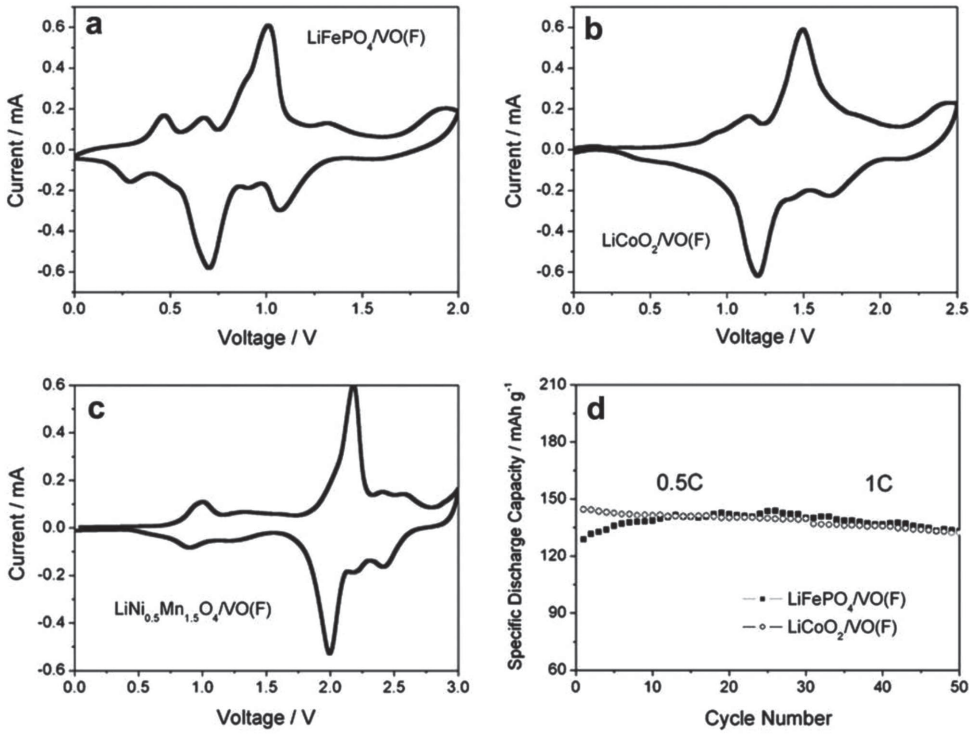

Figure 5. Cyclic voltammograms of the cells: a) $LiFePO_4$/VO(F), b) $LiCoO_2$/VO(F), and c) $LiNi_{0.5}Mn_{1.5}O_4$/VO(F). d) The cycling performance of $LiFePO_4$/VO(F) and $LiCoO_2$/VO(F) cells in the voltage windows of 0–1.5 V and 0–2.5 V, respectively, with 1 M $LiPF_6$/EC-DEC as the electrolyte. Reproduced with permission.[88] Copyright 2009, Elsevier.

bis(trifluoromethanesulfonyl) imide (LiTFSI) additives were reported by Dahn et al.[108] All-solid-state $LiCoO_2/Li_{0.33}La_{0.56}TiO_3/Li_4Ti_5O_{12}$ microbatteries were also reported to have good cycleability.[109] The influence of the synthesis technique (sol-gel, solid-state and combustion) on the electrochemical profiles of $Li_4Ti_5O_{12}$ was evaluated with layered type, Ni- and Mn-doped $LiCoO_2$ ($LiCo_{2/3}Ni_{1/6}Mn_{1/6}O_2$) cathodes with working potentials of ≈2.3 V.[110] Amongst the sol-gel and combustion-derived $Li_4Ti_5O_{12}$ was found to be superior in terms of cycleability (retained ≈90% of initial capacity after 50 cycles) and reversibility compared to solid-state prepared material. Accelerated cycling tests (constant voltage mode) were carried out for $LiCo_{0.5}Ni_{0.5}O_2/Li_4Ti_5O_{12}$ configuration for 50 000 cycles to ensure the long-term stability (by testing them at 2.5 V for 25.6 s and 1.7 V for 25.6 s).[111] About 90% of the initial capacity was retained even the cells were operated at a low current rate. Amatucci et al.[112–114] first suggested the fabrication of a hybrid device by incorporating activated carbon (AC) in both electrodes (AC+$LiCoO_2$/AC+$Li_4Ti_5O_{12}$) to bridge the gap between LIB and supercapacitors, which led to the development of Li-HECs. The same concept has also been adopted for other conventional $LiMn_2O_4$ and $LiFePO_4$ +AC/AC+$Li_4Ti_5O_{12}$ configurations.[115–118] The configuration is currently referred to as "super-redox capacitors".[95,119] The performance of a flexible paper battery with a first generation layered cathode $LiCoO_2$ and a spinel $Li_4Ti_5O_{12}$ anode as reported by several researchers to have appreciable cycleability and an operating potential of ≈2.4 V (here the paper means, free-standing carbonaceous materials);[120–129] for example the full-cell composed of carbon nanotube (CNT)-supported $LiCoO_2$ and $Li_4Ti_5O_{12}$ showed a good cycleability of ≈93% capacity retention after 450 cycles (**Figure 6**).[129] Similarly, carbon- and binder-free $Li_4Ti_5O_{12}$-TiO_2 rutile (3:1) hybrid nanowire arrays were also proposed to overcome the inherent conductivity issue and sustain to deliver high reversible capacity at high current operations.[130] Aging studies were reported that compared the calendar and cycled life of the composite cathode ($LiCoO_2$+$LiMn_2O_4$) in a full-cell assembly with $Li_4Ti_5O_{12}$ anode.[131] The $LiCoO_2/Li_4Ti_5O_{12}$-TiO_2 rutile displayed exceptional cycleability of 3000 cycles with a capacity retention of ≈96% at a current density of 450 mA g^{-1}. A similar capacity profiles were observed while operating at a high current rate of 1750 mA g^{-1} for 2000 cycles. Theoretically, the spinel $Li_4Ti_5O_{12}$ anode paired with a $LiMn_2O_4$ cathode showed a working potential of ≈2.5 V[132,133] and this kind of assembly was extensively investigated by Ohzuku et al.[134,135] The $LiMn_2O_4/Li_4Ti_5O_{12}$ configuration (nanostructured $Li_4Ti_5O_{12}$ anode) has been widely investigated for HEVs, considering the cost, safety, and high power capability.[136–138] At a 10 C rate, the cell displayed excellent cycleability over 1000 cycles under elevated temperature conditions (55 °C) without noticeable capacity fading.[136,139] An excellent long-term cycleability of 30 000 cycles were reported for 100% state-of-charge between 1.8–2.8 V in constant current-constant voltage (CC-CV) mode for a $LiMn_2O_4/Li_4Ti_5O_{12}$ cell at a 10 C rate (1 C = 3 A) with retention of ≈95%.[140] Accordingly, the cycle number and cycle time at a capacity fading of 10%, in accordance with the square root of the cycle number and time rule, are predicted to be 200 000 cycles and 15 years, respectively. On the other hand, the $LiNi_{0.5}Co_{0.2}Mn_{0.3}O_2/Li_4Ti_5O_{12}$ cell showed slightly inferior capacity profiles compared the aforesaid

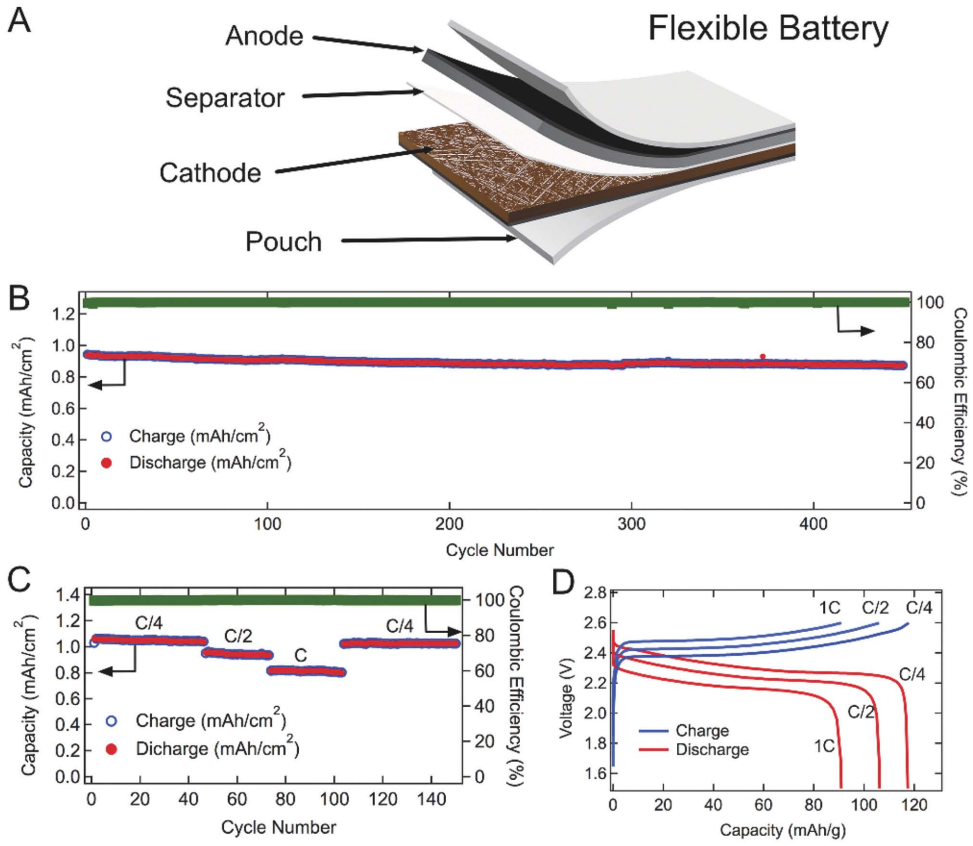

Figure 6. A) Schematic of the flexible battery laminated within aluminum-lined pouch. B) Areal capacity (mAh cm^{-2}) of the full cell ($Li_4Ti_5O_{12}/LiCoO_2$) cycled for 450 cycles at C/2 rate. The full cell had a total active area of 2.5 × 2.5 cm^2 and $Li_4Ti_5O_{12}$ and $LiCoO_2$ loading of 13.4 and 12.5 mg cm^{-2}, respectively. C) Areal capacity (mAh cm^{-2}) and columbic efficiency (%) of the full cell cycled between C/4 and 1C rate. D) Galvanostatic charge/discharge curves for the full cell cycled between C/4 to 1 C rate. The capacity at C/4, C/2 and 1C rate was 117, 104 and 90 mAh g^{-1}, respectively. Columbic efficiency of all the batteries was above 99.5%. Reproduced with permission.[129] Copyright 2014, John Wiley & Sons.

configuration and displayed ≈86% retention after 6000 cycles at a 60 A current rate (3 C). Based on the square root of the cycle number and time rule, the cell is capable of working for 15 years with a loss of 20% capacity. Elevated temperature (55 °C) performance of the $LiMn_2O_4/Li_4Ti_5O_{12}$ system was further improved by Al- and F-doping in the cathode side ($LiAl_{0.1}Mn_{1.8}O_{4-z}F_{0.5}$) with porous PVdF membrane and displayed ≈85% of retention after 400 cycles at 0.14 C rate (7 months).[141,142] Ionica-Bousquet et al.[143] attempted to use two new polyfluorinated boron cluster lithium salts ($Li_2B_{12}F_{12}$ and $Li_2B_{12}F_8H_4$) as the electrolyte for the $LiMn_2O_4/Li_4Ti_5O_{12}$ configuration to improve the initial coloumbic efficiency and high reversibility. $Li_2B_{12}F_{12}$ salt iswas found to be superior than the latter and is comparable to conventional $LiPF_6$ based solutions. The electrochemical performance of $Li_4Ti_5O_{12}$ microspheres was tested with a $LiMn_2O_4$ cathode for 1000 cycles and reversible insertion of more than 3 mole Li was observed.[144] Utilizing a single crystalline $Li_4Ti_5O_{12}$ anode with a $LiMn_2O_4$ cathode was unsuccessful and displayed poor electrochemical behavior even at ambient temperature conditions [145] compared to the previous work by Belharouak et al.[136] At high current cycling, much less generation of heat was observed for the case of $Li_4Ti_5O_{12}$ compared to MCMB[146] and graphite[147] anodes in full-cell assemblies with $LiMn_2O_4$ and $LiFePO_4$, respectively, which is an added advantage. Later, Jiang and Dahn[89,148] confirmed the lower heat evolution (–110 kJ (mol Li)$^{-1}$) in de-lithiated state ($Li_7Ti_5O_{12}$) compared to $Li_{0.81}C_6$ (–215 kJ (mol Li)$^{-1}$). The compatibility with the polymer electrolyte (polyacrylonitrile; PAN) was also evaluated for the configuration with a loss of 0.05% initial capacity only after 200 cycles.[149,150] Christensen et al.[151] found that $Li_4Ti_5O_{12}$ exhibits better high current performance than LiC_6 anode when paired with Li-rich spinel ($Li_{1.16}Mn_{1.84}O_4$). Later, Reale et al.[152,153] demonstrated the compatibility of the $Li_4Ti_5O_{12}$ anode in the presence of a PVdF-based gel polymer electrolyte with spinel $LiMn_2O_4$ and its derivative ($LiNi_{0.5}Mn_{1.5}O_4$) as well as the olivine phase $LiFePO_4$. Electrochemical activity in non-flammable electrolytes, i.e., ionic liquids (LiTFSI in 1-*n*-butyl-1-ethyl-pyrrolidinium bis(trifluoromethane) sulfonamide ($Py_{24}TFSI$) was also evaluated by the same group for the $LiFePO_4/Li_4Ti_5O_{12}$ assembly.[154] However, slightly inferior cycling profiles were noted for the PVdF-based gel polymer system compared to the PAN-based system with the spinel anode. Zr-doping ($Li_4Ti_{5-x}Zr_xO_{12}$) was also performed to improve the electrochemical activity in the full-cell assembly with $LiMn_2O_4$ and no fading was observed for 200 cycles.[155] Electrode thickness is very crucial to yield high performance batteries, however at higher rates the performance is independent of the electrode thickness, which is clearly evident from the $LiMn_2O_4/Li_4Ti_5O_{12}$ cells.[156] Hydrothermally prepared web-like $Li_4Ti_5O_{12}$ anodes

over Ti foil exhibited the extended cycleability of 5000 cycles in a half-cell assembly, irrespective of the applied current rates (2 C and 20 C, 1 C = 175 mA g^{-1}) and they also delivered similar performance to the spinel $LiMn_2O_4$ cathode.[157] Belharouak et al.[158] reported interesting results on such configurations when they were aged at 30, 45, and 60 °C for 5 months; this resulted in a drastic capacity fade, power capability, and H_2 gas production in the cell at high temperature operation. AlF_3 modification was also carried out over a $Li_4Ti_5O_{12}$ surface to suppress the gas evolution when coupled with $LiMn_2O_4$.[159] Gas evolution of the $Li_4Ti_5O_{12}$ anode at elevated temperature operation was further confirmed by Wu et al.[160,161] when paired with a $LiNi_{1/3}Co_{1/3}Mn_{1/3}O_2$ cathode. However, capacity fading is inevitable for such $LiNi_{1/3}Co_{1/3}Mn_{1/3}O_2$ cathodes when coupled with $Li_4Ti_5O_{12}$, irrespective of the operating temperature (55, 75 and 95 °C).[162] Although, capacity fading is unavoidable for $LiNi_{1/3}Co_{1/3}Mn_{1/3}O_2$ based systems, they displayed excellent power capability when paired with spinel $Li_4Ti_5O_{12}$ compared toMCMB anodes.[163,164] The performance of the $LiMn_2O_4$/$Li_4Ti_5O_{12}$ configuration under sub-zero conditions with three different electrolytes (1.0 M $LiPF_6$ in ethylene carbonate (EC): diethyl carbonate (DEC): ethyl methyl carbonate (EMC) (1:1:1, vol%), 1.0 M $LiBF_4$ in propylene carbonate (PC):EMC: methyl butyrate (MB):EC (19:19:57:5, wt%), 1.0 M $LiPF_6$ in EC:EMC:ethyl acetate (EA) (1:5:4, vol%)) was reported by Chen et al.[165] The cell composed of 1.0 M $LiPF_6$ in EC:EMC:EA solution exhibited outstanding performance under low temperature conditions because of the low melting point (-84 °C) and viscosity (0.45 cP at 25 °C) of the EA and it eventually passed the cold cranking test as well. Imazaki et al.[166] suggested the reversible insertion of more than 3 moles of Li in $Li_4Ti_5O_{12}$ without damaging the counter electrode ($Li[Li_{0.1}Al_{0.1}Mn_{1.8}]O_4$) by overcharging to 5.2 V with good stability. Surprisingly, very stable electrochemical profiles were observed when such $Li[Li_{0.1}Al_{0.1}Mn_{1.8}]O_4$ cathodes were paired with $Li_4Ti_5O_{12}$ anodes at –10, 25, and 55 °C temperature conditions.[167] Very negligible capacity fading was observed under sub-zero conditions (–10 °C), whereas 5 and 15% fading was observed after 250 cycles at 25 and 55 °C temperature conditions, respectively. The long-term cycleability of $Li[Li_{0.1}Al_{0.1}Mn_{1.8}]O_4$/$Li_4Ti_5O_{12}$ cells with positive limited (PL) designs was evaluated by means of constant voltage mode (at 3 V for 6 min charge and at 2 V for 6 min discharge) and retained ≈91.7% of initial capacity after 3600 cycles.[168] The influence of the separator (polypropylene microporous membrane or non-woven cloth) on the performance of $Li[Li_{0.1}Al_{0.1}Mn_{1.8}]O_4$/$Li_4Ti_5O_{12}$ and $LiNi_{0.5}Mn_{1.5}O_4$/$Li_4Ti_5O_{12}$ cells was analyzed under elevated conditions (55 °C). Use of non-woven cloths was found appealing in terms of good capacity retention characteristics and high reversibility, and they certainly displayed much better cycleability than commercial polypropylene separators under elevated conditions irrespective of the mentioned ≈2.5 and 3 V configurations.[169] Carbon coating is one of the efficient approaches to overcome the gas evolution observed in $Li_4Ti_5O_{12}$ based cells while operating under elevated conditions. [170] Additionally, the presence of a carbon layer promotes the high power capability of the system. The gassing behavior of the $Li_4Ti_5O_{12}$ anode was not observed when it was paired with layered, spinel, or $LiFePO_4$ systems. This was comprehensively analyzed using online electrochemical mass spectrometry measurements because of the use of poorly dried electrodes and separators and it is in contrast to previous reports.[171] This report confirms that the spinel $Li_4Ti_5O_{12}$ anode is not involved in the gas evolution process while operating under elevated conditions.

Although good cycling profiles were observed for this configuration, elevated temperature profiles of $LiMn_2O_4$ are the main hurdle to using them in practical cells because of the dissolution of Mn^{3+} and the associated Jahn-Teller distortion.[44,137,172] Hence, the well-established low-potential (≈3.4 V *vs.* Li) olivine $LiFePO_4$ was replaced with spinel phase $LiMn_2O_4$, which tends to decrease the net operating potential of the system from ≈2.5 to ≈1.9 V.[70,173–176] The net operating potential is lower, but the olivine phase $LiFePO_4$ exhibits similar characteristics, such ashigh power capability, cost, safety, and high thermal stability.[177–183] The loss in operating potential could be compromised by the high reversible capacity of $LiFePO_4$ (150–160 mAh g^{-1}) compared to $LiMn_2O_4$ (110–130 mAh g^{-1}) in half-cell assemblies.[137] The $LiFePO_4$/$Li_4Ti_5O_{12}$ cells displayed excellent capacity retention characteristics over 1300 cycles for stationary storage[184] and delivered high power capability as well.[185] Yang et al.[186] reported the influence of V-substitution on the Ti sites ($Li_4Ti_{5-x}V_xO_{12}$) and subsequently the full-cell was fabricated and showed an appreciable performance of ≈98.1% retention after 400 cycles. In addition, improved electrochemical reversibility was observed for the $LiFePO_4$/$Li_4Ti_5O_{12}$ cells when casting over free-standing and flexible single-walled carbon nanotube (SWCNT)/polycellulose paper current collectors compared to Al-foil current collectors.[187] Similarly, a wearable configuration was also reported, with the possibility of charging using solar power and utilization of 3D current collectors with notable electrochemical profiles.[188–191] Lei et al.[192] described the advantages of using porous graphitic carbon-$Li_4Ti_5O_{12}$ composites with $LiFePO_4$ to improve the high current cycling. Composite electrodes ($LiFePO_4$ and $Li_4Ti_5O_{12}$) were formulated with graphene foam to construct flexible LIBs for ultrafast charge-discharge capability under harsh conditions (200 C with respect to anode mass) using different orientations of flat and bend modes with good cycleability.[193] Interesting electrochemical and thermal properties are evidenced at sub-zero temperature conditions for 18 650 configurations.[194] Fast charging capability with enhanced safety and long cycle life was noted for $LiFePO_4$ and $Li_4Ti_5O_{12}$ electrodes in 18 650 configurations, in which the electrodes were formulated with water soluble carboxylmethyl cellulose (CMC) binder.[195] The cell retains full-capacity after 20 000 cycles at 6 min charge (10 C) and 12 min (5 C) discharge, and slightly fades to ≈95% after 30 000 cycles, when increasing the charging rate of 15 C (4 min) with 5 C discharge, tested in parallel. In both cases 100% depth-of-discharge and state-of-charge conditions were used. In addition, the mentioned configuration was successfully demonstrated for powering the car on roads. To improve the cell safety under elevated conditions, the $LiFePO_4$/$Li_4Ti_5O_{12}$ configuration was evaluated at 60 °C by incorporating the ionic liquid, 1-hexyl-3-methylimidazolium bis(trifluoromethanesulfonyl) imide (HMIM-TFSI) as the electrolyte.[196] Passerini and co-workers[197,198] also reported the possibility of using *N*-butyl-*N*-methylpyrrolidinium bis(fluorosulfonyl) imide ($PyR_{14}FSI$) and *N*-methoxyethyl-*N*-methylpyrrolidinium fluorosulfonyl-(trifluoromethanesulfonyl) imide ($PyR_{12O1}FTFSI$) ionic liquids

for both ambient and elevated-temperature operation of the $LiFePO_4/Li_4Ti_5O_{12}$ cell. Both electrodes were formulated with CMC binder. Furthermore, ionic liquid based quaternary polymer electrolyte (PVdF + LiTFSI + *N*-methyl-*N*-propylpiperidinium bis(trifluoromethanesulphonyl) imide (PP13-TFSI)+ VC) were also proposed to retard the flammability of the conventional aprotic solvents in the $LiFePO_4/Li_4Ti_5O_{12}$ configuration and they displayed a reversible capacity of ≈161 mAh g^{-1} with good rate performance characteristics.[199] Zaghib et al.[200] suggested that 0.5 mol L^{-1} LiTFSI + 1 mol L^{-1} $LiBF_4$ in EC-γ-butyrolactone (GBL) is found to be a better alternative compared to the thermally unstable $LiPF_6$-based electrolytes when the $LiFePO_4/Li_4Ti_5O_{12}$ cell operates at 60 °C. Notably, the mentioned electrolyte is stable for over thousands of cycles even at ultrafast charging rates such as 30, 60 and 100 C. Redox shuttle additives play a vital role and ensure the cell safety during over charge conditions.[10] Moshuchak et al.[201] studied the usage of 2,5-di-*tert*-butyl-1,4-dimethoxybenzene (DDB) and 4-*tert*-butyl-1,2-dimethoxybenzene (TDB) as the redox shuttle additives for the $LiFePO_4/Li_4Ti_5O_{12}$ configuration and found that the former supports the overcharge protection of ≈200 cycles and the latter supports only 3–15 cycles. Good cycleability of ≈150 mAh g^{-1} under both ambient and elevated temperature conditions for over 100 cycles was reported in the presence of borate ester or aluminium ester-based solid-polymer electrolyte by Wakihara et al.[202] Similarly, the use of patterned current collectors is one of the efficient routes to easily migrate the Li-ions so that high power capability could be realized. Along this line, Choi et al.[203] reported a demonstration of a $LiFePO_4/Li_4Ti_5O_{12}$ cell fabricated using the well patterned (Al and Cu for the cathode and anode, respectively) foils with excellent cycleability at 10 C rate (6 min charge) for 1000 cycles. The cell delivered the reversible capacity of ≈70 mAh g^{-1} after 1000 cycles whereas normal current collector displayed the capacity of ≈8 mAh g^{-1} only under similar testing conditions.

After the successful demonstration of olivine type $LiFePO_4$ in a full-cell assembly with a $Li_4Ti_5O_{12}$ anode, another olivine with a higher redox couple (≈4.1 V *vs.* Li), $LiMnPO_4$, was also used as the cathode active material to fabricate Li-ion power packs for load leveling applications. Similar to $LiFePO_4$ and $LiMn_2O_4$, $LiMnPO_4$ also had similar characteristics, including power capability, cost, safety, high thermal stability, and eco-friendliness.[4] The construction of $LiMnPO_4/Li_4Ti_5O_{12}$ cells with a flat working potential of ≈2.5 V was first reported by Martha et al.[204] The cell displayed an initial reversible capacity of ≈130 mAh g^{-1} (based on cathode loading) at 0.05 C and also exhibited better rate capability profiles. Furthermore, there was no notable capacity loss observed for the cell over the 300 cycles investigated at a 0.5 C rate at 30 °C. Interestingly, there was no such prominent plateau observed at ≈2.5 V while using the carbon-coated $Li_4Ti_5O_{12}$ as the anode with a carbon-coated $LiMnPO_4$ cathode, as reported by Ramar et al.,[205] and it showed a more or less monotonous discharge profile with high power capability. Because of the inferior electrochemical activity of the olivine phase cathode and the different charging protocols (used in conventional mobile phone chargers, CC-CV) fewer reports are available for the case of $LiMnPO_4/Li_4Ti_5O_{12}$ based systems. Therefore, currently, the research activities are focused on the wide range of solid-solutions between $LiFePO_4$-$LiMnPO_4$ ($LiFe_{1-x}Mn_xPO_4$), which are expected to operate between ≈4.1 and 3.4 V vs. Li with two prominent flat potentials.[4,206] For instance, $LiMn_{0.8}Fe_{0.2}PO_4$[204,207–209] and $LiMn_{0.5}Fe_{0.5}PO_4$[208] solid-solutions were reported with spinel $Li_4Ti_5O_{12}$ anodes in full-cell assemblies.

The problems such as anion dissolution in conventional electrolyte solutions and the associated capacity fading reported for the case of high voltage (≈4.8 V *vs.* Li) olivine phase $LiCoPO_4$[210,211] are reported but few reports describing the performance with a $Li_4Ti_5O_{12}$ anode can be found.[212,213] The $LiCoPO_4/Li_4Ti_5O_{12}$ configuration seems promising because of the higher redox potential (≈3.25 V), but an expected capacity fading remains in the full-cell assembly.[212,213] Similar to $LiCoPO_4$, its derivative, Li_2CoPO_4F, also suffers from many issues including poor compatibility with electrolytes,[214] single-phase reaction[215] (whereas $LiCoPO_4$ undergoes a two-phase reaction mechanism),[84,216–219] inherent electrical conductivity,[218] etc., but also, full-cell assembly with $Li_4Ti_5O_{12}$ anode was reported.[220] Unlike that of flat working potential in $LiCoPO_4$ cathodes, a monotonous curve is resulted at ≈3.5 V with capacity fading upon cycling. Furthermore, few reports are available on the spinel $Li_4Ti_5O_{12}$ anode paired with ≈5 V vs. Li type cathodes such as $LiCo_{0.2}Fe_{0.2}Mn_{1.6}O_4$ (working potential: ≈3 V),[221] $LiCoMnO_4$ (working potential: ≈3.2 V)[222], ≈4 V vs. Li class cathodes $LiVPO_4F$ (working potential: ≈2.6 V),[223] $LiNiO_2$ (working potential: ≈ 2 V),[224] and $Li_3V_2(PO_4)_3$ (working potential: ≈2.5 V),[225] and ≈3.4 V vs. Li type layered cathode V_2O_5 (limited for one mole Li-insertion/extraction with operating potential of ≈1.85 V)[75,80] were studied and reported. In addition, an interesting $Li_4Ti_5O_{12}/Na_3V_2(PO_4)_2F_3$ assembly composed of mixed 1 M $LiPF_6$ and 1 M $NaPF_6$ in EC:dimethyl carbonate (DMC) electrolyte solution was reported by Barker et al.[226] The cell displayed reasonable cycling behavior irrespective of either the above solution or $LiPF_6$ based electrolytes with operating potential of ≈2.6 V.

Currently, research is focused on the development of ≈3 V class spinel $LiNi_{0.5}Mn_{1.5}O_4/Li_4Ti_5O_{12}$ systems to fulfil the necessary requirements for zero-emission transportation applications such as EVs and HEVs.[227] Ni-doping in $LiMn_2O_4$ somewhat overcome the Mn^{3+} dissolution and associated Jahn-Teller distortion issues with beneficial higher operating potential (≈4.7 V vs. Li).[46,228–234] Originally, Ohzuku et al.[135,235–238] reported the development of this 3 V class system for high power applications. Demonstrating the influence of particle size on the electrochemical activity of such 3 V class Li-ion cells, $LiNi_{0.5}Mn_{1.5}O_4$ particles prepared at 1000 °C with smooth (111) facets composed of octahedral morphology showed better electrochemical activity with a $Li_4Ti_5O_{12}$ anode compared to low-temperature-synthesized small particulates.[239] The long-term cycleability of such a cell was also evaluated by applying a sinusoidal potential of 1 V at 0.1 Hz with an open-circuit voltage of 3.16 V (5 s charge and 5 s discharge) and 10% power fade was only observed after 200 000 cycles (23 days).Further studies were carried out by several researchers to develop such a zero-strain insertion anode, $Li_4Ti_5O_{12}$-based system for high power applications.[240,241] Apart from the higher operating potential of $LiNi_{0.5}Mn_{1.5}O_4$, the eco-friendliness, low-cost, and high energy density, together with with high power capability and easy production on the industrial

scale are worth mentioning.[242] However, the $Ni^{2+/4+}$ occurs at slightly higher potential than the thermodynamic stability of conventional carbonate-based electrolyte solutions and it is one of the issues when paired with $Li_4Ti_5O_{12}$.[3] This certainly results in the lower coloumbic efficiency of the cell in the initial cycles while using $LiPF_6$ based electrolyte solutions. Therefore, a protective coating (preferably a conductive coating, otherwise it will deteriorate the power capability) or metal co-doping in either transition metal sites (Mn or Ni) or Li-sites is necessary to sustain $LiNi_{0.5}Mn_{1.5}O_4$ as electrochemically active for extended cycling. Wu et al.[243] investigated the electrochemical performance of $LiNi_{0.5}Mn_{1.5}O_4/Li_4Ti_5O_{12}$ with negative limited (NL), PL, and equal-mass ratio (EM) and found that all three configurations showed better electrochemical properties. However, the NL design provides marginally better electrochemical performance than rest after 1000 cycles with retention of ≈98% of the initial capacity compared to ≈96.8% for EM and ≈94% for PL designs. The better electrochemical activity of NL design was further confirmed by Xian et al.[244] and rendered ≈85% capacity compared to ≈56% for PL design after 2900 cycles at a current density of 0.2 mA cm^{-2}. It was also found that EC:DEC solvents exhibit poor compatibility compared to EC:DMC when used for these 3 V class Li-ion cells. Unfortunately, there has been no further improvement to the the columbic efficiency noted when changing the conventional $LiPF_6$ salt to $LiClO_4$, lithium bis(oxalato) borate (LiBOB), or $LiBF_4$.[245] Similar capacity trends were observed for all three salts, and a rapid decrease in the profiles was observed for $LiBF_4$ salts in the 3 V class systems. Li et al.[246] suggested the possibility of using tris(hexafluoro-iso-propyl) aluminate ($Al(HFiP)_3$) as an additive for the PL design cells by considering several aspects including coulombic efficiency, charge at end point capacity slippage, and capacity loss during prolonged storage and capacity retention vs. cycle number. Dimethyl methylphosphonate (DMMP) was also proposed as an additive for the 3 V class systems by considering initial higher coloumbic efficiency and flame retardant characteristics; unfortunately, it offers more fade than additive-free systems upon cycling.[247] To enable the electrochemical activity, preferably the coloumbic efficiency, of such 3 V class cells under sub-zero (–20 °C) and elevated temperature (55 °C) operations, Co co-doping has been performed in the cathodic side.[248] The full-cell $LiNi_{0.45}Co_{0.1}Mn_{1.45}O_4/Li_4Ti_5O_{12}$ with PL design rendered ≈85.4% of initial capacity after 500 cycles at 1 C rate. Irrespective of the operating temperature (–20 to 55 °C), a good cycleability was observed with an expected capacity drop, i.e., less reversibility in sub-zero conditions. On the other hand, Ti substitution in Mn sites ($LiNi_{0.5}Mn_{1.5-x}Ti_xO_4$) results in suppression of the electrolyte decomposition and enables good capacity retention characteristics.[249] Al-co-doping ($LiNi_{0.473}Mn_{1.473}Al_{0.054}O_4$) in spinel cathodes was also reported with nanotube morphology and paired with an $Li_4Ti_5O_{12}$ anode that offered better electrochemical characteristics compared to the micrometer-sized system.[250] However, the obtained results are inferior compared to the aforementioned 3 V class systems reported. Choi et al.[251] reported the synthesis of hierarchical cotton templated electrode materials for the fabrication of $LiNi_{0.5}Mn_{1.5}O_4/Li_4Ti_5O_{12}$ cells with excellent high current performance (3 C) of over 200 cycles with ≈92% capacity retention. No charge capacity end point slippage was observed for $Li_4Ti_5O_{12}$ based cells in either the PL design or NL back-to-back $LiNi_{0.5}Mn_{1.5}O_4/Li_4Ti_5O_{12}$ cells as no interaction between electrodes was observed, whereas rapid fading was observed for normal NL $LiNi_{0.5}Mn_{1.5}O_4/Li_4Ti_5O_{12}$ cells.[252] It is well-known that, $Li_4Ti_5O_{12}$ is a SEI-free electrode; however, the presence of a passivation layer was evident and it was mainly composed of solvated Mn, LiF,and some inorganic species.[253] This might be the result of oxidation of solvent molecules while using high voltage spinel cathodes ($LiNi_{0.5}Mn_{1.5}O_4$). Fabrication of "zero-volt" Li-ion cells with symmetric electrodes ($Li_7Ti_5O_{12}/Li_4Ti_5O_{12}$) is one of the efficient ways to understand capacity fading mechanisms.[254,255] Interestingly, $Li_7Ti_5O_{12}/Li_4Ti_5O_{12}$ symmetric cells were also used to study the parasitic side reaction with various electrolyte solutions and combinations, preferably on a sulfone-based system.[256] This study clearly demonstrated that the surface film formation depends completely on the state-of-charge and the presence of alkyl carbonates (DMC, EMC) in sulfone (**Figure 7**). Thus, alkylcarbonare (EMC) reduction occurred at the $Li_7Ti_5O_{12}$/electrolyte/$Li_4Ti_5O_{12}$ interfaces, which lead to the decomposition products of carbonates, ethers, and mineral compounds such as $ROCO_2Li$ and Li_2CO_3 over titanate electrode surfaces. In addition to above, the large amounts of LiF deposition results in an increase in resistance and subsequently deteriorates the cycling profile upon cycling.

2.4. $LiTi_2O_4$

$LiTi_2O_4$ is the only known cubic spinel superconductor with metallic conductivity and has been proposed as a promising insertion anode for LIB applications; it has a theoretical capacity of ≈161 mAh g^{-1} for the reversible insertion/extraction of one mole of Li ($Li_2Ti_2O_4$ or Ti_2O_4). During the electrochemical Li-insertion/extraction process spinel $LiTi_2O_4$ undergoes a two-phase reaction mechanism at ≈1.5 V *vs.* Li. A small reduction of the lattice parameter value (from 8.416 to 8.380 Å) and unit cell volume variation is also observed during the Li-insertion process.[257,258] The spinel phase exhibits good cycleability in a half-cell assembly, but the very few works only reported for the LIB point of view. This is mainly because of difficulties in the synthesis process, as the preparation of mixed valence of Ti^{3+} and Ti^{4+} is not easy. Similar to Li-insertion, extraction is also plausible because of the presence of Ti^{3+}, which also undergoes a two-phase equilibrium at ≈2.3 V vs. Li and results in the formation of Ramsdellite type TiO_2 (Ti_2O_4) at the end of the charge.[259] Recently, Yang et al.[260] reported a simple carbothermal reduction for the preparation of $LiTi_2O_4$ with good electrochemical properties in the half-cell assembly with a reversible capacity of ≈140 mAh g^{-1} at ≈1.5 V vs. Li region. Persi et al.[261] first reported the performance of a $LiFePO_4/LiTi_2O_4$ system in the presence of PVdF-based gel electrolyte. The cell delivered a reversible capacity of ≈100 mAh g^{-1} (with respect to cathode loading) at a working potential of ≈1.9 V, with meager fading upon cycling (**Figure 8**). Later, Manickam and Takada[262] reported the performance of a $LiMn_2O_4/LiTi_2O_4$ configuration with much less reversibility (≈5 to 15 mAh g^{-1}) in the ≈2.3 V regime.

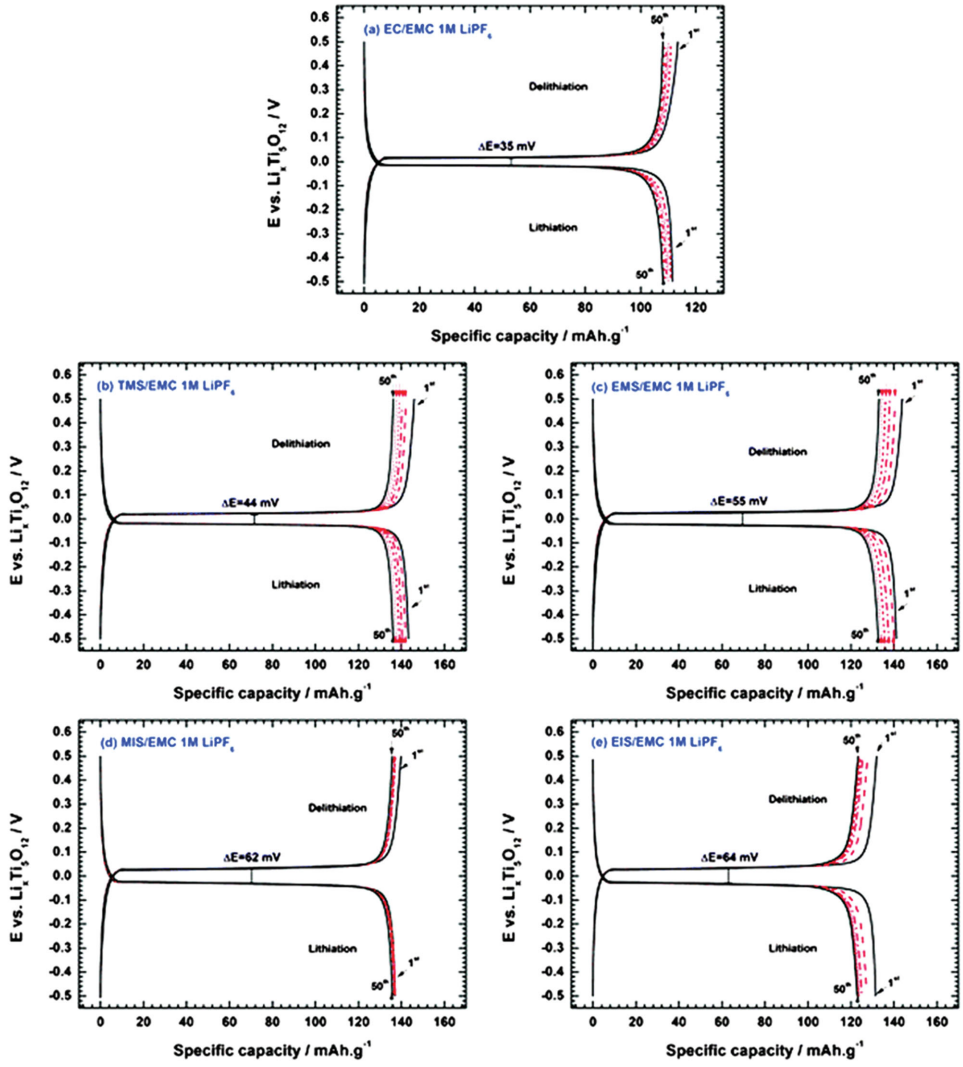

Figure 7. Voltage profiles (C/5 + D/5) at 20.0 ± 0.3 °C for a) EC/EMC 1 M $LiPF_6$, b) tetra methyl sulfone (TMS)/EMC 1 M $LiPF_6$, c) EMC/EMC 1 M $LiPF_6$, d) methyl isopropyl sulfone (MIS)/EMC 1 M $LiPF_6$, and e) ethyl isopropyl sulfone (EIS)/EMC 1 M $LiPF_6$ electrolytes in $Li_{4+x}Ti_5O_{12}/Li_4Ti_5O_{12}$ symmetric cells. Mid-plateau polarization (ΔE) between delithiation and lithiation is indicated for the first cycle. Reproduced with permission.[256] Copyright 2014, PCCP Owner Societies.

2.5. $LiCrTiO_4$

$Li[CrTi]O_4$ is a AB_2O_4 type cubic spinel and exhibits a similar characteristics to those of its counterpart $Li_4Ti_5O_{12}$. Similar to $LiTi_2O_4$, $LiCrTiO_4$ can also be used as a cathode by utilizing the $Cr^{3+/4+}$ redox couple (≈4.5 V *vs.* Li). Unfortunately the electrochemical stability of the $Cr^{3+/4+}$ redox couple is found inferior, hence there has been no further attempt carried out to make use of it. On the other hand, a $Ti^{4+/3+}$ redox couple could be used as a promising ≈1.5 V *vs.* Li insertion anode for LIB applications with theoretical capacity of ≈157 mAh g^{-1} for the reversible insertion of one mole of Li. A unit cell volume variation from 576 to 580 $Å^3$ (+3.7%) is observed during the Li-insertion process at low voltage.[36] As far as the structural prospects of $LiCrTiO_4$ are concerned, the Li is located in the tetrahedral sites 8(a) sites, whereas the transition metal elements Ti^{4+} and Cr^{3+} are randomly distributed in a 1:1 ratio and occupy 100% in the octahedral 16(d) sites in a cubic-closed packed oxygen array in 32(e) sites.[90,263,264] The crystal site formula of $LiCrTiO_4$ can also be written in space notation as $Li^{8(a)}[CrTi]^{16(d)}O_4{}^{32(e)}$. Ohzuku et al.[36,265] first reported the electrochemical activity of a spine framework $LiCrTiO_4$ as a promising electrode for LIB applications. Later, improvement in the electrochemical properties were noted, including N_2 sintering,[266] carbon coating,[267] and $LiCrTiO_4$ with Ramsdellite structure[268,269] in half-cell assembly. Ooms et al.[270] first reported the performance of a $LiMg_{0.1}Ni_{0.4}Mn_{1.5}O_4/LiCrTiO_4$ assembly with a high working potential of ≈3.25 V. The cell delivered an exceptional performance of 175 cycles with stable reversible capacity of ≈120 mAh g^{-1}. On the contrary, a severe fading was noted for the native phase when paired with a $LiCrTiO_4$ anode, for example the full-cell $LiMn_2O_4/LiCrTiO_4$ retained only ≈88% of its initial reversible capacity after 50 cycles with a working potential of ≈2.5 V (**Figure 9**).[263] Apart from the LIB applications,

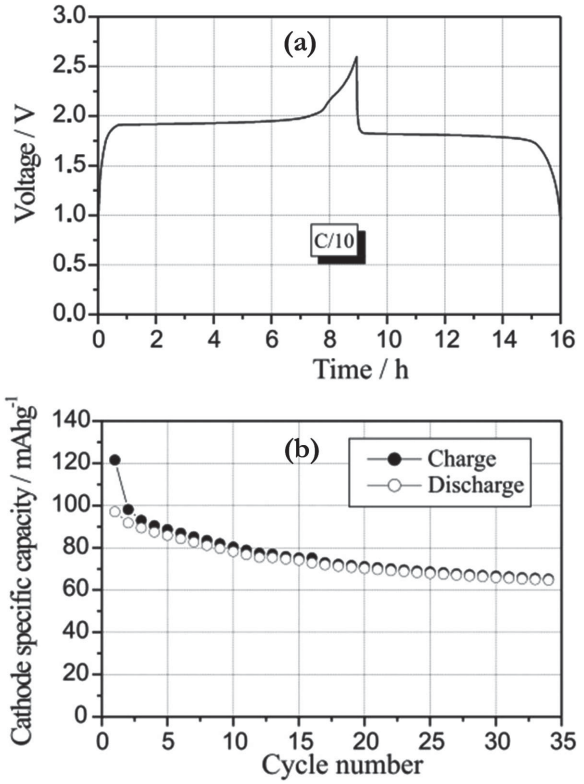

Figure 8. a) Galvanostatic charge–discharge cycle of the polymer $LiTi_2O_4$/$LiClO_4$–EC–PC–PVdF gel/$LiFePO_4$ lithium-ion cell at room temperature and at C/10 rate. b) Capacity upon cycle number for the polymer $LiTi_2O_4$/$LiClO_4$–EC–PC–PVdF gel/$LiFePO_4$ lithium-ion cell at room temperature. Rate: first cycle C/10; following cycles C/5. Voltage limits: charge 2.5 V; discharge 1.1 V. Reproduced with permission.[261] Copyright 2002, Elsevier.

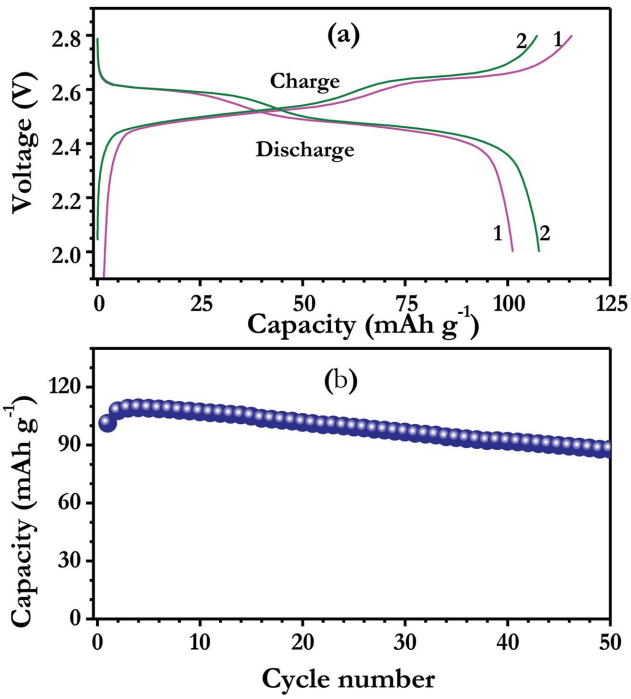

Figure 9. a) Galvanostatic charge-discharge signatures of $LiMn_2O_4$/$LiCrTiO_4$ cell at current density of 15 mA g^{-1} and b) cycling profiles of $LiMn_2O_4$/$LiCrTiO_4$ full-cell with 15 mA g^{-1} current density. Reproduced with permission.[263] Copyright 2012, John Wiley & Sons.

spinel phase $LiCrTiO_4$ has also been used as a promising insertion anode for non-aqueous Li-ion hybrid electrochemical capacitors.[264,271]

2.6. $TiNb_2O_7$

Ti-Nb-O oxides is one of the important insertion anode reported for LIB applications and has two redox species (Ti^{4+} and Nb^{5+}). The monoclinic $TiNb_2O_7$ exhibits a high theoretical capacity of ≈387 mAh g^{-1} for the possible insertion of five mole of Li ($Ti^{4+/3+}$, $Nb^{5+/4+}$, $Nb^{4+/3+}$). Practically, over 280 mAh g^{-1} is possible with a working potential of ≈1.55 V *vs.* Li, irrespective of the synthetic procedures employed.[272–281] Either carbon coating or Nb(IV) doping into Ti sites is required to improve the electrochemical profiles at high current rates.[276] Although, the $TiNb_2O_7$ exhibits the favorable characteristics such as no SEI formation, high reversible capacity, and eco-friendliness, meager capacity fading upon cycling is one of the prime issues.[277,282] This fading mainly originates from the unit cell volume variation during the Li-insertion process likely +≈7.22%, which is much higher compared to the transition from $Li_4Ti_5O_{12}$ in to $Li_7Ti_5O_{12}$ (almost 0%).[282] $TiNb_2O_7$ is a monoclinic layered structure with C2/m space group, in which Ti^{4+} and Nb^{5+} both occupy octahedral sites sharing corners and edges. Anti-site disorder is also possible because of the similar ionic radii of Ti^{4+} and Nb^{5+}. According to Lu et al.,[273] lithium can be reversibly inserted into the (–110) plane of the $TiNb_2O_7$ primitive cell and occupying the interstitial site. Han and Goodenough[272] first reported the performance of a $TiNb_2O_7$/$LiNi_{0.5}Mn_{1.5}O_4$ cell with both cathode- and anode-limiting configurations at an operating potential of ≈3 V. The anode limiting configuration (NL) tested between 3.5 and 1.5 V rendered good electrochemical characteristics compared to the PL one. Unfortunately, both limiting designs exhibited inferior coloumbic efficiency upon cycling (**Figure 10**). Gao et al.[274] reported the excellent performance of a nanoporous $TiNb_2O_7$/$LiNi_{0.5}Mn_{1.5}O_4$ assembly over 1000 cycles with capacity retention and coloumbic efficiency of ≈84% and ≈100%, respectively. Ordered mesoporous $TiNb_2O_7$ exhibits outstanding cycleability of over 1600 cycles at current density of 3.87 A g^{-1} with a $LiFePO_4$ cathode at a working potential of ≈1.8 V. Although, the working potential is found to be low, ≈0.009 mAh g^{-1} loss per cycle was only noted during such prolonged cycling.[279] Very recently, Jayaraman et al.[29,277] realized the performance of electrospun $TiNb_2O_7$ anode in all 1D architecture with electrospun $LiMn_2O_4$ cathode in the presence of an electrospun PVdF-HFP membrane (**Figure 11**). The $TiNb_2O_7$/PVdF-HFP/$LiMn_2O_4$ cell displayed good cycleability irrespective of the applied current rates.

2.7. $SrLi_2Ti_6O_{14}$

A high molecular weight, lower potential anode (≈1.4 V vs. Li) is reported for the alternative to conventional spinel $Li_4Ti_5O_{12}$.

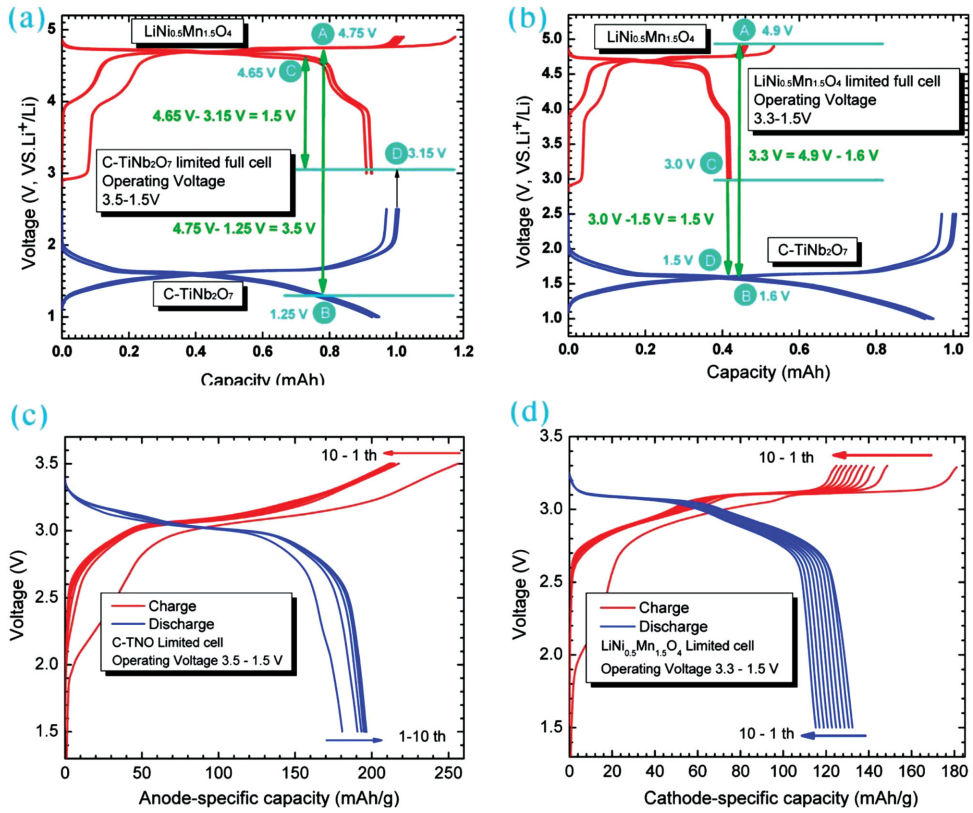

Figure 10. Details of capacity matchup in the a) C-$TiNb_2O_7$-limited and b) $LiNi_{0.5}Mn_{1.5}O_4$-limited full cell, respectively. The charge and discharge voltage profiles of the C-$TiNb_2O_7$/Li cells (blue curves) and $LiNi_{0.5}Mn_{1.5}O_4$/Li (red curves) cells are shown in (a,b) with the electrolyte of 1 M $LiPF_6$/EC + DEC (1:1). The cells operated at the C/10 rate with the cut-off voltages of 1.0–2.5 V for C-$TiNb_2O_7$/Li cell and 3.0–4.9 V for $LiNi_{0.5}Mn_{1.5}O_4$/Li cell. c) Charge/discharge galvanostatic curves for a $LiNi_{0.5}Mn_{1.5}O_4$/C-$TiNb_2O_7$ cell at C/10 with capacity limited by C-$TiNb_2O_7$ cycled between 1.5 and 3.5 V and d) for a $LiNi_{0.5}Mn_{1.5}O_4$/C-$TiNb_2O_7$ full cell at C/10 with capacity limited by the $LiNi_{0.5}Mn_{1.5}O_4$cathode and cycled between 1.5 and 3.3 V. Reproduced with permission.[272] Copyright 2011, American Chemical Society.

The $SrLi_2Ti_6O_{14}$ has a high theoretical capacity of ≈262 mAh g^{-1} for the complete reduction of all six Ti^{4+} atoms in to Ti^{3+}.[283] Furthermore, it has a 3D structure and *Cmca* space group, in which Li-ions can migrate quickly because of the structure's high diffusion coefficient, allowing for excellent high-drain performance. $SrLi_2Ti_6O_{14}$ is made up of edge and corner sharing TiO_6 octahedral units forming layers parallel to the (1 0 0) plane. Consecutive layers (with respect to a mirror plane at $x = 1/2$) are linked by common corners along the *a*-direction. These octahedra constitute a $[Ti_6O_{14}]n^{4n-}$ 3D network. Li atoms in tetrahedral coordination occupy vacancies of the TiO_6 octahedra framework, while Sr atoms lie in 11-coordinated sites between two successive layers.[284,285] Belharouak and Amine[285,286] first reported the electrochemical activity of the Sr-based titanate and found that ≈4.24 mole of Li inserted in to the matrix, contrary to the theoretical value of six mole. Later, the same group reported the performance and compatibility with various anode to cathode mass ratios in the full-cell assembly with a $LiMn_2O_4$ cathode.[287] The full-cell $LiMn_2O_4$/$SrLi_2Ti_6O_{14}$ delivered appreciable cycleability at ≈2.7 V, irrespective of the mass balancing with ≈10% capacity loss after 200 cycles. Later, Liu et al.[288] reported the exceptional cycleability of 1000 cycles with ≈90% capacity retention in the half-cell configuration. Recently, the full-cell was fabricated with a designed capacity of 6 Ah using $LiCoO_2$ and it was compared with $LiCoO_2$/$Li_4Ti_5O_{12}$ configuration for HEV applications.[289] Li-diffusion coefficients and electronic conductivity of $SrLi_2Ti_6O_{14}$ were, respectively, one order and two orders of magnitude higher than commercial $Li_4Ti_5O_{12}$ anodes. As a result, high electronic conductivity and high Li migration capability of $SrLi_2Ti_6O_{14}$ particles leads to excellent power performance in the $LiCoO_2$/$SrLi_2Ti_6O_{14}$ cell compared to the $LiCoO_2$/$Li_4Ti_5O_{12}$ configuration (**Figure 12**).

2.8. $Li_3Nd_3W_2O_{12}$

Garnet framework materials composed of $Li_3A_3B_2O_{12}$ structures have been widely investigated as solid/ceramic electrolytes for LIB applications with ionic conductivities >10^{-4} S cm^{-1} in ambient conditions.[290,291] Very recently, Goodenough and co-workers[292] reported the possibility of using a garnet framework, $Li_3Nd_3W_2O_{12}$, as a low-voltage (≈0.3 V *vs.* Li) insertion anode with high power capability. The garnet framework material exhibits a theoretical capacity of ≈106 mAh g^{-1} for reversible insertion of 4 mole of Li by utilizing the reduction of W^{4+} to W^{2+}. The structural properties of such a lithium garnet framework can be described as $Li_3A_3B_2O_{12}$ in which Li occupies square anti-prismatic, octahedral, and tetrahedral sites in a 3:2:3

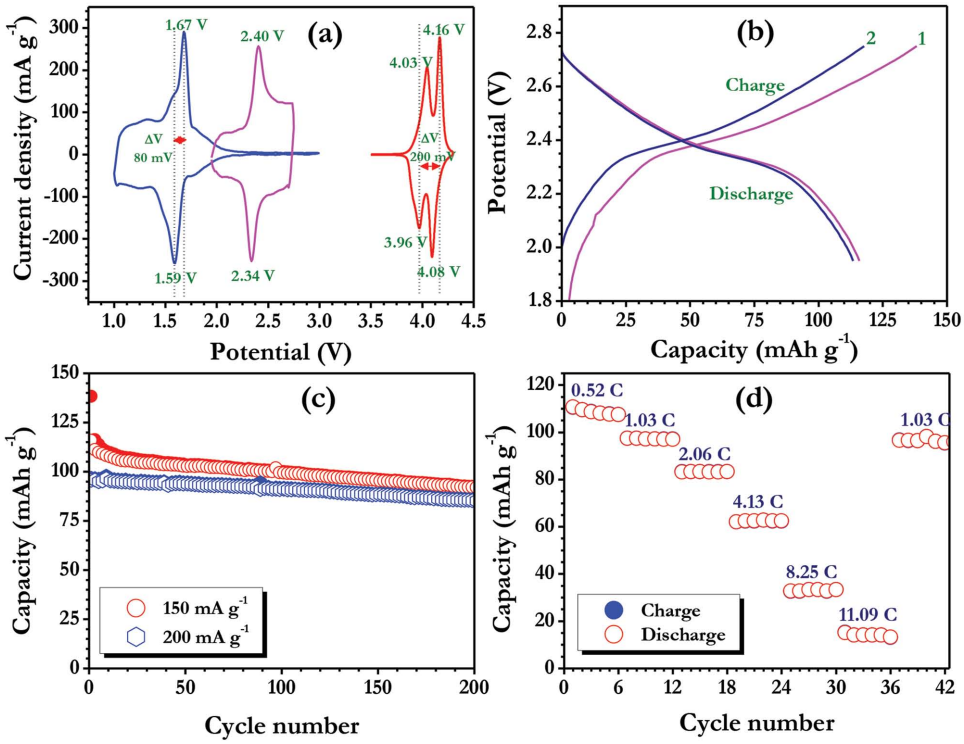

Figure 11. a) CV traces of all one dimensional full-cell, $LiMn_2O_4$|gelled PVdF-HFP|$TiNb_2O_7$ tested between 1.95–2.75 V at scan rate of 0.1 mV s^{-1}. The electrochemical performance of $TiNb_2O_7$ and $LiMn_2O_4$ electrodes in half-cell assembly is also given for the comparison. b) Typical galvanostatic charge-discharge curves of full-cell, $LiMn_2O_4$|gelled PVdF-HFP|$TiNb_2O_7$ at current density of 150 mA g^{-1}. c) Plot of discharge capacity *vs.* cycle number for all 1D full-cell, $LiMn_2O_4$|gelled PVdF-HFP|$TiNb_2O_7$ at current density of 150 and 200 mA g^{-1}. d) Rate capability studies of all one dimensional full-cell, $LiMn_2O_4$|gelled PVdF-HFP|$TiNb_2O_7$ cycled between 1.7–2.5 V at various C rates (1 C is assumed as 150 mAh g^{-1}). Reproduced with permission.[277] Copyright 2014, American Chemical Society.

ratio.[293] The tetrahedral Li-sites are bridged by empty octahedra that share opposite faces with two tetrahedral sites; every face of a Li-site is bridged to neighbouring Li-sites by the means of octahedral sites to provide a 3D interstitial space. This interstitial space can accommodate 9 mole of Li, but a practical limit of 7 mole of Li has been set. However, the material is highly sensitivity towards atmospheres such as H_2O and CO_2 and the garnet framework materials becomes insulating. Hence, the protective coating necessary to keep the lithium garnet framework remains electrochemically active. Satish et al.[294] succeeded at making a uniform carbon coating over $Li_3Nd_3W_2O_{12}$ particulates to realize applications as an anode in LIBs. Subsequently, the full-cell was fabricated with a $LiMn_2O_4$ cathode that had a working potential of ≈3.4 V. The cell, $LiMn_2O_4$/C-$Li_3Nd_3W_2O_{12}$, delivered an exceptional cycleability, irrespective of the applied current rate, for example ≈83% of initial reversible capacity was retained after 300 cycles (**Figure 13**).

2.9. $LiTi_2(PO_4)_3$

$LiTi_2(PO_4)_3$ is one of the widely investigated electro-active materials for LIB applications, independent of anode, cathode, and electrolyte applications. Unfortunately, the operating potential (≈2.6 V vs. Li) of $LiTi_2(PO_4)_3$ is too high from the anode point of view and too low from the cathode perspective.[295] However, it remains attractive as a solid-electrolyte/glass ceramic with room temperature ionic conductivity in the order of ≈10^{-4} S cm^{-1}. It suffers from a lack of electronic conductivity, hence the carbon coating is necessary while employing it as an electrode in LIB applications. $LiTi_2(PO_4)_3$ accommodates two mole of Li with a theoretical capacity of ≈137 mAh g^{-1} and undergoes a two-phase reaction during reversible Li-insertion. Apart from the LIB applications, $LiTi_2(PO_4)_3$ is considered to be a prospective anode material for aqueous rechargeable batteries becausethe redox potential falls well within the H_2 evolution potential;[296,297] it has also been investigated as a prospective anode for Li-HEC applications.[298–300] The structure of NASICON-type $LiTi_2(PO_4)_3$ is similar to $Li_3V_2(PO_4)_3$. Typically, it is a 3D framework and this allows numerous ionic substitutions at various lattice sites. The framework is built of PO_4 tetrahedra linked by the corners of TiO_6 octrahedral units. Each PO_4 tetrahedron is connected with four TiO_6 octahedral units and, conversely, TiO_6 units are connected to six PO_4 tetrahedra. The interstitial cavities generated within the network are of two types known as M1 and M2 sites. The M1 cavity is situated between two TiO_6 octahedral units and is coordinated with the trigonal antiprism of oxygen and occupied by Li. The M2 cavity is composed of distorted eight-fold coordination and is surrounded by M1 interstitial voids. Initially, it was believed that Li would occupy the M2 sites during insertion to form $Li_3Ti_2(PO_4)_3$ However, Aatiq et al.[301] reported that in $Li_3Ti_2(PO_4)_3$ the three Li-ions occupy the two tetrahedral sites, M3 and M'3, within the M2 cavity in a ratio of 2/3:1/3, respectively. Aravindan et al.[302] reported the performance of

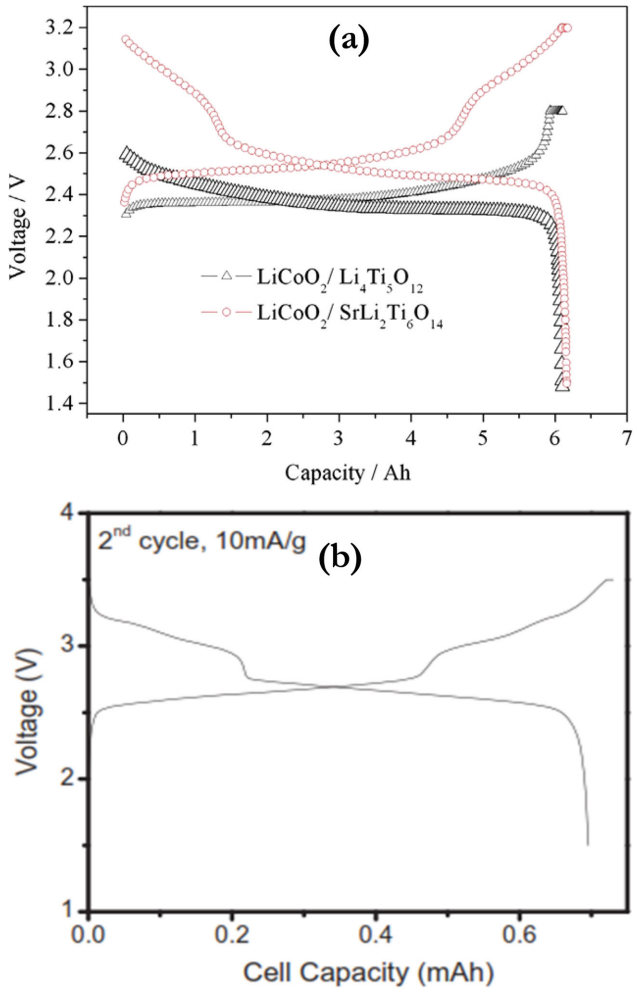

Figure 12. a) Two kinds of full cell charge–discharge curves obtained at a 1.0 C rate,[289] and b) Charge and discharge curves of $LiMn_2O_4$/$SrLi_2Ti_6O_{14}$ full cell cycled between 1.5 and 3.5 V under 10 mA g^{-1}. The full cell is anode limited. Panel (a) reproduced with permission.[289] Panel (b) reproduced with permission.[287] Copyright 2014 and 2011, Elsevier.

a $LiMn_2O_4$/$LiTi_2(PO_4)_3$ cell with a working potential of ≈1.5 V. Unfortunately, the working potential was lower than the redox potential of the $LiTi_2(PO_4)_3$ in the half-cell assembly, and it was much higher than other conventional secondary batteries such as Pb-acid, Ni-MH, Ni-Cd.[5,303] The full-cell $LiMn_2O_4$/$LiTi_2(PO_4)_3$ displayed good capacity retention characteristics and retained ≈72% of its initial reversible capacity after 200 cycles (**Figure 14**). Capacity fading is inevitable for the $LiMn_2O_4$/$LiTi_2(PO_4)_3$ configuration, mainly because of the intrinsic nature of the insertion type NASICON anode.

2.10. $Li_3V_2(PO_4)_3$

NASICON type $Li_3V_2(PO_4)_3$ has been widely investigated as a promising ≈4 V *vs.* Li cathode active material for LIB applications for the extraction of two mole of Li by utilizing $V^{3+/4+}$ redox couple with theoretical capacity ≈132 mAh g^{-1}.[304–306] Removal of a third Li is also plausible by oxidizing one of the V atoms into the 5+ state with a theoretical capacity of ≈197 mAh g^{-1}.[307–310] However, the removal of the last Li is kinetically the most difficult because of the reduced ionic and electronic conductivity of the fully empty $V_2(PO_4)_3$ phase. This certainly results in structural destruction and eventually leads to capacity fade upon cycling. Similar to oxidation of V^{2+} in to V^{5+}, reduction of V^{3+} in to V^{2+} is also possible at ≈1.75 V vs. Li for reversible insertion two mole of Li.[311–315] Practically, a reversible capacity of ≈100 mAh g^{-1} for $Li_3V_2(PO_4)_3$ is observed in theat low voltage region.[311] $Li_3V_2(PO_4)_3$ consists of a 3D framework of metal octahedra (VO_6) and phosphate tetrahedra (PO_4) sharing oxygen vertices. Each VO_6 octahedral unit is surrounded by six PO_4 tetrahedral units. However, each tetrahedral unit is surrounded by four VO_6 octahedral units. This configuration forms a 3D network and the alkali cation, Li, is located in the cavities within the framework. Three four-fold crystallographic positions exist for the Li atoms leading to twelve Li positions within the unit cell.[305,306,309] Kobayashi *et* al.[316] first demonstrated an all-solid-state symmetric $Li_3V_2(PO_4)_3$/$Li_{1.5}Al_{0.5}Ge_{1.5}(PO_4)_3$/$Li_3V_2(PO_4)_3$ cell and found that increasing the temperature from 25 to 80 °C resulted in an increase in the operating voltage (from 1.7 to 2 V) and reversible capacity (from 42 to 104 mAh g^{-1}). This dramatic change in the variation of the working potential and reversible capacity is mainly because of the poor interface between the electrode and solid-electrolyte. Later, Aboulaich et al.[312,314] successfully used the spark plasma sintering (SPS) technique to overcome such interfacial issues for the mentioned configuration (**Figure 15**). Furthermore, the electrochemical profiles of such cells at 80 °C are comparable to the performance of a $Li_3V_2(PO_4)_3$/$Li_3V_2(PO_4)_3$ cell that contains conventional liquid electrolyte at ambient temperature. Apart from the fabrication of all-NASICON-based LIB, the construction of an asymmetric type $LiFePO_4$/$Li_{1.5}Al_{0.5}Ge_{1.5}(PO_4)_3$/$Li_3V_2(PO_4)_3$ cell has been demonstrated using the same SPS technique. However, in both cases, no extended cycleability was reported. A good cycleability with capacity retention of ≈89% was reported after 100 cycles by Mao et al.[315] for a $Li_3V_2(PO_4)_3$/$Li_3V_2(PO_4)_3$ symmetric cell with liquid electrolyte at the predicted operating potential of ≈2.25 V. Plashnitsa et al.[317] also investigated the performance of such $Li_3V_2(PO_4)_3$/$Li_3V_2(PO_4)_3$ symmetric cells in ionic liquid medium to improve the thermal stability of the cells. Very recently, Jian et al.[318] reported the possibility of using rhombohedral structured $Li_3V_2(PO_4)_3$ as possible insertion hosts for both high and low voltage regions. The half-cell displayed a single prominent flat working potential at ≈3.75 V *vs.* Li and variation in the charge discharge curves at lower potential (≈1.75 V vs. Li) was also observed. Although there was no extended cycleability reported for the symmetric $Li_3V_2(PO_4)_3$, a fade in capacity profile was noted for the given three cycles.

2.11. $LiVPO_4F$

Similar to the NASICON framework $Li_3V_2(PO_4)_3$, $LiVPO_4F$ is one of the promising ≈4.2 V *vs.* Li cathodes for LIB applications. Reversible insertion of one mole Li is possible by utilizing the $V^{3+/4+}$ redox couple for the high voltage region with corresponding theoretical capacity of ≈156 mAh g^{-1}.[223,320–324]

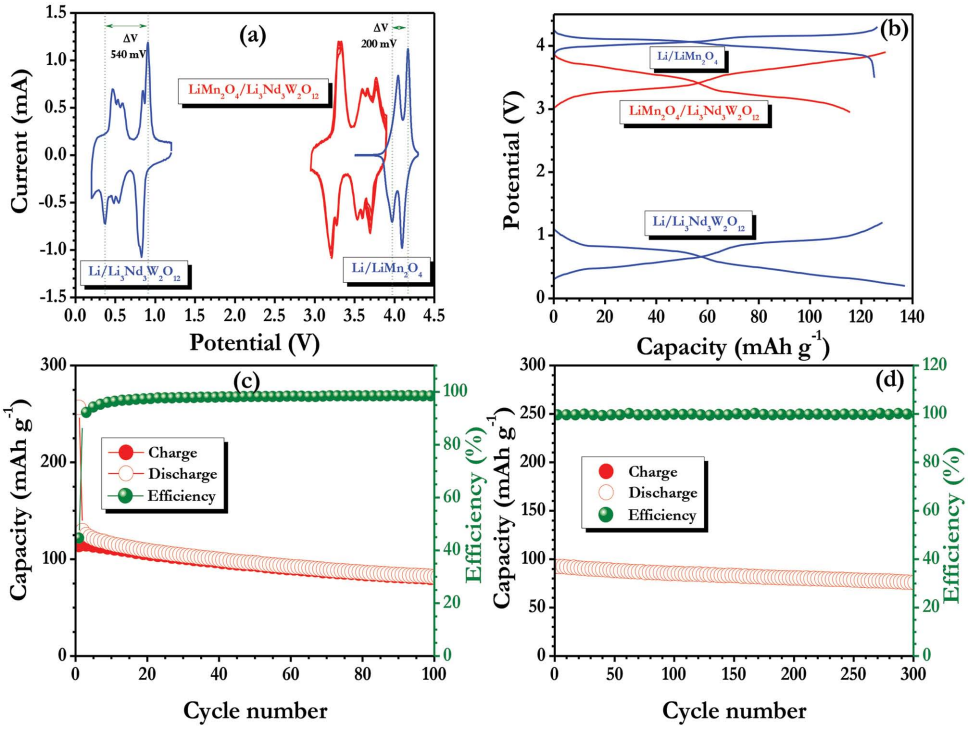

Figure 13. a) Cyclic voltammetric signatures of $LiMn_2O_4$/C-$Li_3Nd_3W_2O_{12}$ cell at slow scan rate of 0.1 mV s^{-1} between 2.95–3.9 V. For comparison, half-cell performances of cathode (Li/$LiMn_2O_4$) and anode (Li/C-$Li_3Nd_3W_3O_{12}$) are also given. b) Galvanostatic charge-discharge profiles of full-cell, $LiMn_2O_4$/C-$Li_3Nd_3W_2O_{12}$ at current density of 100 mA g^{-1} between 2.95–3.9 V. For comparison, half-cell performances of cathode (Li/$LiMn_2O_4$) and anode (Li/C-$Li_3Nd_3W_2O_{12}$) are also given under the same current density. c) Plot of capacity *vs.* cycle number at current density of 100 mA g^{-1} with coulombic efficiency. d) Cycling profiles at current density of 200 mA g^{-1} with coulombic efficiency. Reproduced with permission.[294] Copyright 2014, John Wiley & Sons.

Nevertheless, reversible insertion into tavorite-type $LiVPO_4F$ was also possible at ≈1.8 V vs. Li by using the $V^{3+/2+}$ redox couple.[322–325] Further, two-phase reaction mechanism was clearly evident in the in-situ X-ray diffraction (XRD) measurements at low voltage (≈1.8 V vs. Li) operation during the transition from $LiVPO_4F$ to Li_2VPO_4F.[325] Recently Ma et al.[323] demonstrated that during Li-insertion into $LiVPO_4F$ (174.337 $Å^3$) phase resulted in a huge unit cell variation of ≈53.42% (Li_2VPO_4F 374.231 $Å^3$). As a result, a dramatic fade in the cycling profiles was noted in the half-cell assembly. A similar fading was also demonstrated by Wang et al.[326] when the half-cell was operated at lower potential (≈1.8 V vs. Li). Interestingly, Barker et al.[324] demonstrated the fabrication of ≈2.4 V class Li-ion cells using $LiVPO_4F$ electrodes in a symmetric configuration ($LiVPO_4F$/$LiVPO_4F$). The cell delivered an initial reversible capacity of ≈126 mAh g^{-1} and retained ≈92% of initial capacity after 65 cycles (**Figure 16**). Contrary to Barker et al.[324], Plashnitsa et al.[327] observed the dramatic fading of such symmetric cells in conventional organic electrolytes because of the severe reactivity between $LiVPO_4F$ and acidic $LiPF_6$ based solution. The thermal stability of the $LiVPO_4F$ phase was excellent in the de-lithiated state and was similar to that of olivine type $LiFePO_4$.[328] Later, Plashnitsa et al.[327] attempted to use $LiBF_4$ in 1-ethyl-3-methylimidazolium tetrafluoroborate ($EMIBF_4$) ionic liquid as the electrolyte and the performance was found to be inferior under ambient conditions because of the higher viscosity of the solution. Nevertheless, a good cycleability was noted for $LiVPO_4F$/$LiVPO_4F$ symmetric cells irrespective of the applied current density at elevated conditions.

2.12. TiS_2

TiS_2 is the first insertion type dichalcogenide cathode discovered for the reversible intercalation of Li-ions in organic medium.[72,330,331] TiS_2 is made up of hexagonal close packed structure with $P\bar{3}m1$ space group and exhibits metallic conductivity. Therefore, the inclusion of conductive additive is unnecessary. Ti-ions are in octahedral sites between alternating sulfur sheets. TiS_2 sheets are stacked directly on top of one another by a van der Waals layer, resulting in the sulfur anion stacking sequence ABAB.[72] Because of this unique assembly, it can accommodate a wide range of guest species, in particular Na^+ and Mg^{2+} ions, in addition to Li^+ ions.[332,333] However, an important issue is the huge volume variation of ≈12% upon lithiation[333,334] and this is much higher than conventional intercalating materials such as anatase TiO_2, $LiCrTiO_4$, $Li_4Ti_5O_{12}$, etc.[36] High temperature preparation of TiS_2 leads to the presence of few Ti atoms in the van der Waals layer, which prevents the intercalation of Li. Hence, the dichalcogenide, TiS_2, must be prepared below 600 °C. Theoretically reversible insertion of one mole Li is feasible with a capacity of ≈239 mAh g^{-1}. Upon lithiation process, dichalcogenide, TiS_2 undergo single phase reaction (Li_xTiS_2).[72] TiS_2 primarily focused on the cathode point of

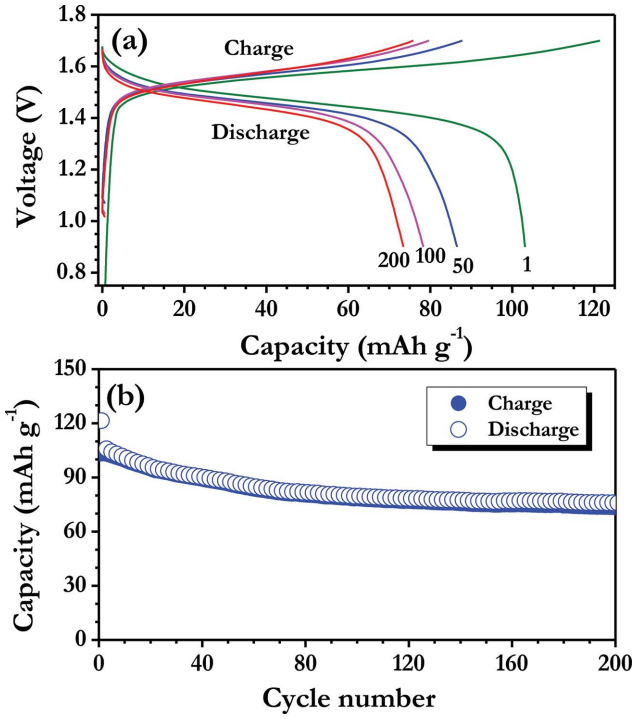

Figure 14. a) Galvanostatic charge-discharge curves of $LiMn_2O_4$/carbon coated-$LiTi_2(PO_4)_3$ cell cycled between 0.9–2.7 V at current density of 150 mA g^{-1} and b) cycling performance of above cell. The integers represent the cycle number. Reproduced with permission.[302] Copyright 2012, The Royal Society of Chemistry.

view, but the working potential is quite low compared to the conventional cathodes including $LiFePO_4$, $LiMn_2O_4$, $LiCoO_2$, and even $LiTi_2(PO_4)_3$ and TiP_2O_7.[38,335] Thus, few reports exist on the utilization of TiS_2 as an anode framework material for the construction of rocking-chair type Li-ion cells with $LiCoO_2$ cathodes. Plichta et al.[336] reported the fabrication of all solid-state Li-ion cells using $LiAlCl_4$ as the solid-electrolyte and $LiCoO_2$ as the cathode ($LiCoO_2/LiAlCl_4/TiS_2$) with a working potential of ≈1.8 V. The cell exhibited an initial reversibility of 0.4 mole Li and faded upon cycling up to 150 cycles at 100 °C. On the other hand, better electrochemical profiles are noted compared to solid-state configuration while employing 1.5 M $LiAsF_6$ in acetonitrile (AN) solution with long cycle life of 500 cycles.[337] Croce et al.[338,339] demonstrated the electrochemical activity of a $LiCoO_2/TiS_2$ cell towards composite polymer electrolyte ($(PEO)_8$-$LiClO_4$–10% γ-$LiAlO_2$) and gel polymer electrolytes (PAN-EC/PC-$LiClO_4$).

3. Conversion

Conversion is a reversible electrochemical reaction (often called a displacement reaction), where the transition metal comprising compound (MX_y, X = P, S, O, F, Cl etc.,) is destroyed electrochemically and subsequently reduced as a metal (M^o) during the process. Upon charging, the electrochemically reduced metallic nanoparticles is theoretically retained in its original state (MX_y), (Figure 1).[340] However, certain ternary oxides are exceptional and the complete reversibility into the parent material is not

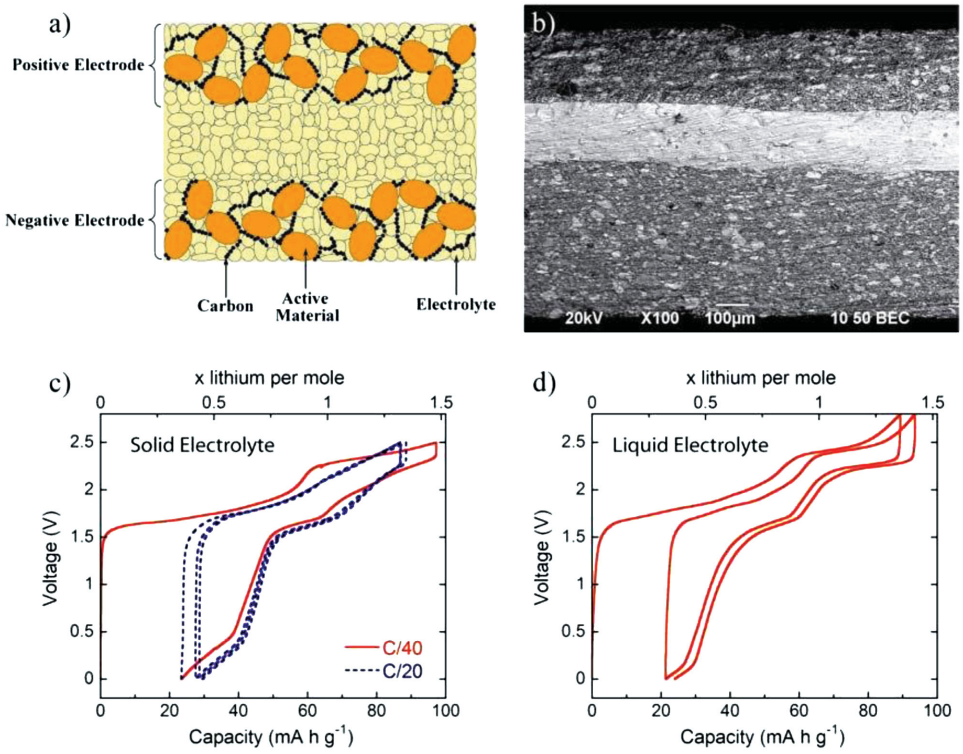

Figure 15. a) Scheme of an all-solid-state Li-ion battery. b) Cross section scanning electron microscopy image in composition mode of an all-solid-state battery prepared in one step by SPS. c) Galvanostatic charge/discharge curves for an all inorganic $Li_3V_2(PO_4)_3/Li_{1.5}Al_{0.5}Ge_{1.5}(PO_4)_3/Li_3V_2(PO_4)_3$ cell (obtained by SPS in one step) at C/40 rate (1 Li^+ in 40 h) and C/20 rate at 80 °C. d) Galvanostatic charge/discharge curves of a $Li_3V_2(PO_4)_3/Li_3V_2(PO_4)_3$ cell using a liquid electrolyte at C/10 rate at room temperature. Reproduced with permission.[314] Copyright 2011, John Wiley & Sons.

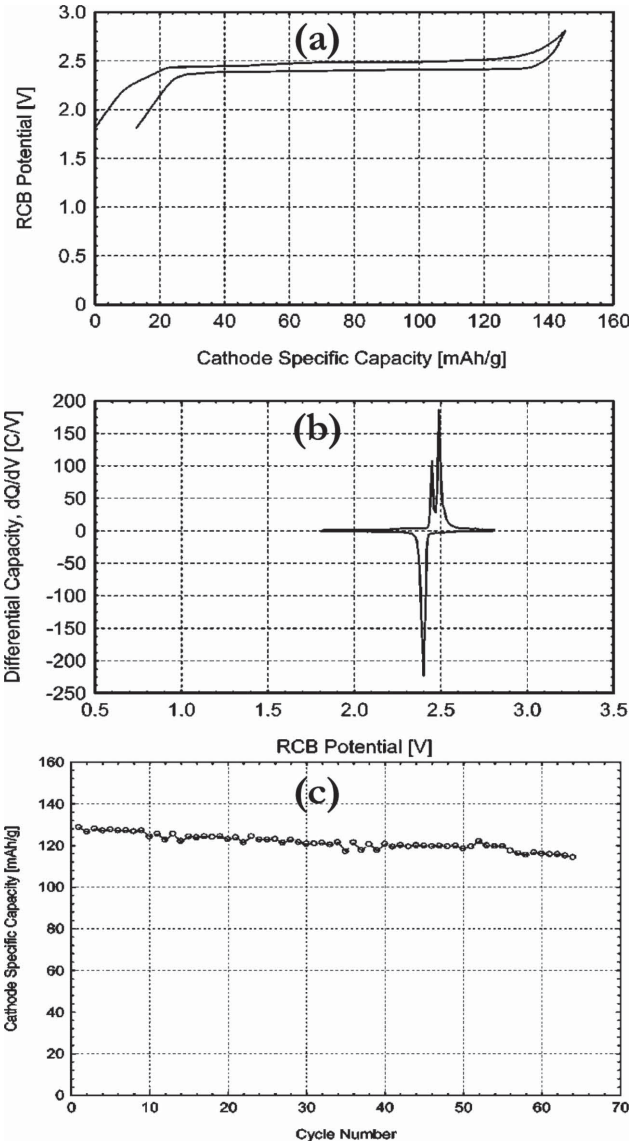

Figure 16. Electrochemical voltage Spectroscopy (EVS) data for a typical $LiVPO_4F/LiVPO_4F$ lithium-ion cell cycled between 1.80–2.80 V. The data shown were collected at 23 °C and are for the first cycle. The electrolyte comprised a 1 M $LiPF_6$ solution in EC/DMC (2:1 by weight). a) EVS voltage profile and b) EVS differential capacity profile. c) Lifetime cycling of representative $LiVPO_4F/LiVPO_4F$ lithium- ion cells cycled between 1.80–2.80 V at a C/5 rate for charge and discharge. The data shown were collected at 23°. Reproduced with permission.[324] Copyright 2005, The Electrochemical Society.

possible; for example in $FeCo_2O_4$, reduction of Fe^o and Co^o is noted upon discharge, whereas FeO and Co_3O_4 only formed while in charge and subsequent cycles as well.[22,23,341] The overall conversion mechanism for the various compounds is represented according to the following equilibrium,

$$M_xP_y + 3ye^- + 3yLi^+ \leftrightarrow xM^o + yLi_3P, \text{ where } M = Ni, Co, Fe, etc.$$
$$M_xS_y + 2ye^- + 2yLi^+ \leftrightarrow xM^o + yLi_2S$$
$$M_xO_y + 2ye^- + 2yLi^+ \leftrightarrow xM^o + yLi_2O$$
$$M_xCl_y + ye^- + yLi^+ \leftrightarrow xM^o + yLiCl$$
$$M_xF_y + ye^- + yLi^+ \leftrightarrow xM^o + yLiF$$

Because of the multiple electron reactions, such conversion type electrodes are able to deliver higher reversible capacity than insertion type materials, including graphite. Similar to graphitic anodes, unavoidable electrolyte decomposition occurs in the first cycle. The decomposition leads to the formation of a SEI layer over the active particle surfaces, which are predominantly composed of insoluble inorganic by products, polymeric films, etc. As a result, a huge irreversible capacity loss in the first cycle is noted compared to graphite. In contrast, the SEI layer formed over conversion anodes is entirely different than graphitic anodes. Large volume variation, higher redox potential, and poor cycleability are other important issues for this type of anode. Polarization of the conversion electrodes is also not to be ruled out. However, carbon coating or forming composites with carbonaceous material/passive elements is proposed to sustain the volume variation and subsequently improve the stability upon cycling. Pre-treating (pre-lithiation) the electrode is one of the efficient approaches to tackle the irreversible capacity loss (ICL) issue, but it involves either use of three-electrode configurations[342] or two-step cell fabrication processes. Recently, Tarascon and co-workers[343] reported the use of "sacrificial-salts" to compensate for the ICL; examples include Li salts of azide, oxocarbons, di-carboxylates, and hydrazides. Anions present in these salts will lose electrons in the first charge with emission of N_2, CO, or CO_2 in the acceptable range of 3–4.5 V vs. Li. As expected, the redox potential of the conversion anodes can be varied from 3d-metal to metal and tailored according to the desired energy density. Indeed, conversion anodes certainly have several advantages over insertion type anodes, and overcoming the mentioned setbacks during the fabrication of the Li-ion cells is a big challenge.[344] Therefore, little work has been reported for such anodes in the full-cell assembly and this is described in the following sections.

3.1. Fe_2O_3

A hematite phase, α-Fe_2O_3 nanostructure has been extensively investigated as the anode material for LIB applications with various morphological features. The α-Fe_2O_3 has a theoretical capacity of ≈1008 mAh g^{-1} for six electron reaction according to the following equilibrium, $Fe_2O_3 + 6Li^+ + 6e^- \leftrightarrow Fe^0 + 3Li_2O$.[345–347] Although the hematite phase shows the favorable advantages such as low cost and eco-friendliness, it has poor electrochemical profiles in the half-cell assembly because of its inherent electrical conductivity. Therefore, several attempts, including carbon coating and making composites with carbonaceous materials, have been performed to improve the electrochemical activity. Apart from the intrinsic properties, the testing potential also plays a vital role in the electrochemical stability. Hassoun et al.[342] first reported the fabrication of a Li-iron battery using the bulk hematite phase as the anode and $LiFePO_4$ as the cathode (**Figure 17**). As expected in the half-cell assembly, very poor cycling profiles were noted for the conventional range (0.3–3 V vs. Li) and, hence, the capacity was limited to 300 mAh g^{-1} (0.3–1.8 V vs. Li) to sustain stability. Both electrodes were pre-treated before conducting the full-cell assembly using reference electrode Li; likewise $LiFePO_4$ was charged (Li_0FePO_4) and α-Fe_2O_3 anode was discharged ($Fe^0 + 3Li_2O$) to

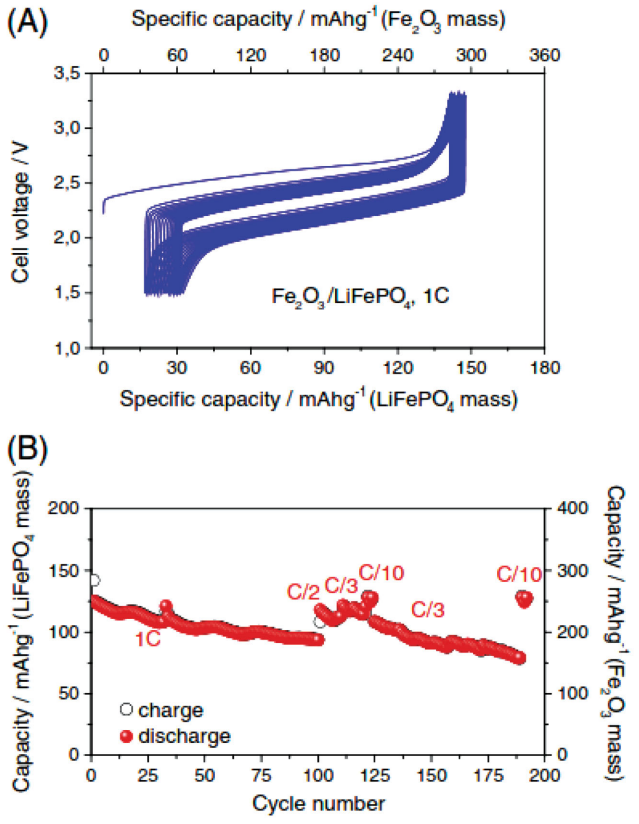

Figure 17. A) Voltage *vs.* specific capacity at 1C rate and B) specific capacity *vs.* cycle number at different c-rates profiles of the Fe_2O_3/$LiFePO_4$ lithium ion battery, where 1 C = 170 mA g^{-1} is referred to the cathode mass. EC:DMC, $LiPF_6$ electrolyte. Room temperature. Reproduced with permission.[342] Copyright 2011, Elsevier.

overcome the ICL issue in the $LiFePO_4$/α-Fe_2O_3 configuration. The cell had good cycleability and high current performance for the investigated 190 cycles. However, much worse electrochemical profiles were noted while paring with a $LiFePO_4$ cathode and porous α-Fe_2O_3 nanosheet anode i.e., without any pre-treatment.[348] Mesoporous α-Fe_2O_3-graphene composite was also explored as a possible anode for LIB applications.[349] It is unfortunate that the cell exhibited inferior cycleability in the full-cell configuration with both spinel $LiMn_2O_4$ or layered $LiCoO_2$ cathodes. Among the worst performances, spinel $LiMn_2O_4$ was observed to have better compatibility than layered counterpart in terms of reversibility and cycleability. In addition, >34% of ICL was noted in the first cycle because of the presence of graphene nanosheets, which undergo huge ICL in first cycle. Hariharan et al.[350] reported the electrochemical activity of the template synthesized α-Fe_2O_3 with an olivine phase $LiMn_{0.8}Fe_{0.2}PO_4$ cathode. There were no efforts taken to circumvent the ICL, as the authors mentioned very little irreversible capacity only noted in half-cell assembly, i.e., coloumbic efficiency was found to be ≈90% in the first cycle. The full-cell $LiMn_{0.8}Fe_{0.2}PO_4$/α-Fe_2O_3 had a reasonable reversibility of ≈83 mAh g^{-1} (based on cathode loading) over 30 cycles with a working potential of ≈2.3 V. This study also showed the influence of electrode heat treatment on half-cell assembly, but not on the full-cell. Maghemite phase (γ-Fe_2O_3) was also explored as a possible anode material for the fabrication of high power LIBs with graphene composites.[351] The pre-treatment was carried out by placing the γ-Fe_2O_3 electrode in contact with a Li foil soaked in LiBOB solution. The pre-treated electrode in the full-cell, $LiFePO_4$/γ-Fe_2O_3 with LiBOB-based electrolyte, showed an initial reversible capacity of ≈130 mAh g^{-1} (based on cathode mass) in both pure and graphene composites. The presence of graphene nanosheets was certainly beneficial for the retention of capacity upon cycling and in high current testing compared to native maghemite phase.

3.2. Fe_3O_4

The magnetite phase showed much better electrical conductivity than its counterpart hematite phase because of the electron exchange between the Fe^{2+} and Fe^{3+} centers. The magnetite phase is a perfect example of the inverse spinel structure with cubic close packed array of ions, where half of the octahedral sites are filled by all the Fe^{2+} ions and Fe^{3+} ions occupy the remaining octahedral and tetrahedral sites. It is interesting to note that, both magnetite and maghemite phases exhibit very similar XRD patterns and, therefore, careful analysis must be performed to distinguish between the phases. The magnetite phase exhibits the theoretical capacity of ≈926 mAh g^{-1} for eight electron reaction according to the following equilibrium, $Fe_3O_4 + 8Li^+ + 8e^- \leftrightarrow Fe^0 + 4Li_2O$.[352] Ji et al.[353] first demonstrated the performance of the Fe_3O_4-graphene composite as a conversion anode with layered type $LiNi_{1/3}Mn_{1/3}Co_{1/3}O_2$ as the cathode. No pre-treatment was used for the anode, so $LiNi_{1/3}Mn_{1/3}Co_{1/3}O_2$/$Fe_3O_4$-graphene cell experienced the ICL of ≈38% in the first cycle. This huge ICL certainly affected the cell performance and it displayed a reversible capacity of ≈85 mAh g^{-1} (based on cathode mass) at 0.1 C with a capacity retention of ≈90.3% after 10 cycles. Excellent long-term cycling profiles (over 100% retention after 600 cycles) of carbon encapsulated 3D hierarchical Fe_3O_4 spheres were reported in the half-cell assembly by Fan et al.[354] Unusually, ≈58% irreversibility was observed for such spheres when coupled with a $LiMn_2O_4$ cathode. The $LiMn_2O_4$/Fe_3O_4 cell exhibits a lack of irreversibility in the first cycle, but it retains the initial reversible capacity of ≈800 mAh g^{-1} after 50 cycles. CF_x modified Fe_3O_4 nanoparticles were reported with excellent cycleability of over 100 cycles in the half-cell assembly and they were subsequently fabricated with a full-cell with high-voltage $LiNi_{0.5}Mn_{1.5}O_4$ cathodes.[355] A reversible capacity of ≈111 mAh g^{-1} (based on cathode mass) was observed at a current density of 100 mA g^{-1} and it retained ≈67% of capacity retention after 300 cycles. In addition, elevated temperature (45 °C) performance was also evaluated with inferior columbic efficiency and reported. Recently, Ming et al.[356] extensively investigated the fabrication and electrochemical profiles of porous carbon-Fe_3O_4 composite with a layered $LiNi_{0.59}Co_{0.16}Mn_{0.25}O_2$ cathode (**Figure 18**). In the full-cell assembly, both chemically and electrochemically treated porous carbon-Fe_3O_4 composite showed exceptional electrochemical profiles when paired with the cathode. The $LiNi_{0.59}Co_{0.16}Mn_{0.25}O_2$/porous carbon-$Fe_3O_4$ cell had ≈64 and ≈58% of the initial capacity after 1000 cycles for the chemically and electrochemically lithiated anodes, respectively. A maximum energy density of ≈483 Wh kg^{-1} was

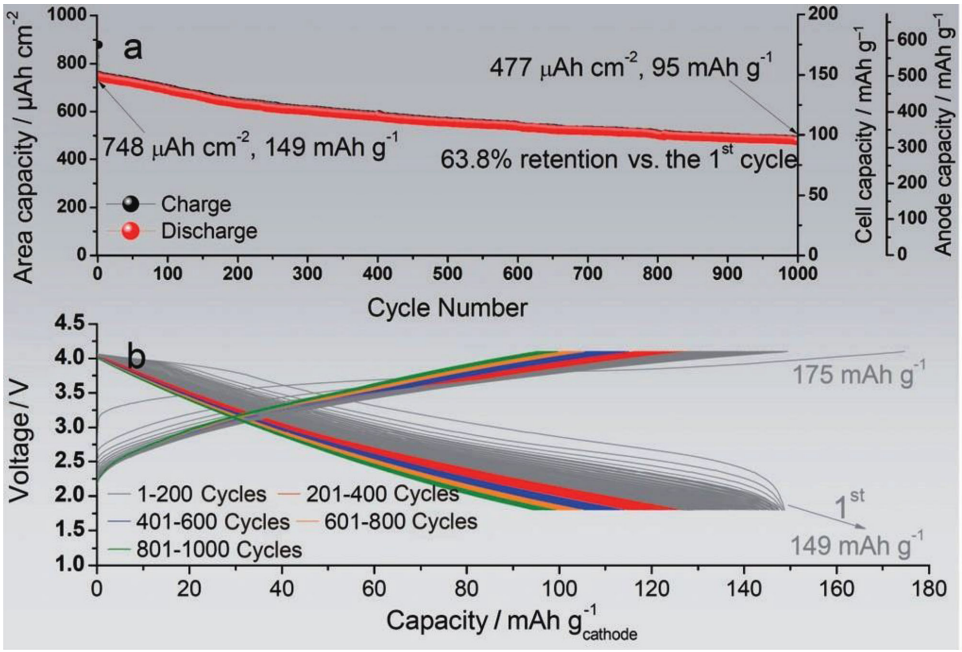

Figure 18. a) Area capacity and capacity for the full-cell of lithiated porous carbon–Fe_3O_4 (30 g cm^{-2}/15 min)/$LiNi_{0.59}Co_{0.16}Mn_{0.25}O_2$ in the cycling test. b) Charge–discharge curves over the initial 1000 cycles. Reproduced with permission.[356] Copyright 2014, John Wiley & Sons.

achieved for this configuration. This clearly indicates that, no matter what kind of lithiation procedure is used to overcome the ICL while fabricating the cell with cathodes.

3.3. CuO

CuO is a very important p-type semiconductor with a band gap of 1.2 eV and has been extensively studied for multifarious applications such as catalysts, gas sensors, photoconductive/photochemical cells, and other electronic devices. Furthermore, CuO can also be used as a promising anode for LIB applications via conversion pathways, with a theoretical capacity of ≈674 mAh g^{-1} for two electron reaction ($CuO + 2Li^+ + 2e^- \leftrightarrow Cu^0 + Li_2O$).[22,340,357–360] CuO belongs to the monoclinic crystal structure with space group of *C2/c*. Verrelli et al.[361] first reported the performance of a CuO-MCMB (1:1 ratio) composite anode with a high voltage $LiNi_{0.5}Mn_{1.5}O_4$ cathode. Before fabricating the $LiNi_{0.5}Mn_{1.5}O_4$/CuO-MCMB cell, the anode was pre-treated/cycled in half-cell configuration (Li/CuO-MCMB) to overcome the ICL issue. On the other hand, the ICL observed when paired with high voltage cathodes cannot be ruled out in full-cell assembly. The $LiNi_{0.5}Mn_{1.5}O_4$/CuO-MCMB cell displayed excellent electrochemical profiles in terms of higher operating potential (≈4 V) and cycleability (no fade was observed for 100 cycles). Even under harsh conditions (5 C where 1 C = 148 mA g^{-1}), the full-cell as capable of delivering a reversible capacity over 100 mAh g^{-1} (based on cathode mass loading). The same group of authors reported the performance of CuO-MCMB composite anodes with spinel $Li_{0.85}Ni_{0.46}Cu_{0.1}Mn_{1.49}O_4$ cathodes in the presence of 1 M $LiPF_6$ in PC solution rather than conventional 1 M $LiPF_6$ in EC:DMC.[362] As expected, the $Li_{0.85}Ni_{0.46}Cu_{0.1}Mn_{1.49}O_4$/CuO-MCMB cell delivered good cycleability and reversibility at ≈3.6 V (**Figure 19**). Zhang et al.[363] reported the performance of CuO grown over Cu foil as an anode with a high voltage $LiNi_{0.5}Mn_{1.5}O_4$ cathode without any pre-lithiation process in the NL configuration. Good cycleability (≈84% capacity retention after 100 cycles at current density of 337 mA g^{-1}) was observed with initial reversible capacity of ≈516 mAh g^{-1}.

3.4. MnO

It is well known that Mn-based materials are attractive as electrode materials for LIB applications by virtue of their abundance, low cost, and eco-friendliness.[364] The binary metal oxide, MnO, undergoes a metallic reduction (Mn^0) according to the conversion reaction mechanism $MnO + 2Li + 2e^- \leftrightarrow Mn^0 + Li_2O$, with a corresponding theoretical capacity of ≈756 mAh g^{-1}. In addition, MnO has much lower redox potential ≈0.5 V vs. Li than rest of the binary and ternary metal oxide that have been investigated for LIB applications.[22] The lower redox potential and higher theoretical capacity are certainly beneficial for the development of high energy density Li-ion power packs. However, inherent electronic conductivity and large volume variation during the conversion reaction are the main issues for these materials. Therefore, either carbon coating or making composites with MnO were attempted to overcome the issues and thereby improve the electrochemical activity. Chae et al.[365] first reported the fabrication of a full-cell assembly with a MnO_x-C composites as anode and $LiMn_2O_4$ as the cathode. Prior to the full-cell assembly, the MnO_x-C composite was pre-treated with Li to overcome the ICL observed in first cycle. The $LiMn_2O_4$/MnO_x-C cell delivered a reversible capacity of ≈105 mAh g^{-1} (with respect to cathode mass loading) at

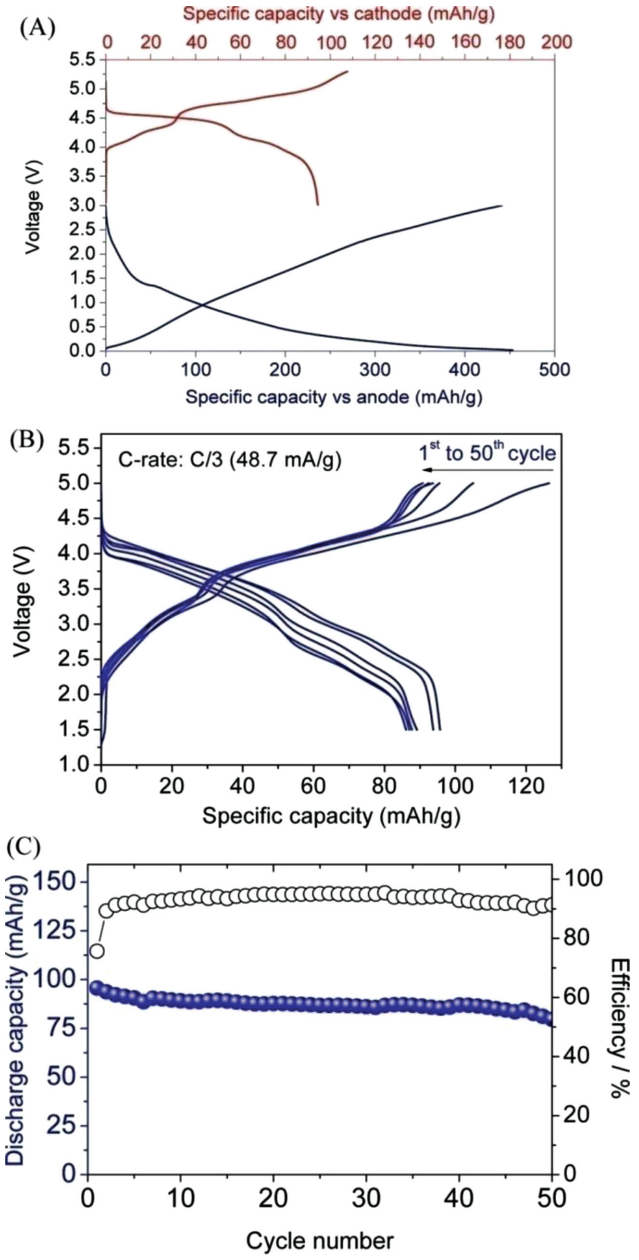

Figure 19. Typical charge–discharge voltage profiles of the $Li_{0.85}Ni_{0.46}Cu_{0.1}Mn_{1.49}O_4$ cathode and of the CuO–MCMB anode (A), response of the CuO–MCMB/1 M $LiPF_6PC/Li_{0.85}Ni_{0.46}Cu_{0.1}Mn_{1.49}O_4$ lithium ion cell in terms of voltage profiles (B), and capacity versus cycle number at C/3 rate (C). Reproduced with permission.[362] Copyright 2014, American Chemical Society.

0.2 C rate with a working potential and energy density of ≈3.5 V and 350 Wh kg^{-1}, respectively. Furthermore, excellent cycleability was observed for $LiMn_2O_4/MnO_x$-C cells for about 195 cycles without any significant fade (**Figure 20**). Olive-shaped MnO nanostructures were prepared by the decomposition of $MnCO_3$ in Ar atmosphere and they were subsequently paired with high voltage $LiNi_{0.5}Mn_{1.5}O_{4-\delta}$ cathodes.[366] The full-cell $LiNi_{0.5}Mn_{1.5}O_{4-\delta}$/MnO delivered a maximum energy density of ≈390 Wh kg^{-1} at 0.1 C (1 C = 148 mA g^{-1}) and showed excellent cycleability for the investigated 300 cycles without noticeable fade upon cycling.

3.5. Mn_2O_3

Similar to MnO, Mn_2O_3 also showed a lower operating potential vs. Li with a theoretical capacity of ≈1018 mAh g^{-1} for six electron reaction. Metallic reduction (Mn^0) is also possible for the Mn (III) oxide according to the multi-step reaction described by Fang et al.[367] as follows:

$$3Mn_2O_3 + 2Li + 2e^- \rightarrow 2Mn_3O_4 + Li_2O$$

$$Mn_3O_4 + Li + e^- \rightarrow LiMn_3O_4$$

$$LiMn_3O_4 + Li + e^- \rightarrow 3MnO + Li_2O$$

$$MnO + 2Li + 2e^- \leftrightarrow Mn^0 + Li_2O$$

Several works have been reported for this material, however a huge ICL, i.e., over 50% loss in first cycle, is the main issue for this Mn_2O_3 via the conversion pathway, irrespective of the synthesis procedures and morphology.[364] It is noteworthy that various Mn-based binary oxides (MnO, Mn_2O_3, and Mn_3O_4) have been evaluated as conversion type anodes, but the cycleable redox reaction were found in MnO and its reactivity is only with Li ($MnO + 2Li^+ + 2e^- \leftrightarrow Mn^0 + Li_2O$).[367]. Wang et al.[368] reported the synthesis of Mn_2O_3 nanowires using a two-step hydrothermal approach,followed by a solid-state reaction. In the half-cell assembly, Mn_2O_3 nanowires displayed an initial reversible capacity of 502 mA h g^{-1} at a current density of 100 mA g^{-1}. Prior to the full-cell fabrication, the Mn_2O_3 was cycled for three cycles in the half-cell assembly to avoid the ICL. $LiMn_2O_4/Mn_2O_3$ cell delivered the discharge capacity of ≈99 mAh g^{-1} with an operating potential of ≈3 V. Furthermore, a good cycling profile was evident for 40 cycles in both flat and folded pouch cells (**Figure 21**).

3.6. CoO and Co_3O_4

Co-based materials are one of the important materials of interest for LIBs and include the layered cathode, $LiCoO_2$.[15] Although favorable electrochemical properties are noted for the Co-based compounds, toxicity and high cost cannot be ruled out. Co-based binary metal oxide, CoO, is one of the widely investigated anode materials for LIB applications that showed a theoretical capacity of ≈715 mAh g^{-1} for two electron reactions and is composed of a rock salt type structure. The conversion mechanism can be described as follows

$$CoO + 2Li + 2e^- \leftrightarrow Co^0 + Li_2O$$

Tarascon and co-workers [369,370] first reported the fabrication of CoO anode based cells with either layered $LiCoO_2$ or spinel $Li_{1+x}Mn_2O_4$ cathodes. Interestingly the CoO electrodes exhibited

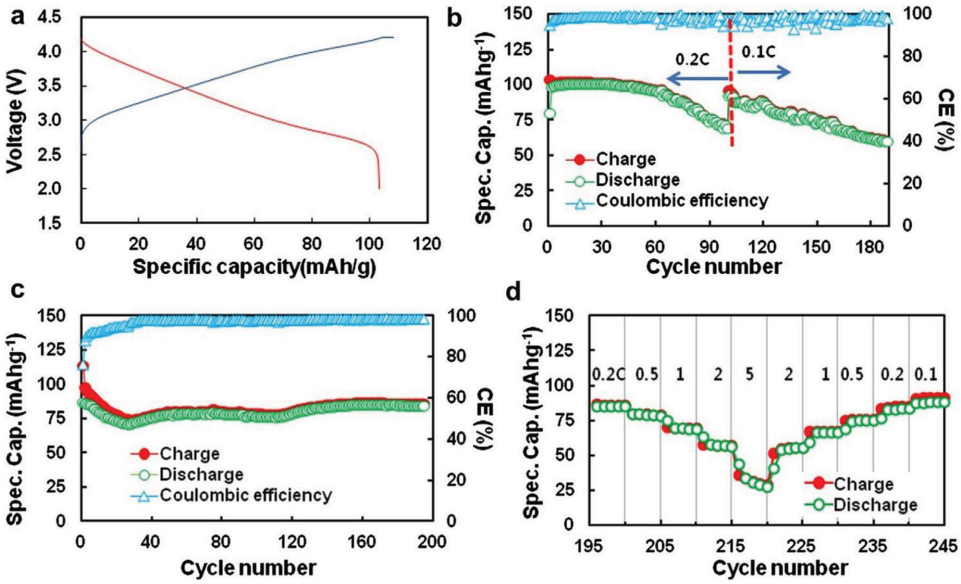

Figure 20. a) Voltage profile, b) cycling performance of LMn_2O_4/MnO_x–C (A) cell at 0.2 C for 100 cycles and then at 0.1 C for up to 188 cycles, c) cycling performance of LMn_2O_4/MnO_x–C (B) cell at 0.2 C for up to 195 cycle, and d) rate performance of LMn_2O_4/MnO_x–C (B) cell. Voltage cut-off range is between 2.0 and 4.1 V. Reproduced with permission.[365] Copyright 2013, Elsevier.

much higher reversible capacity than the theoretical limitations in half-cell assembly, which was widely accepted because of the contribution from interfacial storage. A maximum reversible capacity of ≈950 mAh g^{-1} was reported for the Li/CoO cell. Except in the first cycle, the $LiCoO_2$/CoO cell displayed excellent cycleability for 80 cycles with a working potential of ≈2 V. 100% reversibility was noted for first 50 cycles and thereafter fading was observed, which was a replica of the half-cell performance of CoO. Here, the main issue was the excess loading of $LiCoO_2$, which simultaneously diluted the energy density of the LIB. Thus, the authors attempted to avoid such excess loading by using a Li-rich spinel $Li_{1.3}Mn_2O_4$ cathode and the presence of excess Li in ≈3 V vs. Li region was expected to compensate the ICL. Accordingly, the CoO/$Li_{1.3}Mn_2O_4$ assembly displayed much better performance than the normal spinel (CoO/$LiMn_2O_4$) configuration in the view of reversibility, for instance, a reversible capacity of ≈110 and ≈90 mAh g^{-1} (based on cathode mass loading) was observed for the former and latter configurations, respectively. Except in the first cycle, the Li-rich spinel cathode acted as the normal spinel in the subsequent cycles. However, coupling of CoO anode with $LiCoO_2$ or $Li_{1+x}Mn_2O_4$ cathode resulted in a working potential of more or less 2 V (**Figure 22**).

Cobalt (II, III) oxide ($CoO.Co_2O_3$) is a perfect example for normal spinel structure, where Co^{2+} ions occupy the tetrahedral sites and octahedral sites are filled with Co^{3+} ions. The spinel Co_3O_4 has been extensively investigated for the LIB anode point of view because of its easy synthesis procedure and high reversible capacity.[340,371] Similar to CoO, Co_3O_4 also undergoes the redox reaction for the eight electron reaction with a corresponding theoretical capacity of ≈890 mAh g^{-1} according to the following mechanism

$$Co_3O_4 + 8Li + 8e^- \leftrightarrow Co^0 + 4Li_2O$$

The Tarascon and co-workers[370] first reported the performance of Co_3O_4 in a full-cell assembly with layered type $LiCoO_2$. In the half-cell assembly, the anode was capable of delivering a reversible capacity of >900 mAh g^{-1} irrespective of both ambient and elevated temperature (55 °C) conditions. An excess loading of $LiCoO_2$ was used in order to overcome the ICL issues. Therefore, based on the electrochemical profiles of individual electrodes, the mass ratio between the anode and cathode was adjusted to 1:8.4. The full-cell $LiCoO_2/Co_3O_4$ was capable of delivering the reversible capacity of ≈120 mAh g^{-1} (with respect to cathode loading) at a 0.2 C rate under ambient conditions with a working potential of 2 V. The same capacity profiles were observed under elevated conditions with different current densities (0.1 C and 0.2 C). The cycling trend of $LiCoO_2/Co_3O_4$ cell was a replica of the performance of Co_3O_4 in the half-cell assembly (Li/Co_3O_4).

3.7. FeS

Sulfide based electrode materials have an advantage over oxide based materials for LIB applications in terms of safety. Similar to binary and ternary metal oxides, research has been reported on the possibilities of using them in LIB applications.[330,372] Transition metal monosulfides (MS, where M = Ti, V, Cr, Fe, Co, and Ni) are found impressive because of their favorable electrochemical properties. The mentioned monosulfides undergo a displacement reaction (except TiS) according to the following equilibrium, $MS + Li^+ + e^- \leftrightarrow M^0 + Li_2S$. The conversion reaction for TiS occurs at negative Fermi energy of the Li. However, the metal formation of V^0 and Ti^0 via conversion reaction is still a debate. It is interesting to note that for metal monosulfides, an increase in the atomic number results in the increase in redox potential. FeS is found to be more interesting because of its very flat operating potential (≈1.4 V vs. Li), high theoretical

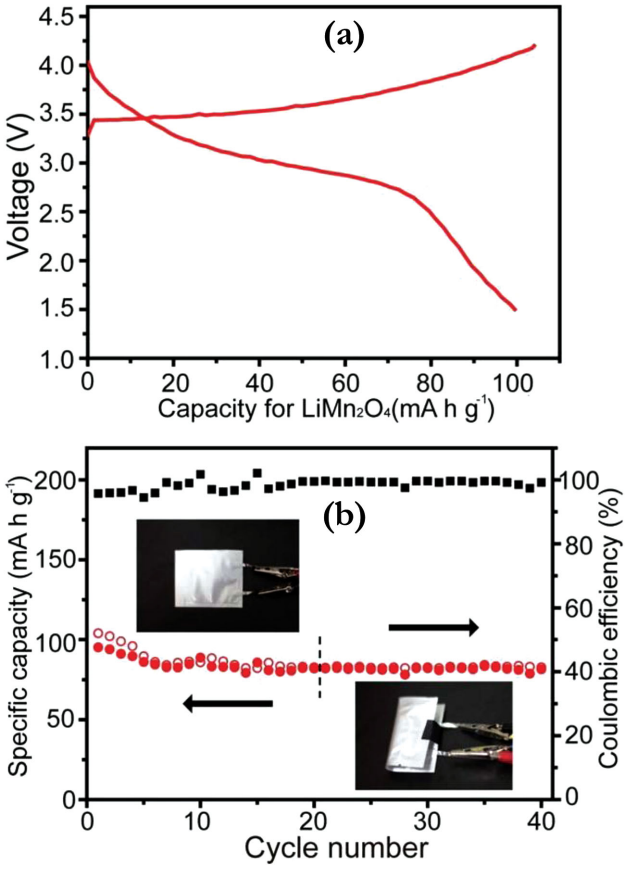

Figure 21. a) Charge-discharge curves of a flexible Mn_2O_3/$LiMn_2O_4$ LIB full-cell at the first cycle. b) Cycling performance (red curve) and Coulombic efficiency (black curve) of a representative flexible Mn_2O_3/$LiMn_2O_4$ full cell. The cell is fully extended in the first 20 cycles and folded from the 21st to 40 cycles, as optical images and the black arrows are shown in the insets. Reproduced with permission.[368] Copyright 2014, American Chemical Society.

capacity (≈610 mAh g^{-1}) and eco-friendliness.[373] The higher redox potential certainly avoids the electrolyte decomposition, which results in less ICL for during the displacement reaction (no need for deep cycling). In addition, the observed redox potential for FeS is found to be much lower (≈0.15 V vs. Li) than the well-established insertion type $Li_4Ti_5O_{12}$ with high reversibility. However, the electrochemical stability of FeS is another issue upon cycling. The deep cycling not only results in the higher ICL, it also leads to the disappearance of the prominent ≈1.4 V *vs.* V plateau. Wang et al.[374] reported the synthesis of FeS nanostructures by a hydrothermal approach with and without TiO_2 modification.No prominent flat potentials are noted, but the TiO_2 modified FeS showed a reversible capacity of ≈430 mAh g^{-1} after 500 cycles. The Li-ion cells were fabricated with a $LiMn_2O_4$ cathode. A high ICL of ≈125 mAh g^{-1} was observed at a current density of 100 mA g^{-1} under ambient temperature conditions in $LiMn_2O_4$/TiO_2-FeS cell. The test cell delivered a reversible capacity of ≈350 mAh g^{-1} (at 100 mA g^{-1}) and was capable of delivering >150 mAh g^{-1} at a current density of 1500 mA g^{-1}.

3.8. MoS_2

MoS_2 is a layered structured dichalcogenide that shows similar appearance to that of a conventional graphitic anode. MoS_2 is a diamagnetic semiconductor with an indirect band gap of 1.2 eV. Initially, similar to TiS_2, MoS_2 was also investigated as insertion electrode for LIB applications with an insertion potential and theoretical capacity of ≈1.1 V vs. Li and ≈167 mAh g^{-1}, respectively.[330,375,376] The insertion reaction is highly reversible and the mechanism can be schematically represented as follows

$$MoS_2 + xLi^+ + xe^- \leftrightarrow Li_xMoS_2$$

The reversible capacity and flat operating potential was found to be inferior to TiS_2, and therefore less research activity was carried out for this material. The conversion mechanism has been successfully used for the metal oxides and the same strategy has been extended for sulfides as well. Among the sulfides investigated, MoS_2 is appealing because of its high theoretical capacity (≈670 mAh g^{-1}) for four electron reaction during deep cycling according to the following mechanisms

$$MoS_2 + xLi^+ + xe^- \rightarrow Li_xMoS_2$$

$$Li_xMoS_2 + (4-x)Li^+ + (4-x)e^- \rightarrow Mo^0 + 2Li_2S$$

$$Mo^0 + 2Li_2S \leftrightarrow MoS_2 + 4Li^+ + 4e^-$$

Interestingly, a very small ICL was only observed for the case of MoS_2 compared to metal oxides in the half-cell assembly. Similar to oxides, MoS_2 also suffers a lack of cycleability because of the volume variation upon redox reaction. Therefore, most of the work has been reported with carbonaceous materials in the half-cell assembly and this has been clearly described in recent review by Stephenson et al.[375] In addition, a much higher reversible capacity than theoretical capacity was reported by the researchers, with speculation that the excess capacity was obtained from the interfacial storage. Hwang et al.[377] synthesized disordered graphene-like MoS_2 nanoplates using a hydrothermal approach and delivered a reversible capacity of 917 mAh g^{-1} in the first cycle with a coloumbic efficiency of 87% in a half-cell assembly. Furthermore, ≈98% capacity was retained after 50 cycles at a current density of 1062 mA g^{-1}. Full-cell $LiCoO_2$/MoS_2 was fabricated with a layered type $LiCoO_2$ cathode and the electrochemical performance at a high current rate of 1062 mA g^{-1} was investigated. The cell delivered an initial reversible capacity of 114 mAh g^{-1} with retention of ≈89% capacity after 60 cycles (**Figure 23**). MoS_2 nanoflakes grown over carbon cloth were also reported by Yu et al.[378] and appreciable areal capacity was noted for such a composite. The full-cell $LiCoO_2$/MoS_2 over carbon cloth was also demonstrated to power light-emitting diodes (LEDs).

4. Alloying and De-Alloying

Simply, an alloy is described as a mixture of two or more elements. In LIBs, such alloying reactions are feasible in reversible

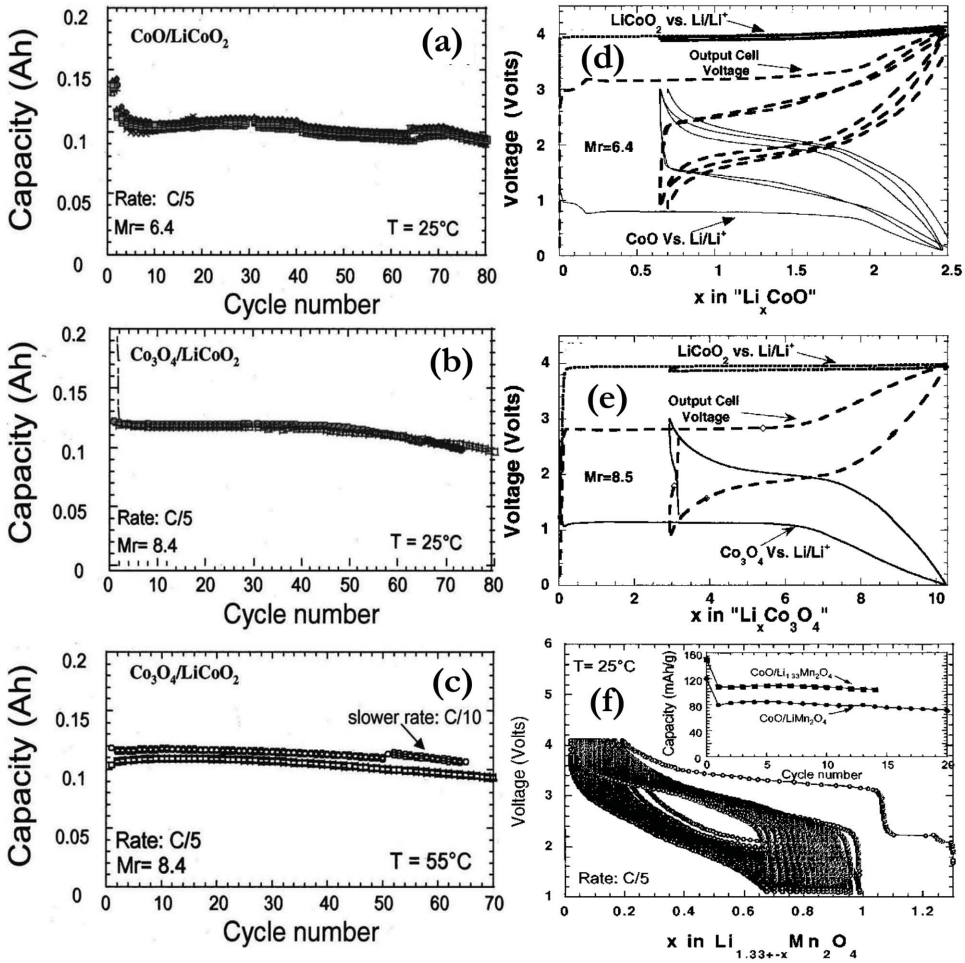

Figure 22. Capacity retention at room temperature for a) a plastic $CoO/LiCoO_2$ Li-ion cells (Mass ratio, Mr = 6.4) and b) for a plastic $Co_3O_4/LiCoO_2$ Li-ion cell assembled at a Mr value of 8.4. The 55 °C capacity retention for this $Co_3O_4/LiCoO_2$ ion cell is shown in (c). The cells were cycled at a C/5 rate between 0.9 and 4.1 V. To stress the reproducibility of the experiments the data for 4 and 2 different cells has been reported in (a–c), respectively. Two – and three-electrode potential data for $CoO/LiCoO_2$ (curve d) and $Co_3O_4/LiCoO_2$ (e) cells balanced at Mr ratios of 6.4 and 8.5, respectively. Note a 2 V cell output voltage and the large irreversible capacity during the first cycle. The cycling was done at a C/5 rate. f) Voltage vs. composition profile for a $CoO/LiMn_2O_4$ Li-ion cell demonstrating the possible use of $Li_{1.33}Mn_2O_4$ as a Li reservoir. The capacity at a 3 V plateau is used to compensate for the first cycle irreversibility observed with CoO. The inset shows the capacity retention for this cell and illustrates the beneficial effect of using the Li reservoir on cell capacity as compared to $CoO/LiMn_2O_4$ Li-ion cells. Reproduced with permission.[370] Copyright 2002, The Electrochemical Society.

manner for wide range of semi-metal or metallic compounds (or elements) in the presence of aprotic organic solvents.[379] The spontaneously formed alloys during electrochemical reaction with metallic Li are same as those of metallurgically prepared ones and few exceptional cases also exist, for example $Li_{15}Si_4$.[21,379,380] Numerous original and review articles have described the potential importance of such anodes and their necessity for the development for high energy LIB applications.[3,22,24,380–396]. Moreover, Sony (Sn-Co-Ti-C) and Panasonic (Si) companies have already commercialized such alloy-based anodes in high power Li-ion packs for consumer applications. The reason behind the research activities on such alloy-based anodes are their high theoretical capacity and lower working potential (except graphite) compared to the insertion and displacement type anodes, especially for group IV elements (Si, Ge, Pb and Sn).[397] Several binary and ternary metal oxides, including ZnO, SnO_x, Sb_2O_3, $ZnFe_2O_4$ etc., also undergo conversion reactions upon charge-discharge processes, in addition to the alloying reaction at a lower working potential. As a result, the theoretical capacity has been elevated compared to pure metals. On the other hand, the main issue for such anodes is associated with their huge volume variation upon lithiation and de-lithiation, in addition to the very high ICL observed in first cycle. This severely affects the electrochemical profiles of such anodes and also cracks and detaches the active particles (i.e., pulverization of the electro-active particulates) from the current collector.[22] Therefore, carbon coating or composites with carbonaceous materials or prepared with either active or inactive matrix elements to sustain the volume variation were proposed. However, ICL remains an issue for such anodes. In the recent past, a pre-treating procedure was successfully adopted for the case of conversion type anodes and the same strategy can also be extended for these alloy type anodes during the fabrication of Li-ion power packs. Unstable SEI formation

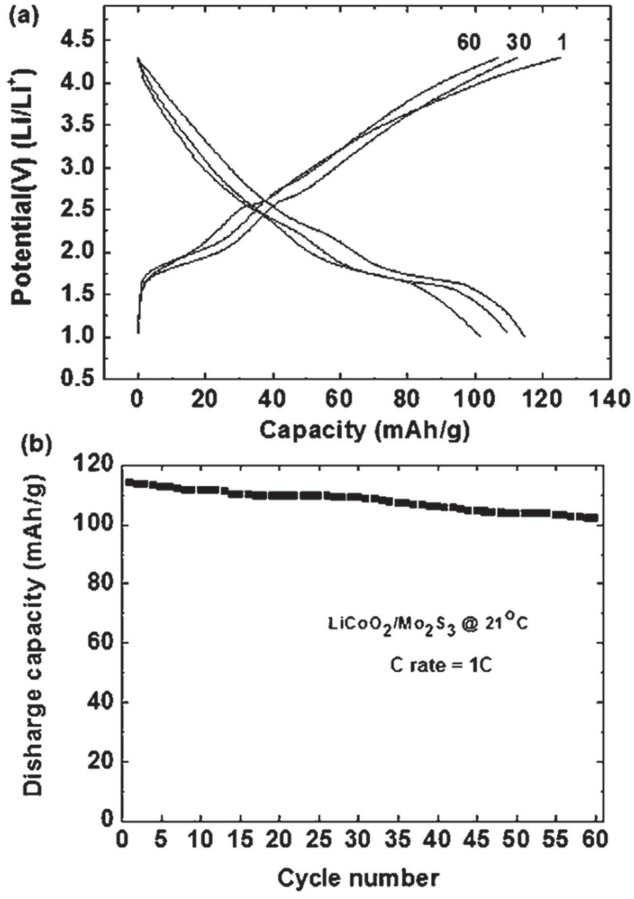

Figure 23. a) Voltage profiles of MoS_2 nanoplates in a full cell (MoS_2/$LiCoO_2$) between 1 and 4.3 V at a rate of 1C (1 C = 1062 mA g^{-1}) (charge and discharge rates were same) at room temperature and b) plot of discharge capacity as a function of cycle number from (a). Reproduced with permission.[377] Copyright 2011, American Chemical Society.

over active material is another important issue that in turn provides a continuous reaction of active particles with the electrolyte counterpart and forms a very thick layer upon cycling resulting in an increase in cell resistance.[20] It is well understood that the SEI formed over alloy anodes is in contrast to that formed in conventional graphitic anodes. In addition, the SEI formed in alloy type anodes seems to be a dynamic process of breaking off and reforming because of the unavoidable volume variation upon alloying/de-alloying process.[382] Because of the mentioned setbacks, limited reports are available for such fascinating anodes in full-cell assemblies and these are discussed in the next sections.

4.1. Si and its Derivative

Silicon is one of the very important Group IV elements and is extensively studied as a potential candidate to replace the conventional graphitic anode because of its lower working potential, high volumetric (≈9786 mAh cm^{-3}) and gravimetric capacities (≈3579 mAh g^{-1}), and its abundance on earth's crust. Interestingly, the theoretical capacity ($Li_{15}Si_4$) is closer to that of metallic Li (≈3862 mAh g^{-1}) and, therefore, extensive research activities have been carried out.[383,388,398–402] The main issue for this material is the poor reversibility upon cycling because of the huge volume variation during lithiation and de-lithiation processes (434% for amorphous and 399% for crystalline Si),[397] which results in the detachment of active particles from the substrate.[403] As a consequence, a dramatic capacity fading is observed. Other issues such as the ICL observed in the first cycle and the unstable SEI formation upon cycling are not to be ruled out.[387,404] The main cause of the volume variation is its reaction with Li.[383]

During discharge: Si (crystalline) + xLi$^+$ + xe$^-$ → Li_xSi (amorphous) + (3.75 − x)Li$^+$ + (3.75 − x)e$^-$ → $Li_{15}Si_4$ (crystalline)

During charge: $Li_{15}Si_4$ (crystalline) → Si (amorphous) + yLi$^+$ + ye$^-$ + $Li_{15}Si_4$ (residual)

The two-phase reaction is observed in all the stages of the first discharge and completely vanishes once it reaches the binary $Li_{15}Si_4$ alloy formation; single phase reaction only resulted with subsequent cycles.[388,405] Electrochemical aggregation of particles was observed because of the welding effect during the charge process (i.e., pressure induced from the enormous amount of volume expansion/contradiction) not ruled out for the capacity fade.[406] Undoubtedly, Si-based active materials should be either prepared with a carbonaceous matrix or synthesized with active/inactive matrix elements to uphold the volume variation before formulating the electrodes. Utilization of hollow structured materials is more preferable, and can sustain certain amounts of variation.[407] The use of various binders (CMC, polyacrylic acid (PAA), teflonized acetylene black (TAB), etc.) and additives to form a the stable SEI to improve the cycleability also been reported;such binders enable self-heating.[408] As a consequence, binders also contribute to upholding the volume variation upon alloying/de-alloying.Much research into the synthesis of Si nanostructures with various morphologies has been reported, but unfortunately few of them were only explored in practical configuration. Si-based materials are the only extensively studied anodes for practical LIB configurations among the alloy-type materials. However, the electrochemical profiles are different for thin films and powders and, similarly, for amorphous and crystalline Si.

Lee et al.[409] first reported the successful fabrication of a full-cell assembly with a $LiMn_2O_4$ cathode prepared by radio frequency (RF) magnetron sputtering. The sputtered Si anode exhibited much better cycleability and reversibility in PC-based solution than EC:DMC. Furthermore, the authors attempted to overcome the ICL by cycling the Si anode in the half-cell assembly for five cycles and subsequently paired it with a spinel cathode, $LiMn_2O_4$. The pre-lithiated Si anode displayed much better cycleability than the untreated Si anode in a full-cell assembly. Under the optimized conditions, the $LiMn_2O_4$/Si cell maintained a reversible capacity of 16 μAh cm^{-2} $μm^{-1}$ compared to its initial reversible capacity of 24 μAh cm^{-2} $μm^{-1}$ after 100 cycles. Amorphous Si is believed to be as efficient as and a better candidate than its crystalline state. Baranchukov et al.[410] reported the preparation of amorphous Si by direct current (DC) magnetron sputtering and fabricated the full-cell with $LiCoO_2$ (60% excess relative to Si) in the presence of 1 M LiTFSI in 1-methyl-1-propylpiperidinium bis(trifluoromethylsufonyl) imide (MPPpTFSI) ionic liquid. As expected, a large ICL of ≈1000 mAh g^{-1} was noted with a reversible capacity of

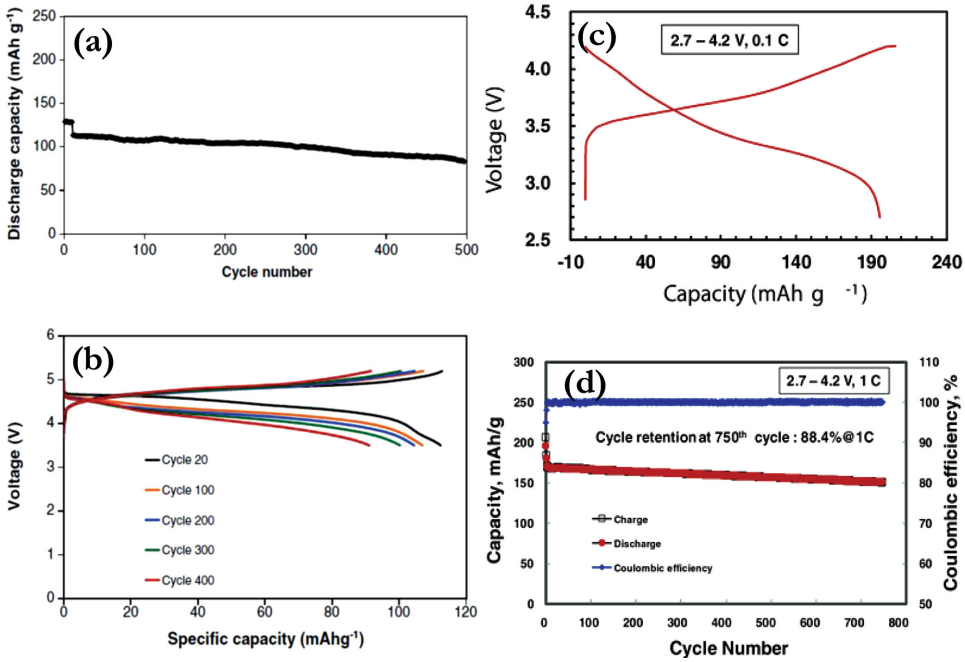

Figure 24. Typical curve of discharge capacity vs. cycle number (a) and voltage profile (b) obtained upon galvanostatic cycling of $LiNi_{0.5}Mn_{1.5}O_4$/Si cells at 0.5 C rate (10 initial cycles at C/8 rate) in the FEC-based electrolyte solution. Reproduced with permission.[417] Copyright 2013, Elsevier. c) Voltage profile of the lithium ion battery based on the Si/C-internally wired with graphene sheets anode and full concentration gradient cathode cycled between 2.7 and 4.2 V at a 0.1 C rate, and d) Cycling performance of the lithium ion battery based on the Si/C-internally wired with graphene sheets anode and full concentration gradient cathode cycled between 2.7 and 4.2 V at a 1.0 C rate. Reproduced with permission.[425] Copyright 2014, John Wiley & Sons.

≈2500 mAh g^{-1}. However, a drastic fade was noted for the $LiCoO_2$/Si cell upon cycling and it showed a reversible capacity of ≈1200 mAh g^{-1} within 32 cycles. Yang et al.[411] reported the exceptional performance of a DC magnetron sputtered amorphous Si anode with a layered $LiCoO_2$ cathode. The $LiCoO_2$/Si cell displayed a very stable cycleability of over 300 cycles with loss of only 0.01% per cycle and good capacity retention properties at high current rates were also noted. Electron beam deposited amorphous Si also showed similar stability when paired with a $LiCoO_2$ cathode over 200 cycles.[412] Similar stability was reported for spinel $LiMn_2O_4$/amorphous Si by a low pressure chemical vapor deposition (LPCVD) process for 400 cycles in the presence of 1 M $LiClO_4$ in PC.[413] On the other hand, there is no such stability when coupled with $LiFePO_4$ and amorphous Si prepared by RF magnetron sputtering.[414] The authors employed Ni as the under layer between Si and the Cu current collector, but the capacity fading was found to be very severe compared with the $LiCoO_2$ and $LiMn_2O_4$ cathodes. Recently, exceptional performance of columnar Si thin film anodes was clearly seen when coupled with a traditional TiS_2 cathode in the presence of 1 M $LiPF_6$ in fluoro ethylene carbonate (FEC):DMC (1:4).[415] The anode was pre-lithiated to ensure the $Li_{15}Si_5$ phase before conducting the full-cell assembly with TiS_2. The full-cell TiS_2/lithiated Si cell showed a capacity of ≈240 mAh g^{-1} and displayed a very stable capacity for 300 cycles. The observed reversibility and cycleability were a replica of the performance of the TiS_2 electrodes in the half-cell assembly, except for the 250 mV reduction in the operating potential. This outstanding performance was due to the stable SEI formation over Si electrodes upon cycling, which predominantly contains the polyenes, LiF, and dominance of $Li_xPO_yF_z$ species compared to Li_xPF_y while using the standard solutions.[416] To ensure the favorable properties of FEC-based solutions in Si anodes, the same group of authors used the same strategy in high voltage and high capacity configurations, i.e., $LiNi_{0.5}Mn_{1.5}O_4$ and $xLi_2MnO_3.(1–x)LiNi_yMn_zCo_{1-y-z}O_2$.[11,416–418] (**Figure 24**). A similar electrochemical stability was observed for the Si anodes with the aforementioned cathode, for instance ≈74.2 (after 500 cycles) and ≈89% (after 200 cycles) capacity was retained for a Si anode coupled with $LiNi_{0.5}Mn_{1.5}O_4$ and $xLi_2MnO_3.(1–x)LiNi_yMn_zCo_{1-y-z}O_2$ cathodes, respectively.

The Si-C composite prepared by pyrolysis with polyvinylchloride (PVC) and successive high energy mechanical milling and showed stable electrochemical profiles >950 mAh g^{-1}.[419] The full-cell with layered $LiCo_{0.2}Ni_{0.8}O_2$ displayed a reversible capacity of over 600 mAh g^{-1} with a working potential of ≈3.5 V. However, no cycleability was reported for the mentioned configuration. Park et al.[420] reported the fabrication of LIBs with carbon-coated Si nanotubes anodes and layered $LiCoO_2$ cathodes. The test cell delivered a reversible capacity of ≈3247 mAh g^{-1} with a high coloumbic efficiency of ≈89%. Furthermore, excellent cycleability over 200 cycles was reported with a retention of ≈89% of the initial reversible capacity. In addition, the observed capacity of the $LiCoO_2$/Si cell after 200 cycles was 10 times higher than graphite-based LIBs and displayed high reversibility of >3000 mAh g^{-1}, even at rates of 5 C and 2 C (1 C = 3 A g^{-1}). Cui et al.[421] proposed the concept of fabricating core-shell structured carbon-Si nanowires to uphold the volume variation. Usually Si is in the core and carbon is in the shells, whereas in the present case, they were reversed.

Amorphous Si was prepared over the carbon nanofibers and evaluated as a possible anode. It displayed a stable reversible capacity of ≈2000 mAh g^{-1} for about 30 cycles. In the full-cell assembly with a $LiCoO_2$ core-shell, carbon-Si nanowires showed good capacity retention characteristics (≈80% after 30 cycles) and reversibility (≈1400 mAh g^{-1}). Similarly, Si nanowires over carbon textiles were also reported as free-standing electrodes with a reversible capacity of over ≈1600 mAh g^{-1} and compatibility at various temperatures (10–45 °C) conditions and bending states were reported.[422] Forney et al.[423] attempted to deposit the Si nanostructures over SWCNTs using a plasma-enhanced chemical vapor deposition (PECVD) process with low (≈26%), medium (≈53%), and high (≈68%) loadings. The higher loading leads to a severe capacity fading upon cycling in both the half-cell and full-cell assemblies (with $LiNi_{0.8}Co_{0.1}Al_{0.1}O_2$ as the cathode). However, very stable cycling profiles are noted for medium and low level Si loadings for the investigated 100 cycles with targeted 40% of the depth of discharge (DOD). It is strongly believed that the presence of carbonaceous material upholds the volume variation during lithiation and de-lithiation processes, nevertheless a stainless steel fibril mat was also used for the same propose. In this scenario, Song et al.[424] reported the preparation of a binder-free Si deposited metal fibril mat as a promising anode with good cycleability (≈2000 mAh g^{-1} in the half-cell). Notable electrochemical profiles were observed when coupled with a $LiFePO_4$ cathode and it retained ≈76% of initial capacity (≈1300 mAh g^{-1}) after 50 cycles. Ultralong cycleability (750 cycles) was observed for a Si-carbon composite internally wired with graphene nanosheets paired with Ni-rich layered full concentration gradient cathode ($Li.[Ni_{0.75}Co_{0.1}Mn_{0.15}]O_2$).[425] The full-cell retained ≈88.4% of initial capacity after 750 cycles, i.e., the loss of 0.016% capacity per cycle (Figure 24). Similarly, cycling stability was observed in a Si-nanoparticle backboned graphene composite for 1000 cycles with almost 100% capacity retention and a reversibility of ≈1000 mAh g^{-1} in the half-cell assembly.[426] A full-cell with a $LiCoO_2$ cathode was capable of delivering the high reversibility at high currents (5, 10, 15 and 20 C rates), for instance ≈90 mAh g^{-1} (based on cathode mass) was observed at 20 C with good capacity retention characteristics. Multi-layered Si and graphene structures (five layers) were prepared using PECVD and an anodic aluminium oxide (AAO) template approach, respectively, and these were subsequently evaluated as an anode.[427] The full-cell composed of a layered $LiNi_{1/3}Mn_{1/3}Co_{1/3}O_2$ as cathode and multi-layered Si-graphene structure as the anode showed a poor cycleability of ≈70.4% retention within 15 cycles. Surface modification was one of the efficient approaches to suppress the unwanted side reaction with electrolyte counterpart and it was effectively adopted for a Si-graphene composite via atomic layer deposition (ALD) (Al_2O_3 coating).Enhanced cycleability was observed for such an Al_2O_3-modified Si-graphene composite compared to an unmodified one in a half-cell assembly, but severe fading upon cycling was experienced when it was paired with a Li-rich layered-layered cathode ($Li_{1.2}Ni_{0.2}Mn_{0.6}O_2$).[408] This fading was mainly because of the excess Li-removal during the first charge process. The influence of the thickness of the native oxide (SiO_x) on the electrochemical profiles of the Si anode was studied and it was found that increasing the SiO_x thickness (2–15 nm) results in enhanced capacity retention; however the dilution of reversible capacity is inevitable.[428] It is well known that, the SiO_x is also electrochemically active and it contributes a small amount of capacity. As expected, the SiO_x modified Si was paired with $LiCoO_2$ and showed capacity retentions of ≈67 and ≈48% after 130 cycles with coating thicknesses of ≈7 and ≈2 nm, respectively. The mentioned coating was certainly beneficial for the nanowire thickness of <100 nm, but if it exceeds that size, it is not possible for such a metal oxide coating to suppress the volume variation. Similarly, a Sb-doped tin oxide coating over both the anode (Si) and the cathode ($LiCoO_2$) was suggested by Lee et al.[429] to realize the ultrahigh energy density of a LIB. Apart from the prevention of side reactions with the electrolyte, the coating increases the electronic conductivity of both electrodes to an order of magnitude higher than the native phases. As a result, excellent cycleability was noted for the $LiCoO_2$/Si cells composed of surface-modified electrodes compared to a bare $LiCoO_2$/Si cell. Choi et al.[430] performed a metallo-thermic reduction process to prepare a shape-preserving macro-/nanoporous Si particulate via alumino-thermic and subsequent magnesio-thermic reaction of porous silica particles with various concentrations.Si/Al_2O_3 with 7:3 was found to be more stable in the half-cell assembly, but experienced severe fading when paired with $LiCoO_2$. SnC_2O_4 modification over the Si anode as also reported and it is well known that SnC_2O_4 is also electrochemically active, similar to SiO_x and Sb-doped tin oxide.[431] Introduction of SnC_2O_4 certainly improves the cycling profiles, however an increase in SnC_2O_4 concentration leads to a decrease in reversible capacity. Si-70%SnC_2O_4 was found to have an optimum concentration to yield a high performance anode. The full-cell was fabricated with a $LiFePO_4$ cathode; nevertheless, prior to the cell assembly the anode was cycled in a half-cell assembly to overcome the ICL. A very stable capacity of ≈140 mAh g^{-1} was noted for the reported 200 cycles without any noticeable fade. In addition, the cell was capable of displaying a similar stability independent of the working environment, including under sub-zero (–20 and –5 °C) and elevated conditions (60 °C). There was no smoke or flame observed during the nail penetration or the over charge tests. Core-shell Si@SiO_x nanowires over carbon textiles are reported as substrate free anodes for the fabrication of high energy density LIBs with $LiCoO_2$ cathodes.[432] The full-cell $LiCoO_2$/Si@SiO_x was capable of displaying a reversible capacity of ≈1949 mAh g^{-1} at a current density of 2 A g^{-1} and upheld ≈93.4% of the initial capacity after 50 cycles.

Flexible and bendable electronics are one of the fast growing frontier areas of research. In order to power such miniature electronic appliances, the fabrication of Li-ion power packs is warranted and Si-based materials are found to be promising for use as the anodes. Such LIBs with fast charging capabilities are reported for Si nanoparticle decorated expandable graphite anodes and V_2O_5 modified $LiNi_{0.75}Co_{0.11}Mn_{0.14}O_2$ cathodes.[433] Before conducting the fabrication of an assembly, honeycomb patterned Al and Cu current collectors are prepared using a reactive-ion etching process. The full-cell displayed a maximum reversible capacity of ≈185 mAh g^{-1} at 0.1 C, was capable of delivering a good reversibility at 12 C rate (1 C = 15.6 mAh), and retained ≈50% of its initial capacity after 600 cycles. In-situ bending studies were also conducted at a speed of 30 mm min^{-1} with a simultaneously applied torque of 11 N to ensure

the similar electrochemical profiles. Similarly, nanohair structured Cu current collectors were patterned with thermal evaporation over polyimide and were subsequently deposited by Si.[434] An outstanding electrochemical profile of ≈2775 mAh g^{-1} (at 0.05 C) was reported for such a unique structure in the half-cell assembly and for high currents as well. A full-cell was fabricated with $LiNiCoAlO_2$ oxide with working potential of ≈3.74 V. The nanohair structured electrode containing cell delivered favorable electrochemical properties compared to the planner substrate. Furthermore, the mechanical stability of the mentioned cells was evaluated against bending fatigue and the working potential of the nanohair electrode composed cell remained constant for 3000 bending cycles compared to planner electrodes. Vlad et al.[435] also reported a rolled up LIB composed of $Si_{core}@Cu_{shell}$ nanostructures as the anode with a layered $LiCoO_2$ cathode.

Apart from the pure Si nanostructures in thin film or powder form, electro-active Si with either active or inactive materials are also equally important. A multilayer Si-Ge thin films and composites were prepared using RF magnetron sputtering for various compositions.[436] Among these, $Si_{0.84}Ge_{0.16}$ composites showed better reversibility and cycleability in half-cell assemblies. The composite anode $Si_{0.84}Ge_{0.16}$, paired with $LiCoO_2$, displayed an initial reversible capacity of 213 mAh g^{-1} with a retention rate of 52.4% after 100 cycles.

Silicon monoxide (SiO) is considered to be a promising substitute for the fascinating Si anode, andis expected to sustain the volume variation observed during lithiation/de-lithiation process. SiO undergoes structural destruction upon the first discharge process according to the following reaction[437,438]

$$SiO + 5.75Li^+ + 5.75e^- \rightarrow Li_{3.75}Si + Li_2O$$

$$Li_{3.75}Si + Li_2O \leftrightarrow 3.75Li + Si + Li_2O$$

The cycleability of SiO is found to be superior compared to its metallic form (Si). Zeng et al.[439] attempted to fabricate a non-flammable LIB using a DMMP-based electrolyte solution (0.8 M $LiPF_6$ in DMMP) in the presence of FEC additive (10% by vol.). In this NL design, an excess of $LiFePO_4$ was used to overcome the ICL issue observed in carbon-coated-SiO anodes. An excellent cycleability was seen for both the anode and the cathode in the half-cell assembly, but a capacity fade in full-cell configuration was observed; for example, reversible capacities of ≈900 and ≈570 mAh g^{-1} were observed for first and 50th cycles, respectively. Carbon-coated SiO was prepared using a thermal evaporation procedure and it was evaluated as a promising anode that has better cycleability than carbon-coated Si anodes.[440] The SiO-carbon composite showed much better electrochemical performance than the SiO-graphite composite in the half-cell assembly and it showed reversibilities of ≈870 and 740 mAh g^{-1}, for the former and latter cases, respectively. Eventually, the full-cell was fabricated with a manually mixed cathode $LiCoO_2$ and $LiCo_{1/3}Ni_{1/3}Mn_{1/3}O_2$ (3:7 ratio) and it showed a practical capacity of over 700 mAh g^{-1} after 100 cycles. The capacity retention was observed to be over ≈85% after 100 cycles. The electrochemical charging process was carried by a CC-CV mode for such mixed cathodes at 4.2 V for 3 h. A 14 500 prototype was reported with various current rates and temperature conditions with a retention of ≈700 mAh capacity after 300 cycles for the designed 1 Ah.[441] The cell passed the safety profiles including over charge tolerance (at 1 C charging to 12 V), a nail penetration test, and heating the fully-charged battery to 150 °C for 2 h. A diamond-like carbon coating was also carried out over SiO_x-graphite by PECVD to improve the cycleability.[442] A reversible capacity of ≈520 mAh g^{-1} was observed for both bare and diamond-like carbon-coated composites when paired with $LiCoO_2$, but the electrochemical stability of the latter one became superior compared to the bare composite. For instance, the ≈52 and 78.2% initial reversible capacity was noted for bare and diamond-like carbon-coated SiO-graphite composites after 100 cycles, respectively. A high reversible capacity of over 1000 mAh g^{-1} was noted under elevated temperature conditions (60 °C) with an increase in the upper cut-off potential, i.e., different working potential 3 to 4, 4.1, and 4.2 V when paired with a layered $LiNi_{0.8}Co_{0.15}Al_{0.05}O_2$ cathode.[443] However, drastic fading was observed for the potential window of 3 to 4.2 V, whereas notable fading was observed for rest of the potential window. This was because the working potential played a vital role for the stability of the cell. However, in the present case, the poor thermal stability of the electrolyte was responsible for the capacity fade. Liu et al.[444,445] reported the performance of 50% SiO_x- 50% Sn-Co-C composite (Sn-Co-C is the alloy-based anode developed and used in Sony's Nexelion batteries[4,446]) as a high capacity anode for LIB applications with Li-rich cathodes such as $Li_{1.2}Ni_{0.2}Mn_{0.6}O_2$ and $Li_{1.2}Ni_{0.15}Co_{0.10}Mn_{0.55}O_2$. Before conducting the full-cell assembly, the mentioned composite electrodes were coated with solid lithium metallic powder (SLMP) to overcome the ICL issue. The $Li_{1.2}Ni_{0.2}Mn_{0.6}O_2$ or $Li_{1.2}Ni_{0.15}Co_{0.10}Mn_{0.55}O_2$/50% SiO_x-50% Sn-Co-C cell showed a good reversibility of ≈77.7 (after 100 cycles) and ≈72% (after 200 cycles) initial reversible capacity for former and latter configurations, respectively.

4.2. Sn and its Derivative (Sn-Cu, Sn-WC, and SnO_2)

Metallic Sn has been widely investigated as a possible anode for LIB applications and its composite (Sn-Co-Ti-C) has already been commercialized by Sony in high power Nexelion configurations.[446] This clearly shows the promising feature of this element. Sn showed favorable features such as lower reaction potential (≈0.3 V vs. Li) and high theoretical capacity (≈993 mAh g^{-1} for the reversible formation of $Li_{4.4}Sn$ alloy) compared to the conventional graphitic anodes.[381] The high power capability of Sn compared to graphite is worth mentioning. During the lithiation/de-lithiation process Sn undergoes a (alloying) reaction with metallic Li according to the following equilibrium: $Sn + 4.4Li^+ + 4.4e^- \leftrightarrow Li_{4.4}Sn$. However, a large unit cell volume variation (≈259% for crystalline and ≈305% for amorphous).[397] upon alloy formation results in the possible use of carbon as the matrix element to sustain such variation without affecting its electrical conductivity. This translates to a Sn anode in composite form with carbonaceous material, which is found to be superior in terms of cycleability and high reversible capacity. Apart from the carbonaceous matrix, several active and inactive matrices have also been proposed to sustain such volume variation. Highly stable cycling

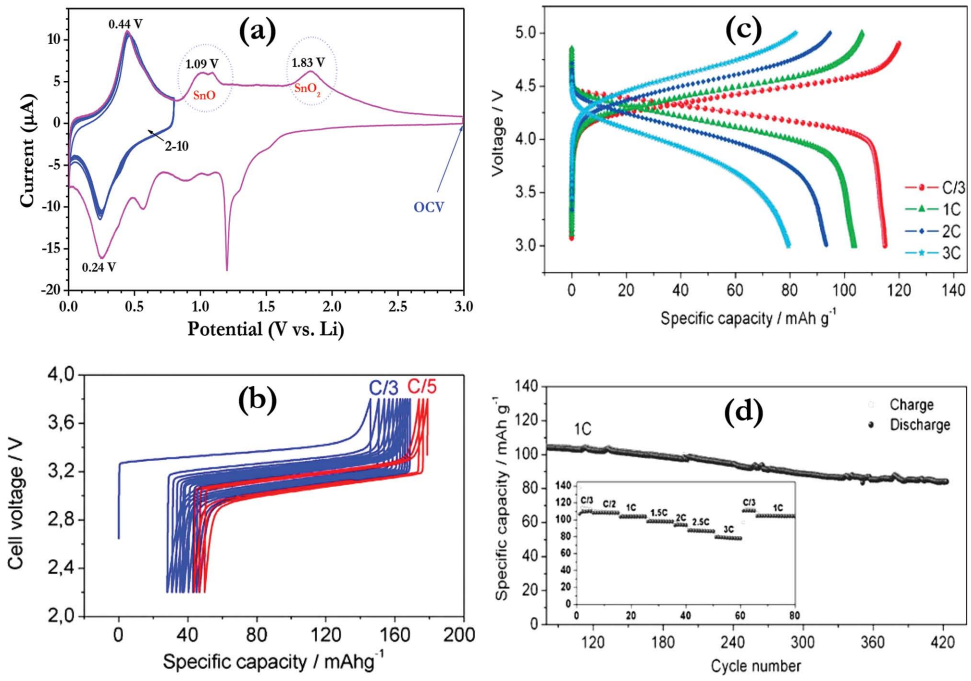

Figure 25. a) Cyclic voltammograms of ALD SnO_2 anodes in half-cell configuration (Li/SnO_2) cycled between different potential ranges at slow scan rate of 50 μV s^{-1}, in which metallic lithium acts as both counter and reference electrode. Reproduced with permission.[448] Copyright 2013, Elsevier. b) Voltage vs. specific capacity profile of a Li-ion battery using a pre-treated Sn–C anode, a $LiFePO_4$ cathode, and a LiBOB, EC:PC:DMC (1:1:3) electrolyte solution, galvanostatically cycled at a C/3 rate (1 C = 170 mA g^{-1}). Reproduced with permission.[461] Copyright 2011, Elsevier. c) Voltage profiles of the Sn-C/gel polymer electrolyte (GPE)/$LiNi_{0.5}Mn_{1.5}O_4$ battery at various rates (1 C about 0.2 A cm^{-2} g^{-1} respect the cathode mass) and at room temperature. d) Capacity delivery versus cycle number for the Sn-C/GPE/$LiNi_{0.5}Mn_{1.5}O_4$ battery at 1 C rate and at room temperature. The inset shows the cycling response at various rates. Reproduced with permission.[452] Copyright 2009, John Wiley & Sons

profiles were observed. Accordingly, the derivatives of Sn, such as SnO and SnO_2, have also been explored as possible anodes for LIBs.[447] In addition to the mentioned alloying reaction, the presence of oxide promotes the oxidation of de-alloyed Sn to its native phase, i.e., SnO and SnO_2 via the conversion reactions:

$$SnO_x + 2xLi^+ + 2xe^- \rightarrow Sn^0 + xLi_2O \quad (1)$$

$$Sn^0 + xLi^+ + xe^- \leftrightarrow LixSn (0 \le x \le 4.4) \ (< 0.8V \text{ vs. Li}) \quad (2)$$

$$Li_xSn \leftrightarrow Sn^0 + Li_2O \leftrightarrow SnO \ (> 0.8V \text{ vs. Li}) \quad (3)$$

$$Li_xSn \leftrightarrow Sn^0 + Li_2O \leftrightarrow SnO \leftrightarrow SnO_2 \ (> 1.65V \text{ vs. Li}) \quad (4)$$

Accordingly the theoretical capacity can be extended from ≈993 mAh g^{-1} for Sn metal (4.4 mole Li) to ≈1138 and ≈1494 mAh g^{-1} for SnO (≈6.4 mole Li) and SnO_2 (≈8.4 mole Li), respectively. Apart from the material choice, the mentioned reaction can be made possible by adjusting the testing potential while using SnO_2 as the anode[448,449] (**Figure 25**). Apart from the commercialization of Sn-Co-Ti-C composite anodes in the Nexelion configuration by Sony, Derrien et al.[450] first reported the possibility of using Sn-C composites with average particle size of ≈30 nm an the anode for LIB applications. In the half-cell assembly, these showed a reversible capacity of ≈497 mAh g^{-1}, which includes a small contribution (≈23 mAh g^{-1}) from the carbon matrix via an insertion/extraction mechanism. Prior to the full-cell assembly, the anode was tested for 20 cycles and discharged to 0.01 V vs. Li in the half-cell, whereas the cathode $LiNi_{0.5}Mn_{1.5}O_4$ was charged to an open-circuit voltage (OCV) (≈5 V vs. Li) for the removal of Li. The $LiNi_{0.5}Mn_{1.5}O_4$/Sn-C cell displayed a reversible capacity of ≈120 mAh g^{-1} (based on cathode loading) with very stable cycleability (over 100 cycles) and efficiency (almost 100%). A marginal improvement in the electrochemical reversibility (≈120 mAh g^{-1}, based on cathode loading) was noted in the $LiNi_{0.5}Mn_{1.5}O_4$/Sn configuration when the metallic Sn anode was electroplated over Cu foil.[451] As expected, the cell delivered a good cycling profile for the reported 50 cycles and the same pre-treating procedure was adopted for the fabrication of the full-cell. Furthermore, the authors attempted to improve the safety of the high power $LiNi_{0.5}Mn_{1.5}O_4$/Sn-C configuration by using polymer membranes prepared by conventional (1 M $LiPF_6$ in PVdF-EC-PC) (Figure 25).[452] and electrospinning (1 M $LiPF_6$-EC-DMC in polyvinylidenefluoride-*co*-chlorotrifluoroethylene (PVdF-CTFE))[453] techniques. In both cases, good reversibility, cycleability, and high current performances were noted. Instead of using the resorcinol derived Sn-C composite, mechanically milled Sn-C was also considered with the high voltage $LiNi_{0.5}Mn_{1.5}O_4$ cathode and ensured the previous reversibility (≈120 mAh g^{-1}, based on cathode loading) and cycling stability.[454] The performance of such a cathode under sub-zero conditions (0 to –30 °C) delivered a reasonable capacity profile when paired with a Sn-C anode, particularly at –5 °C.[455] The Li-ion cell delivered

excellent capacity with a reversibility of ≈105 mAh g^{-1} over 200 cycles under sub-zero temperature conditions (–5 °C). An attempt has also been made to evaluate the compatibility with other high voltage configurations such as $LiNi_{0.45}Co_{0.1}Mn_{1.45}O_4$ and similar performance was observed.[456] Fe-doped $LiCoPO_4$ ($LiFe_xCo_{1-x}PO_4$) is considered to be one of the promising solutions for the fabrication of high energy density Li-ion power packs.[217,218,457] To keep the issues of $LiCoPO_4$ based cathodes with conventional electrolyte, $PyR_{14}FSI$-LiTFSI was used as a cathode.[458] This eventually destroys the reversible capacity of the cathode, for example the reversible capacity of ≈90 mAh g^{-1} was only noted for $LiFe_{0.1}Co_{0.9}PO_4$ in the half-cell assembly with the expected high charge capacity. Despite the loss of the first charge, reasonable cycling profiles were noted when paired with Sn-C for about 7 cycles. Li_2MnO_3 based derivatives were believed to be high capacity cathodes for the fabrication of next generation LIB. Elia et al.[459] reported the performance of such a Li-rich cathode, $Li[Li_{0.2}Ni_{0.4/3}Co_{0.4/3}Mn_{1.6/3}]O_2$ with a Sn-C anode, and it displayed capacity retention of ≈75% after 500 cycles at various current densities. Once of the interesting configuration of the Sn-C composite is with a $LiFePO_4$ cathode because of the low cost, high power, and eco-friendliness of the system. Unfortunately, the $LiFePO_4$/Sn-C system showed more fading than the layered and spinel-type cathodes described above.[460] However, several approaches, including utilization of LiBOB-based solutions (0.7 M LiBOB in EC:PC:DMC, 1:1:3, Figure 27)[461], polyethylene oxide (PEO)-based polymer electrolyte (PEO_{20}-$LiCF_3SO_3$):ZrO_2, 90:10 wt%),[462] and ionic liquid LiTFSI-Py_{24}TFSI,[463] were also used to improve the electrochemical performance. However, there are no long-term cycling profiles (*i.e.*, beyond 100 cycles; most of them are up to just 10–30 cycles) or in-depth studies are available at the moment. A free-standing yolk-shell structured Sn-C composite was also reported with a layered $LiCoO_2$ with various cut-off potentials, but such an assembly exhibits very poor cycleability.[464]

Kim et al.[465] reported the synthesis of novel core-shell Sn-Cu anodes, although these offer lower reversible capacity compared to Sn-C in the half-cell assembly. However, much higher power capability and cycleability was noted compared to Sn-Cu anodes. The full-cell was fabricated with $LiCoO_2$ ($LiCoO_2$/Sn-Cu) and delivered a reversible capacity of ≈670 mAh g^{-1} (based on anode loading) with retention of ≈85% after 170 cycles. The observed cycleability of the Sn-Cu anode was consistent with the natural graphite reported by the authors. Yao et al.[466] suggested the possibility of using 3D current collectors to improve the rate capability and the stability of Sn-Cu anodes when paired with $LiFePO_4$ cathode. Poor cycleability was noted for the conventional Cu current collector formulated with PVdF binder, which was substantially improved by heat treating them in Ar atmosphere. However, the capacity fading remains an issue. The combined advantages of using a 3D current collector (Ni-Cr) and formulating with CMC binder certainly enable excellent cycleability and allows retention of over ≈90% of the initial capacity after 200 cycles. Trilayer Sn-WC-few-layer graphene was prepared using a ball-milling procedure and was proposed as a promising anode for LIB applications; it has good reversible capacity (≈400 mAh g^{-1}) and capacity retention characteristics.[467] In the trilayer system, the inner (WC) and outer layers (few layers graphene) were anticipated to sustain the volume variation during the alloying/de-alloying reaction. The electrode was prelithiated before the full-cell assembly, as suggested by Hassoun et al.[456] The $LiNi_{0.5}Mn_{1.5}O_4$/Sn-WC-few layer graphene cell delivered good reversibility (≈400 mAh g^{-1}) and rendered ≈87% of initial capacity after 50 cycles. Cable-type flexible LIBs fabricated with hollow multi-helix electrodes, i.e., $LiCoO_2$ coated Al wire and Sn-Ni coated over Cu wire,were reported for miniature electronic applications.[468] The hollow structured anode exhibited much higher reversibility and cycleability than solid anodes.

Apart from the Sn composite with carbonaceous materials and other matrix elements such as Cu, Ni, and WC, the derivative SnO_2 was also explored as a possible anode for practical cells. To sustain the volume variation the SnO_2 microtubes were grown over carbon cloth and subsequently used as binder free anodes.[469] The full-cell was fabricated with a NL design using such a binder-free anode along with $LiCoO_2$ as the cathode for self-powered photo-etector applications. Because there was no pre-treating for the SnO_2 anode, a this results in a huge ICL during the first charge when paired with a layered cathode. The full-cell delivered a reversible capacity of ≈863 mAh g^{-1} at a current density of 200 mA g^{-1} with an ICL of ≈800 mAh g^{-1}. The full-cell $LiCoO_2$/SnO_2 renders ≈64% of the initial reversible capacity after 60 cycles. The same group of authors attempted to improve the cycleability by making heterostructures with TiO_2 over carbon cloth for the mentioned photodetector applications.[470] As observed in the previous case, a huge ICL was also observed in the SnO_2@TiO_2 heterostructure when coupled with $LiCoO_2$. However, the improvement in the reversible capacity (≈960 mAh g^{-1}) and cycling stability was noted for the reported 25 cycles while utilizing SnO_2@TiO_2 heterostructures compared to SnO_2 microtubes.

4.3. Ge and its Derivative

Ge is one of the important Group IV elements that have been widely exploited as promising anodes for LIB applications. Despite its salient features, which include high theoretical and lower working potential (≈0.5 V *vs.* Li), the cost of this material remains a main hurdle for the extensive research. As a result fewer research activities have been carried out compared to its counterparts such as Si and Sn. Formation of the end product in the first cycle is still a debate that leads to deviation in the exact theoretical capacity of Ge ($Li_{15}Ge_4$ (≈1384 mAh g^{-1}),[471] $Li_{22}Ge_5$ (≈1624 mAh g^{-1}),[472] or $Li_{17}Ge_4$ (≈1568 mAh g^{-1})[473]). Generally, the reaction mechanism can be described as follows $Ge \rightarrow Li_9Ge_4 \rightarrow Li_7Ge_2 \rightarrow Li_{15}Ge_4 + Li_{22}Ge_5$.[383] Still, the practical reversibility (>1000 mAh g^{-1}) in the half-cell assembly is much higher than that for conventional graphitic or Sn-Co-Ti-C anodes. In addition, the three orders of magnitude higher electrical conductivity (≈2.1 S m^{-1}) and two orders of magnitude higher ionic diffusivity (6.25×10^{-12} cm^2 s^{-1}), i.e., 400 times higher than its counterpart Si (electrical conductivity ≈1.6 mS m^{-1} and ionic diffusivity 1.9×10^{-14} cm^2 s^{-1}), indicates the high power capability of this unique anode.[473] This is mainly because of the smaller band gap (0.6 eV) of the Ge. Furthermore, the ICL observed in the first cycle is also found to be minimal compared to Si- and Sn-based anodes. Therefore,

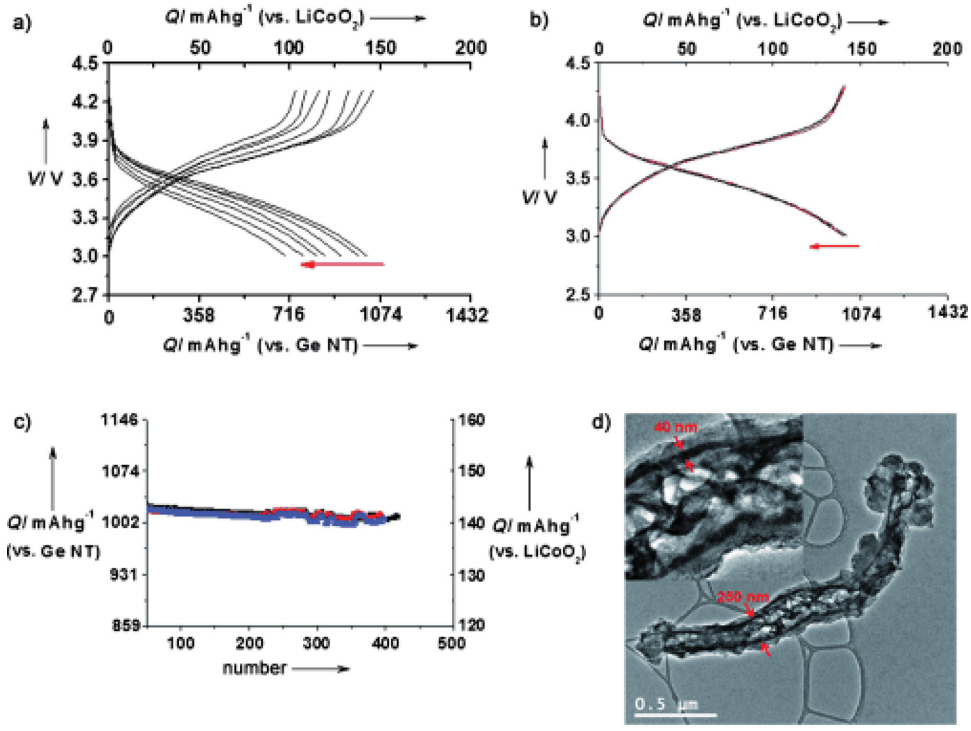

Figure 26. a,b) Voltage profiles of pouch-type lithium-ion cells: a) cycled between 3 and 4.3 V at different C rates: 1C, 5 C, 7C, and, 20 C, 30 C, and 40 °C (charge rate = discharge rate, 1 C = 1 A g^{-1}), b) after 1, 150, 300, and 400 cycles between 3 and 4.3 V (charge rate 0.5 °C, discharge rates 1 °C). c) Plot of capacity *vs.* cycle number in three different lithium-ion cells, (d) TEM image of a Ge nanotube after 400 cycles; inset: expanded view. As the nanotube was extracted from the composite electrode, its surface was covered by binder and carbon black. Reproduced with permission.[474] Copyright 2011, John Wiley & Sons.

research efforts on Ge-based anodes are worth investigating from the EV and HEV point of view, for example nanocrystalline Ge thin films are capable of delivering higher reversible capacity even at 1000 C rates.[472] Similar to rest of the alloy and conversion anodes, Ge also suffers upon cycling because of the pulverization of the electrode during the lithiation/de-lithiation process. Typically, the crystalline and amorphous phases of Ge undergo ≈353 and ≈382% of variation, respectively.[383,397] Therefore, strategies adapted to the alloy type and conversion anodes to sustain the volume variation are desperately needed to improve the cycleability.

Park et al.[474] first reported the performance of carbon-coated Ge nanotubes (obtained from the Kirkendall effect at 700 °C) in a full-cell assembly with layered $LiCoO_2$ **(Figure 26)**. As expected, carbon-coated Ge anodes delivered a reversible capacity of ≈716 mAh g^{-1} at a 40 C rate (40 A g^{-1}),which is much better rate performance than its counterpart Si (reported only up to 15 C or 15 A g^{-1}). In addition, an exceptional cycleability was noted, for example the cell showed a reversible capacity of 1020 and 1002 mAh g^{-1} at a 1 C discharge rate (charging at 0.5 C) for first and 400th cycles, respectively. The enhanced cycleability of dodecanethiol-passivated Ge nanowires was capable of delivering better electrochemical performance than bare nanowires, irrespective of the applied current rates or working conditions (both room and elevated temperatures).[475] Without proper optimization, the full-cell assembly with the $LiFePO_4$ cathode showed a reversible capacity of over 1000 mAh g^{-1} for the investigated 30 cycles. Later the same group attempted to synthesize high loading of Ge nanoparticles over graphene sheets with a carbon coating.[476] The Ge-reduced graphene oxide (RGO)-C composite had very stable cycleability over 600 cycles in a half-cell assembly at a 1 C rate with a reversible capacity of ≈1000 mAh g^{-1}. As expected, the $LiCoO_2$/Ge-RGO-C cell retained a capacity of 900 mAh g^{-1} after 100 cycles with an initial reversible capacity of ≈1234 mAh g^{-1}.

Similar to Ge, the derivative germanium oxide (GeO_x) is also equally promising from an anode point of view according to the following equilibrium: $GeO_x + 2Li^+ + 2e^- \rightarrow Ge + Li_2O$. Subsequently, Ge will form a reversible alloy with Li according to the above equation and translate the high reversible capacity. Another advantage of using GeO_x is translating additional two Li via the conversion reaction for high reversible capacity, which can be utilized by widen the operating potential.[477] Wang et al.[478] first reported the synthesis of amorphous hierarchical porous GeO_x as promising anode with ultralong cycleability of 600 cycles in half-cell assembly at 0.5 C rate. The full-cell was fabricated with a layered type $Li(NiMnCo)_{1/3}O_2$ and the cell delivered the initial coloumbic efficiency of ≈85%. The $Li(NiMnCo)_{1/3}O_2/GeO_x$ cell displayed outstanding cycleability of 200 cycles with reversible capacity of ≈144 mAh g^{-1} (based on cathode mass) at 0.5 C rate by CC-CV mode of charging. The cell experiences capacity loss of only ≈0.028% per cycle upon cycling after 200 cycles. In addition to the alloying reaction, the conversion reaction was also utilized for the GeO_x-RGO composite to

yield a higher reversible capacity.[477] Fabrication of the full-cell assembly as carried out with a spinel $LiNi_{0.5}Mn_{1.5}O_4$ cathode and the GeO_x-RGO composite was pre-lithiated prior to the full-cell assembly according to the procedure described by Derrien et al.[450] The full-cell, $LiNi_{0.5}Mn_{1.5}O_4/GeO_x$-RGO showed a reversible capacity of ≈120 mAh g^{-1}. Very high reversible capacity was observed, independent of the applied current density, and it retained ≈83% of the initial capacity at a current density of 560 mA g^{-1}.

Germanate nanowires with active and inactive matrices are also worth investigating as possible anodes by sustaining the unit cell variation. Lin et al.[479,480] reported a series of germinate nanowire arrays including $SrGe_4O_9$, $BaGe_4O_9$, Zn_2GeO_4, and $Ca_2Ge_7O_{16}$ over carbon textiles, which undergo both alloy and conversion reactions. Irrespective of the germanate nanowires, all four phases experienced a huge ICL observed in the first cycle, which was much higher than the native and oxide forms. On the other hand, the presence of a carbonaceous matrix promotes the electrochemical activity of such nanowires, which is clearly evident from the half-cell studies and delivers the reversible capacity of ≈1000 mAh g^{-1} for all the cases. However, an ICL of over 800–1200 mAh g^{-1} was noted and no information was available about how it was circumvented during the fabrication of the full-cell assembly with a layered $LiCoO_2$ cathode. The full-cell $LiCoO_2/BaGe_4O_9$ or $Ca_2Ge_7O_{16}$ delivered a stable reversible capacity of ≈900 and ≈1100 mAh g^{-1} for the former and latter configurations, respectively.

5. Combined Conversion and Alloying

Binary metal oxides exhibits simpler conversion reaction with metallic Li and eventually showed good electrochemical activity. Interestingly, the introduction of alloying components in to the aforesaid matrices leads to a widening of reversible capacity and stability. As a result, certain materials exhibit combined conversion and alloying reactions with Li during charge-discharge process, for example, $ZnCo_2O_4$, $ZnMn_2O_4$, $ZnFe_2O_4$, SnO, and SnO_2, etc. In this special kind of material, the testing potential plays a crucial role to determine in the electrochemical performances and it has been clearly described for Sn-based derivatives. This kind of material is also studied and paired with conventional cathodes and this is described in the following sections.

5.1. $ZnFe_2O_4$

Spinel phase zinc ferrite has been extensively studied as a promising conversion-type anode for LIB applications and has a maximum theoretical capacity of 1000 mAh g^{-1} for the nine electron reaction. Although metallic reduction of Zn and Fe atoms is possible by conversion pathways, Zn is effectively involved in the alloy formation with Li according to the following equilibrium[22,481,482]

$$ZnFe_2O_4 + 8Li^+ + 8e^- \rightarrow Zn^0 + 2Fe^0 + 4Li_2O$$

$$Zn^0 + Li^+ + e^- \leftrightarrow LiZn$$

$$Zn^0 + Li_2O \leftrightarrow ZnO + 2Li^+ + 2e^-$$

$$2Fe^0 + 3Li_2O \leftrightarrow Fe_2O_3 + 6Li^+ + 6e^-$$

Xie et al.[483] first demonstrated the fabrication of a $ZnFe_2O_4$-graphene composite with olivine $LiFePO_4$. In half-cell assembly itself, a notable capacity fade was observed irrespective of the applied current rates with an ICL of ≈37%. Interestingly, the full-cell $LiFePO_4/ZnFe_2O_4$ experienced a huge ICL of ≈60% in the first cycle, which is almost twice that of the performance in the half-cell assembly. As a result, poor cycling profiles were noted for the $LiFePO_4/ZnFe_2O_4$ configuration, for instance an initial reversible capacity of ≈715 mAh g^{-1} was dramatically decreased to ≈450 mAh g^{-1} within 10 cycles. Later, Varzi et al.[484] demonstrated the ultralong cycling profiles of over 10 000 cycles for carbon-coated $ZnFe_2O_4$ with a $LiFePO_4$-CNT composite in the full-cell assembly (**Figure 27**). Here, the $ZnFe_2O_4$ electrodes were pre-lithiated in different levels to avoid the ICL observed in first cycle. It is interesting to note that the increase in pre-lithiation (an extended lithiation process towards lower potential with respect to metallic Li) results overcome the ICL issue and elevate the operating potential in the full-cell assembly; for example the pre-lithiated $ZnFe_2O_4$ anode exhibits a ≈0.43 V higher working potential than the untreated one when coupled with a $LiFePO_4$-CNT composite cathode. The full-cell composed of pre-treated $ZnFe_2O_4$ anode retained ≈86% initial reversible capacity after 10 000 cycles compared to ≈46% retention for the untreated electrode. The test electrodes were formulated with CMC binder to yield such a high performance configuration. Furthermore, the authors claimed that the observed maximum specific energy and power of 202 Wh kg^{-1} and 3.72 kW kg^{-1} (referring to the total electrode mass loading) are much higher than the Li-ion capacitors.[18,98]

5.2. $ZnMn_2O_4$

Similar to above-mentioned Co- and Fe-based spinels, manganite-based spinels with the general formula AMn_2O_4, where, A = Co, Ni, or Zn, were found to be attractive for LIB applications and were extensively studied by Courtel et al.[485]. All transition metals undergo the metallic reduction (Zn^0, Co^0, Ni^0 and Mn^0) via conversion reaction and, in addition, Zn involves the reversible alloy formation with Li (<1 V vs. Li), which, in turn, provides extra capacity for the spinel oxides.[364] More clearly, $CoMn_2O_4$ and $NiMn_2O_4$ are the purely conversion type anodes, whereas $ZnMn_2O_4$ undergo both conversion and alloy type reactions according to the following reactions

$$ZnMn_2O_4 + 8Li^+ + 8e^- \rightarrow Zn^0 + 2Mn^0 + 4Li_2O$$

$$Zn^0 + Li^+ + e^- \leftrightarrow LiZn$$

$$Zn^0 + Li_2O \leftrightarrow ZnO + 2Li^+ + 2e^-$$

$$2Mn^0 + 2Li_2O \leftrightarrow 2MnO + 4Li^+ + 4e^-$$

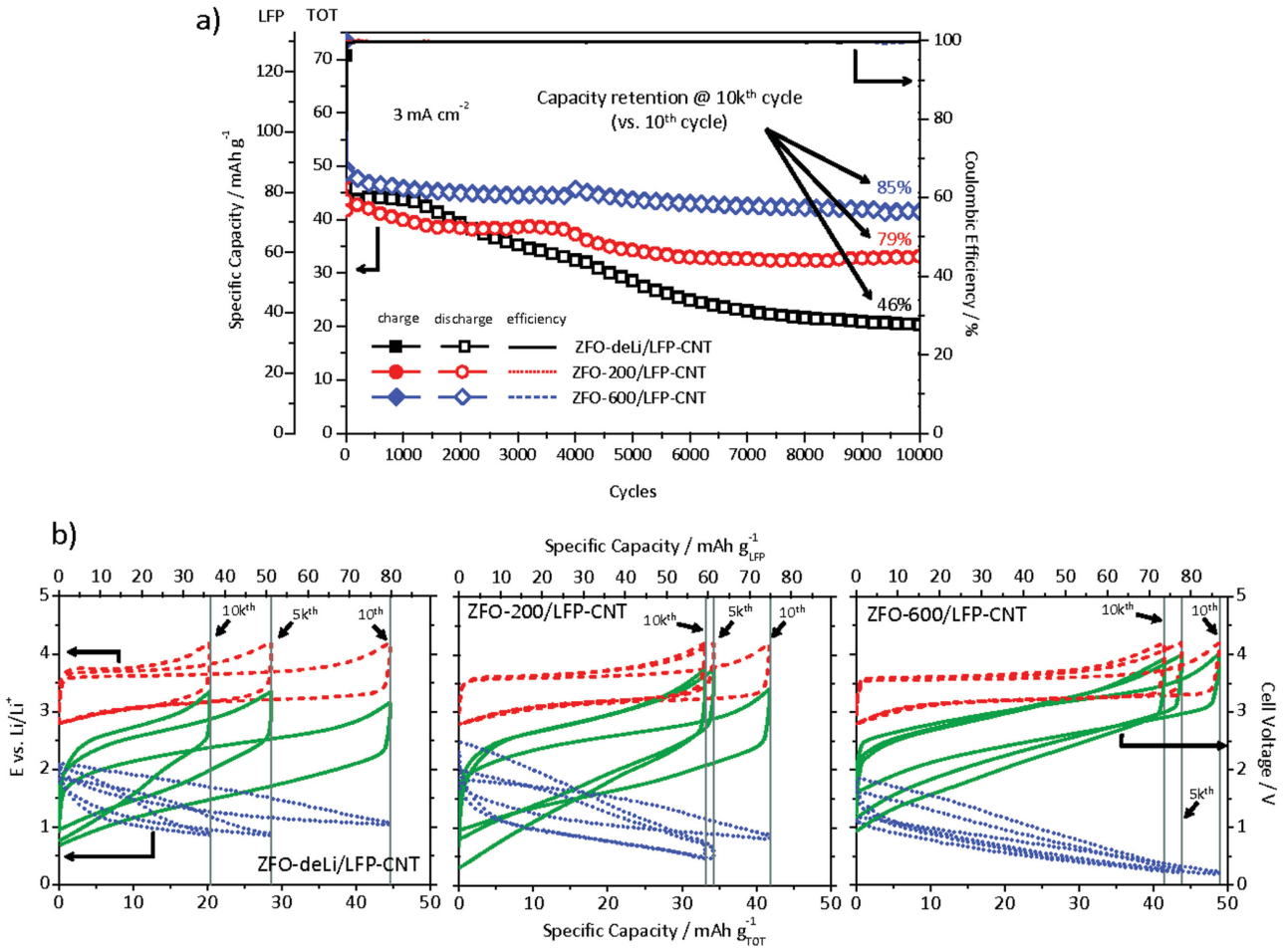

Figure 27. a) Long-term cycling stability applying a high current density of 3 mA cm^{-2} and the coulombic efficiency of $ZnFe_2O_4$ (ZFO)/$LiFePO_4$ (LFP)-CNT full-cells employing anodes with different degrees of lithiation. b) Selected electrode and cell voltage profiles evolution upon cycling. Specific capacity values are referred to the active material amount of both the limiting cathode (i.e., $LiFePO_4$) and the sum of the anode and cathode (i.e., TOT = $LiFePO_4$ + $ZnFe_2O_4$). Reproduced with permission.[484] Copyright 2014, John Wiley & Sons.

It was found that $ZnMn_2O_4$ that was co-precipitated, followed by sintering at 800 °C, was superior in terms of high reversible capacity and capacity retention characteristics compared to the rest of the spinels ($CoMn_2O_4$ and $NiMn_2O_4$) and its individual oxides (ZnO and Mn_2O_3) in the half-cell assembly. Li-CMC and 1 M $LiPF_6$ in EC:DEC (3:7 by volume) were found to be better binders and electrolytes for $ZnMn_2O_4$ anode, respectively. Eventually, the full-cell was fabricated with a high voltage $LiNi_{0.5}Mn_{1.5}O_4$ cathode in the presence of the mentioned electrolytes. Here, the cathode to anode mass as adjusted to 5:1 with 30% excess loading of $LiNi_{0.5}Mn_{1.5}O_4$ used to overcome the ICL issue. As expected, a dramatic fade in capacity profiles was noted; for example reversible capacities of 108 and 68 mAh g^{-1} were observed in the first and 20th cycles, respectively, with poor coulombic efficiency throughout the cycling (**Figure 28**). There are several reasons for this poor performance, for instance the choice of electrolyte; usually for such high voltage cathode configurations DMC-based solution are preferred over DEC.

5.3. $ZnCo_2O_4$

Even though Co-based compounds such as $LiCoO_2$ were claimed to be toxic for the LIB applications, research activities are still in full swing, for instance, $ZnCo_2O_4$ was proposed as an attractive material for the anode point of view. Similar to $ZnFe_2O_4$, $ZnCo_2O_4$ shows a cubic spinel structure where Co^{3+} ions occupy the octahedral sites and divalent Zn ions fill the tetrahedral sites. It is worth mentioning that both Zn and Co are found to be electrochemically active with Li according to the following equilibrium

$$ZnCo_2O_4 + 8Li^+ + 8e^- \rightarrow Zn^0 + 2Co^0 + 4Li_2O$$

$$Zn^0 + Li^+ + e^- \leftrightarrow LiZn$$

$$Zn^0 + Li_2O \leftrightarrow ZnO + 2Li^+ + 2e^-$$

$$2Co^0 + 2Li_2O \leftrightarrow 2CoO + 4Li^+ + 4e^-$$

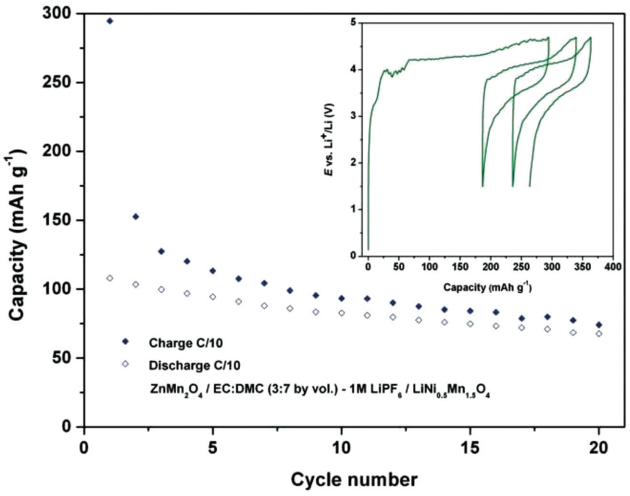

Figure 28. Charge and discharge capacity of a $ZnMn_2O_4/LiMn_{1.5}Ni_{0.5}O_4$ full cell. Inset: voltage–capacity curve of $ZnMn_2O_4/LiMn_{1.5}Ni_{0.5}O_4$ full cell. Reproduced with permission.[485] Copyright 2011, The Royal Society of Chemistry.

However, it is well established that CoO will be further oxidized into Co_3O_4 according to Sharma et al.[486] ($2CoO + 2/3Li_2O \leftrightarrow 2/3Co_3O_4 + 4/3Li^+ + 4/3e^-$). Liu et al.[487] successfully synthesized 3D architectured $ZnCo_2O_4$ nanowire arrays-carbon cloth composites and fabricated a full-cell assembly with a layered-type $LiCoO_2$ cathode. As expected, an irreversible capacity of ≈300 mAh g^{-1} was noted for the first cycle in the half-cell assembly. The NL configuration $LiCoO_2/ZnCo_2O_4$ nanowire array-carbon cloth cell displayed a good cycleability of ≈96% initial capacity retention (≈1300 mAh g^{-1} with respect the anode loading) after 40 cycles. The same group reported the synthesis of $ZnCo_2O_4$ urchins in carbon fiber cloth in a similar process and by varying the reaction time in autoclave.[488] A full-cell $LiCoO_2/ZnCo_2O_4$ urchin-carbon cloth cell with a NL design showed a reversible capacity of ≈1176 mAh g^{-1} with an exceptional cycleability of 50 cycles. Furthermore, bending studies from 30° to 180°were also conducted to ensure the integrity of such a flexible LIB design. Here, 100% reversibility was noted for $ZnCo_2O_4$ nanostructures when coupled with a $LiCoO_2$ cathode, which is somewhat unbelievable. How the authors achieved 100% reversibility in first cycle is a mystery because there was no pre-lithiation conducted for such $ZnCo_2O_4$ nanostructures. Additionally, the authors used an aqueous solution of 1.05 M $LiPF_6$ in EC:DMC as the electrolyte in the full-cell assembly in both works. Although the works reported such spinel $ZnCo_2O_4$ based composites are interesting, we are not sure about the reliability and originality of the mentioned works.

6. Summary and Outlook

Several transition metal based insertion materials are proposed to be the potential alternative to replace the graphitic anodes, but few of them, including $Li_4Ti_5O_{12}$, bronze phase TiO_2, and $TiNb_2O_7$, are only found appealing in terms of cell-safety, cost-effectiveness, compatibility with cathodes, and improved electrochemical activity. Irrespective of the insertion anodes evaluated, the intercalation potential is found to be much higher (>1 V vs. Li) for all the cases compared to the graphitic anodes (<0.1 V vs. Li). Similar to higher insertion potential, the practical reversible capacity is less than that of graphite. Nevertheless, the superior rate capability and redox couple located in the thermodynamic stability window of the conventional aprotic solvents, i.e., SEI–free, makes them attractive candidates to fabricate high power Li-ion power packs. After extensive investigation for over two decades, the spinel $Li_4Ti_5O_{12}$ anode reached into the commercial market with spinel cathodes for EV applications. However, the high performance is realized for the mentioned anode in practical-cell configurations, but unfortunately the reversible capacity is limited to only ≈175 mAh g^{-1}. Therefore, research activities are focused on using anatase TiO_2 as the anodes for LIB applications because of their high theoretical capacity (≈335 mAh g^{-1}), but they show slightly higher potential (≈1.75 V vs. Li) compared to the $Li_4Ti_5O_{12}$ anode (≈1.5 V vs. Li). Unfortunately, the reversibility is limited to ≈0.5 mole instead of one mole, which is inferior compared to the well-established $Li_4Ti_5O_{12}$ chemistry. Nevertheless, the successful reversible Li-insertion into the nanostructured bronze phase with similar physico-chemical properties made a significant breakthrough in the anode research.[61] Interestingly, the insertion potential (≈1.55 V vs. Li) is almost same that of $Li_4Ti_5O_{12}$, which results in a net increase in the energy density of the cell. This is because of the structural arrangement of bronze phase and its capable of delivering high reversibility even at high current rates, i.e., high power capability. This is clearly evident when the bronze phase is coupled with either $LiFePO_4$ or $LiNi_{0.5}Mn_{1.5}O_4$ cathodes compared to $Li_4Ti_5O_{12}$.[60,70] Similar to the bronze phase, $TiNb_2O_7$ is also promising in the recent past because of its high reversible capacity (≈300 mAh g^{-1}), similar working potential (≈1.5 V vs. Li), high power capability, and excellent electrochemical stability upon cycling. The preliminary results indicate that the compatibility and long-term cycleability with spinel cathodes (about 1000 cycles) are promising and could be used to replace the $Li_4Ti_5O_{12}$ anode for the fabrication of high power Li-ion power packs.[274] However, further in-depth studies are required to make them as potential anodes in practical cells before reaching the commercialization. On the other hand, other insertion anodes described displayed either less reversible capacity or higher working potential compared to those three anodes and are interesting for small scale applications and academic research only.

Displacement type anodes exhibit high reversible capacity and high rate capability, but the huge polarization is the main issue while fabricating the full-cell assembly, apart from ICL. Mitigating the ICL issue has been well matured, for example in the beginning days both the cathode and anode were pre-treated to eliminate and accommodate the Li, either chemically or electrochemically. Some reports have also been reported with excess loading of the cathode to overcome the ICL. Presently, only the anode has is pre-treated with Li for few cycles and it is fabricated with conventional cathodes. Nevertheless, the electrochemical pre-treating procedure certainly beneficial in two ways: i) to overcome the ICL and ii) to ensure the electrode performance observed in the respective half-cell assembly. Favorable long-term cycleability (over 1000 cycles) and high power capability were recently reported for Fe_3O_4-porous carbon composites after both chemical and electrochemical

lithiation, but unavoidable variation in the structural changes has to be sacrificed upon cycling, which is clearly evident from the deviation of charge-discharge curves.[355] Similarly, outstanding 10 000 cycles with ≈85% retention was reported for $ZnFe_2O_4$ with a $LiFePO_4$ assembly, however the Zn-based ternary oxides ($ZnFe_2O_4$, $ZnMn_2O_4$, $ZnCo_2O_4$ etc.,) do not fall into the category of pure conversion type anodes.[484] Generally, Zn undergoes an alloying reaction with Li (Li_xZn), apart from the conversion of its respective oxides (ZnO and Fe_2O_3). On the other hand, power capability of the cell is much better than the insertion type anodes based cells, but the energy density has been diluted because of the polarization and wider working potential. The research activities on the development of conversion-type-anode- based practical cells are strongly encouraged from an academic point of view, but very little scope is available for the practical aspects.

Alloying type anodes are fascinating electrodes among the rest discussed above because of their lower working potential (very close to graphite and Li), large reversible capacity, and high power capability. This type of anode has already been commercialized, for example Sony's Nexelion is composed of a Sn-based nanocomposite with mixed layered type cathodes ($LiCoO_2$ + $Li(NiMnCo)O_2$), but unfortunately this has not been extended for high power applications such as EVs and HEVs. Although hundreds of research articles are available for such alloy type anodes, very few of them report practical cell configurations. Initially, Si-based anodes were expected to dominate the future Li-ion battery market due to their salient features described, but they failed to deliver satisfactory results in the half-cell assembly itself. This limited full-cell work is not only for the Si-based anodes and also inclusive of Sn and Ge based materials as well. Moreover the reported limited works in the full-cell configuration are also composed of inferior cycleability, i.e., 100 to 200 cycles only. The performance of alloy-based anodes in thin film conditions displayed much better performance than those in powdered form.[410,415,448] However, such thin film anodes have fewer practical applications and using such anodes to realize the goal of EVs and HEVs is impossible. In addition, the main reason for the limited work on alloy-based materials is ascribed to the unusual volume variation in both crystalline and amorphous conditions upon alloying/de-alloying processes. Either active or inactive matrix element are necessary to uphold such issue and this makes them attractive candidates for the construction of high energy density Li-ion power packs with high power capability. On the contrary, the presence of an amorphous matrix such as Li_2O during deep discharge certainly sustains the unusual unit cell variation for some extend. As a result, improved electrochemical profiles are noted, more clearly SiO_x, and SnO_x is a marginally better candidate than its metallic form in the presence of a carbonaceous matrix. Although a small amount of reversible capacity loss has to be sacrificed, long-term cycleability would be assured. Presently, fabricating a full-cell with either conversion or alloy type anodes is well-matured and long-term cycleability of thousands of cycles has been reported using displacement type anodes. A similar type of strategy is strongly encouraged for alloy-based anodes to realize them in the fabrication of practical cells. Therefore, many research activities are strongly anticipated to demonstrate them in practical configurations with long-term cycleability and high power capability, rather than just testing in half-cell assemblies.

To conclude, significant progress in the insertion type anodes development has been realized and has matured, for example spinel $Li_4Ti_5O_{12}$ anode-based cells have reached the commercial market after the commercialization of graphitic anodes. Bronze phase and $TiNb_2O_7$ exhibit favorable characteristics including high power capability, high reversibility, and similar operating potential to spinel $Li_4Ti_5O_{12}$ and are lined up for commercialization. On the other hand, several alloy-type anodes are potential candidates and are expected to replace the conventional graphitic anodes, but the unusual volume variation and associated cyclic stability hinders them for potential use in practical LIBs. Therefore, much research is anticipated to focus on them to overcome the issues described above and to realize them for the fabrication of high energy density Li-ion power packs with lighter weight and high power capability and to eventually power EVs and HEVs.

Acknowledgments

V.A. and S.M. are thankful for financial support from the Singapore National Research Foundation under its Campus for Research Excellence And Technological Enterprise (CREATE) programme. Y.S.L. acknowledges support from the International Cooperation of the Korea Institute of Energy Technology Evaluation and Planning (KETEP) Grant funded by the Korea government Ministry of Knowledge Economy (No. 20128510010050).

Received: January 13, 2015
Revised: February 16, 2015
Published online:

[1] Y. Nishi, *Chem. Rec.* **2001**, *1*, 406.
[2] N.-S. Choi, Z. Chen, S. A. Freunberger, X. Ji, Y.-K. Sun, K. Amine, G. Yushin, L. F. Nazar, J. Cho, P. G. Bruce, *Angew. Chem. Int. Ed.* **2012**, *51*, 9994.
[3] H. D. Yoo, E. Markevich, G. Salitra, D. Sharon, D. Aurbach, *Mater. Today* **2014**, *17*, 110.
[4] V. Aravindan, J. Gnanaraj, Y.-S. Lee, S. Madhavi, *J. Mater. Chem. A* **2013**, *1*, 3518.
[5] M. M. Thackeray, C. Wolverton, E. D. Isaacs, *Energy Environ. Sci.* **2012**, *5*, 7854.
[6] J. M. Tarascon, M. Armand, *Nature* **2001**, *414*, 359.
[7] P. Saha, M. K. Datta, O. I. Velikokhatnyi, A. Manivannan, D. Alman, P. N. Kumta, *Prog. Mater. Sci.* **2014**, *66*, 1.
[8] T. Sasaki, Y. Ukyo, P. Novák, *Nat. Mater.* **2013**, *12*, 569.
[9] M. S. Whittingham, *Dalton Trans.* **2008**, 5424.
[10] K. Xu, *Chem. Rev.* **2004**, *104*, 4303.
[11] E. M. Erickson, C. Ghanty, D. Aurbach, *J. Phys. Chem. Lett.* **2014**, *5*, 3313.
[12] R. Yazami, P. Touzain, *J. Power Sources* **1983**, *9*, 365.
[13] R. Fong, U. vonSacken, J. R. Dahn, *J. Electrochem. Soc.* **1990**, *137*, 2009.
[14] J. B. Goodenough, K.-S. Park, *J. Am. Chem. Soc.* **2013**, *135*, 1167.
[15] K. Mizushima, P. C. Jones, P. J. Wiseman, J. B. Goodenough, *Mater. Res. Bull.* **1980**, *15*, 783.
[16] E. J. Cairns, P. Albertus, *Annu. Rev. Chem. Biomol. Eng.* **2010**, *1*, 299.
[17] F. Béguin, V. Presser, A. Balducci, E. Frackowiak, *Adv. Mater.* **2014**, *26*, 2219.

[18] V. Aravindan, J. Gnanaraj, Y.-S. Lee, S. Madhavi, *Chem. Rev.* **2014**, *114*, 11619.
[19] V. Aravindan, J. Gnanaraj, S. Madhavi, H.-K. Liu, *Chem. Eur. J.* **2011**, *17*, 14326.
[20] K. Xu, *Chem. Rev.* **2014**, *114*, 11503.
[21] M. N. Obrovac, V. L. Chevrier, *Chem. Rev.* **2014**, *114*, 11444.
[22] M. V. Reddy, G. V. Subba Rao, B. V. R. Chowdari, *Chem. Rev.* **2013**, *113*, 5364.
[23] J. Cabana, L. Monconduit, D. Larcher, M. R. Palacín, *Adv. Mater.* **2010**, *22*, E170.
[24] M. R. Palacin, *Chem. Soc. Rev.* **2009**, *38*, 2565.
[25] P. G. Bruce, B. Scrosati, J.-M. Tarascon, *Angew. Chem. Int. Ed.* **2008**, *47*, 2930.
[26] V. Aravindan, Y. S. Lee, R. Yazami, S. Madhavi, *Mater. Today* **2015**, DOI: 10.1016/j.mattod.2015.02.015
[27] L. Kavan, *Chem. Rec.* **2012**, *12*, 131.
[28] Z. Liu, Y. G. Andreev, A. Robert Armstrong, S. Brutti, Y. Ren, P. G. Bruce, *Prog. Nat. Sci.Mater. Int.* **2013**, *23*, 235.
[29] V. Aravindan, S. Jayaraman, Y.-S. Lee, M. Srinivasan, S. Ramakrishna, P. Suresh Kumar, *Chem. Commun.* **2015**, *51*, 2225.
[30] M. Lazzeri, A. Vittadini, A. Selloni, *Phys. Rev. B* **2001**, *63*, 155409.
[31] W. Q. Fang, X.-Q. Gong, H. G. Yang, *J. Phys. Chem. Lett.* **2011**, *2*, 725.
[32] L. H. Nguyen, V. Aravindan, S. A. Kulkarni, F. Yanan, R. R. Prabhakar, S. K. Batabyal, S. Madhavi, *ChemElectroChem* **2014**, *1*, 539.
[33] Z. Yang, D. Choi, S. Kerisit, K. M. Rosso, D. Wang, J. Zhang, G. Graff, J. Liu, *J. Power Sources* **2009**, *192*, 588.
[34] P. Suresh Kumar, V. Aravindan, J. Sundaramurthy, V. Thavasi, S. G. Mhaisalkar, S. Ramakrishna, S. Madhavi, *RSC Adv.* **2012**, *2*, 7983.
[35] X. Zhang, P. Suresh Kumar, V. Aravindan, H. H. Liu, J. Sundaramurthy, S. G. Mhaisalkar, H. M. Duong, S. Ramakrishna, S. Madhavi, *J. Phys. Chem. C* **2012**, *116*, 14780.
[36] K. Mukai, K. Ariyoshi, T. Ohzuku, *J. Power Sources* **2005**, *146*, 213.
[37] J.-Y. Shin, D. Samuelis, J. Maier, *Adv. Funct. Mater.* **2011**, *21*, 3464.
[38] V. Aravindan, N. Shubha, Y. L. Cheah, R. Prasanth, W. Chuiling, R. R. Prabhakar, S. Madhavi, *J. Mater. Chem. A* **2013**, *1*, 308.
[39] V. Aravindan, N. Shubha, W. C. Ling, S. Madhavi, *J. Mater. Chem. A* **2013**, *1*, 6145.
[40] I. Exnar, L. Kavan, S. Y. Huang, M. Grätzel, *J. Power Sources* **1997**, *68*, 720.
[41] S. Y. Huang, L. Kavan, I. Exnar, M. Grätzel, *J. Electrochem. Soc.* **1995**, *142*, L142.
[42] V. Subramanian, A. Karki, K. I. Gnanasekar, F. P. Eddy, B. Rambabu, *J. Power Sources* **2006**, *159*, 186.
[43] A. Moretti, G.-T. Kim, D. Bresser, K. Renger, E. Paillard, R. Marassi, M. Winter, S. Passerini, *J. Power Sources* **2013**, *221*, 419.
[44] V. Aravindan, J. Sundaramurthy, P. S. Kumar, N. Shubha, W. C. Ling, S. Ramakrishna, S. Madhavi, *Nanoscale* **2013**, *5*, 10636.
[45] X. Xin, X. Zhou, J. Wu, X. Yao, Z. Liu, *ACS Nano* **2012**, *6*, 11035.
[46] N. Arun, V. Aravindan, S. Jayaraman, N. Shubha, W. C. Ling, S. Ramakrishna, S. Madhavi, *Nanoscale* **2014**, *6*, 8926.
[47] S. Brutti, V. Gentili, P. Reale, L. Carbone, S. Panero, *J. Power Sources* **2011**, *196*, 9792.
[48] N. Plylahan, M. Letiche, M. K. S. Barr, T. Djenizian, *Electrochem. Commun.* **2014**, *43*, 121.
[49] D. Choi, D. Wang, V. V. Viswanathan, I.-T. Bae, W. Wang, Z. Nie, J.-G. Zhang, G. L. Graff, J. Liu, Z. Yang, T. Duong, *Electrochem. Commun.* **2010**, *12*, 378.
[50] X. Zhang, V. Aravindan, P. S. Kumar, H. Liu, J. Sundaramurthy, S. Ramakrishna, S. Madhavi, *Nanoscale* **2013**, *5*, 5973.
[51] M. Mancini, F. Nobili, R. Tossici, M. Wohlfahrt-Mehrens, R. Marassi, *J. Power Sources* **2011**, *196*, 9665.
[52] F.-F. Cao, X.-L. Wu, S. Xin, Y.-G. Guo, L.-J. Wan, *J. Phys. Chem. C* **2010**, *114*, 10308.
[53] P. Prosini, C. Cento, A. Pozio, *J. Solid State Electrochem.* **2014**, *18*, 795.
[54] H. Ming, J. Ming, S.-M. Oh, E.-J. Lee, H. Huang, Q. Zhou, J. Zheng, Y.-K. Sun, *J. Mater. Chem. A* **2014**, *2*, 18938.
[55] E. Baudrin, S. Cassaignon, M. Koelsch, J. P. Jolivet, L. Dupont, J. M. Tarascon, *Electrochem. Commun.* **2007**, *9*, 337.
[56] Y. S. Hu, L. Kienle, Y. G. Guo, J. Maier, *Adv. Mater.* **2006**, *18*, 1421.
[57] J. Hassoun, M. Pfanzelt, P. Kubiak, M. Wohlfahrt-Mehrens, B. Scrosati, *J. Power Sources* **2012**, *217*, 459.
[58] A. R. Armstrong, G. Armstrong, J. Canales, R. García, P. G. Bruce, *Adv. Mater.* **2005**, *17*, 862.
[59] S. Brutti, V. Gentili, H. Menard, B. Scrosati, P. G. Bruce, *Adv. Energy. Mater.* **2012**, *2*, 322.
[60] G. Armstrong, A. R. Armstrong, P. G. Bruce, P. Reale, B. Scrosati, *Adv. Mater.* **2006**, *18*, 2597.
[61] A. R. Armstrong, G. Armstrong, J. Canales, P. G. Bruce, *Angew. Chem. Int. Ed.* **2004**, *43*, 2286.
[62] Y. Ren, Z. Liu, F. Pourpoint, A. R. Armstrong, C. P. Grey, P. G. Bruce, *Angew. Chem. Int. Ed.* **2012**, *51*, 2164.
[63] G. Armstrong, A. R. Armstrong, J. Canales, P. G. Bruce, *Chem. Commun.* **2005**, 2454.
[64] A. R. Armstrong, G. Armstrong, J. Canales, P. G. Bruce, *J. Power Sources* **2005**, *146*, 501.
[65] P. G. Bruce, *Solid State Ionics* **2008**, *179*, 752.
[66] Y. G. Andreev, P. M. Panchmatia, Z. Liu, S. C. Parker, M. S. Islam, P. G. Bruce, *J. Am. Chem. Soc.* **2014**, *136*, 6306.
[67] M. Zukalová, M. Kalbáč, L. Kavan, I. Exnar, M. Graetzel, *Chem. Mater.* **2005**, *17*, 1248.
[68] A. G. Dylla, G. Henkelman, K. J. Stevenson, *Acc. Chem. Res.* **2013**, *46*, 1104.
[69] M. Edisson Jr., P. M. Jardim, A. M. Bojan, C. R. Fernando, A. S. d. A. Marco, L. Z. José, S. A. Antonio, *Nanotechnol.* **2007**, *18*, 495710.
[70] Z. Guo, X. Dong, D. Zhou, Y. Du, Y. Wang, Y. Xia, *RSC Adv.* **2013**, *3*, 3352.
[71] N. Takami, Y. Harada, T. Iwasaki, K. Hoshina, Y. Yoshida, *J. Power Sources* **2015**, *273*, 923.
[72] M. S. Whittingham, *Chem. Rev.* **2004**, *104*, 4271.
[73] N. A. Chernova, M. Roppolo, A. C. Dillon, M. S. Whittingham, *J. Mater. Chem.* **2009**, *19*, 2526.
[74] Y. L. Cheah, V. Aravindan, S. Madhavi, *ACS Appl. Mater. Interfaces* **2012**, *4*, 3270.
[75] Y. L. Cheah, V. Aravindan, S. Madhavi, *ACS Appl. Mater. Interfaces* **2013**, *5*, 3475.
[76] V. Aravindan, Y. L. Cheah, W. F. Mak, G. Wee, B. V. R. Chowdari, S. Madhavi, *ChemPlusChem* **2012**, *77*, 570.
[77] Y. L. Cheah, V. Aravindan, S. Madhavi, *J. Electrochem. Soc.* **2012**, *159*, A273.
[78] Y. L. Cheah, N. Gupta, S. S. Pramana, V. Aravindan, G. Wee, M. Srinivasan, *J. Power Sources* **2011**, *196*, 6465.
[79] Y. L. Cheah, V. Aravindan, S. Madhavi, *J. Electrochem. Soc.* **2012**, *159*, A273.
[80] Y. L. Cheah, V. Aravindan, S. Madhavi, *J. Electrochem. Soc.* **2013**, *160*, A1016.
[81] Y. L. Cheah, R. vonHagen, V. Aravindan, R. Fiz, S. Mathur, S. Madhavi, *Nano Energy* **2013**, *2*, 57.
[82] T. Chirayil, P. Y. Zavalij, M. S. Whittingham, *Chem. Mater.* **1998**, *10*, 2629.
[83] G. Armstrong, J. Canales, A. R. Armstrong, P. G. Bruce, *J. Power Sources* **2008**, *178*, 723.
[84] V. Aravindan, Y. L. Cheah, W. C. Ling, S. Madhavi, *J. Electrochem. Soc.* **2012**, *159*, A1435.
[85] G. Wee, H. Z. Soh, Y. L. Cheah, S. G. Mhaisalkar, M. Srinivasan, *J. Mater. Chem.* **2010**, *20*, 6720.

[86] M. Ulaganathan, A. Jain, V. Aravindan, S. Jayaraman, W. C. Ling, T. M. Lim, M. P. Srinivasan, Q. Yan, S. Madhavi, *J. Power Sources* **2015**, *274*, 846.
[87] L. Kong, Z. Liu, M. Shao, Q. Xie, W. Yu, Y. Qian, *J. Solid State Chem.* **2004**, *177*, 690.
[88] N. Ding, X. Feng, S. Liu, J. Xu, X. Fang, I. Lieberwirth, C. Chen, *Electrochem. Commun.* **2009**, *11*, 538.
[89] J. Jiang, J. R. Dahn, *J. Electrochem. Soc.* **2006**, *153*, A310.
[90] S. Patoux, C. Masquelier, *Chem. Mater.* **2002**, *14*, 5057.
[91] K. Ariyoshi, R. Yamato, T. Ohzuku, *Electrochim. Acta* **2005**, *51*, 1125.
[92] S. Scharner, W. Weppner, P. Schmid-Beurmann, *J. Electrochem. Soc.* **1999**, *146*, 857.
[93] T. Ohzuku, A. Ueda, N. Yamamoto, *J. Electrochem. Soc.* **1995**, *142*, 1431.
[94] A. Jain, V. Aravindan, S. Jayaraman, P. S. Kumar, R. Balasubramanian, S. Ramakrishna, S. Madhavi, M. Srinivasan, *Sc. Rep.* **2013**, *3*, 3002.
[95] K. Naoi, W. Naoi, S. Aoyagi, J.-i. Miyamoto, T. Kamino, *Acc. Chem. Res.* **2013**, *46*, 1075.
[96] K. Naoi, S. Ishimoto, Y. Isobe, S. Aoyagi, *J. Power Sources* **2010**, *195*, 6250.
[97] S. Takai, M. Kamata, S. Fujine, K. Yoneda, K. Kanda, T. Esaka, *Solid State Ionics* **1999**, *123*, 165.
[98] K. Naoi, S. Ishimoto, J.-i. Miyamoto, W. Naoi, *Energy Environ. Sci.* **2012**, *5*, 9363.
[99] K. Naoi, *Fuel Cells* **2010**, *10*, 825.
[100] K. Naoi, Y. Nagano, *Supercapacitors*, Wiley-VCH Verlag GmbH & Co. KGaA, Weinheim, Germany, **2013**, pp. 239–256.
[101] E. Ferg, R. J. Gummow, A. deKock, M. M. Thackeray, *J. Electrochem. Soc.* **1994**, *141*, L147.
[102] N. Takami, H. Inagaki, T. Kishi, Y. Harada, Y. Fujita, K. Hoshina, *J. Electrochem. Soc.* **2009**, *156*, A128.
[103] G. X. Wang, D. H. Bradhurst, S. X. Dou, H. K. Liu, *J. Power Sources* **1999**, *83*, 156.
[104] A. N. Jansen, A. J. Kahaian, K. D. Kepler, P. A. Nelson, K. Amine, D. W. Dees, D. R. Vissers, M. M. Thackeray, *J. Power Sources* **1999**, 81–82, 902.
[105] M. Majima, S. Ujiie, E. Yagasaki, K. Koyama, S. Inazawa, *J. Power Sources* **2001**, *101*, 53.
[106] A. M. Stux, K. E. Swider-Lyons, *J. Power Sources* **2007**, *165*, 635.
[107] J. H. Kim, S.-y. Bae, J.-H. Min, S.-W. Song, D.-W. Kim, *Electrochim. Acta* **2012**, *78*, 11.
[108] J. C. Burns, G. Jain, A. J. Smith, K. W. Eberman, E. Scott, J. P. Gardner, J. R. Dahn, *J. Electrochem. Soc.* **2011**, *158*, A255.
[109] T. Brousse, P. Fragnaud, R. Marchand, D. M. Schleich, O. Bohnke, K. West, *J. Power Sources* **1997**, *68*, 412.
[110] A. Mahmoud, J. M. Amarilla, K. Lasri, I. Saadoune, *Electrochim. Acta* **2013**, *93*, 163.
[111] K. Sawai, R. Yamato, T. Ohzuku, *Electrochim. Acta* **2006**, *51*, 1651.
[112] A. D. Pasquier, I. Plitz, J. Gural, F. Badway, G. G. Amatucci, *J. Power Sources* **2004**, *136*, 160.
[113] G. G. Amatucci, F. Badway, A. Du Pasquier, T. Zheng, *J. Electrochem. Soc.* **2001**, *148*, A930.
[114] I. Plitz, A. DuPasquier, F. Badway, J. Gural, N. Pereira, A. Gmitter, G. G. Amatucci, *Appl. Phys. A* **2006**, *82*, 615.
[115] X. Hu, Z. Deng, J. Suo, Z. Pan, *J. Power Sources* **2009**, *187*, 635.
[116] S. Chen, H. Hu, C. Wang, G. Wang, J. Yin, D. Cao, *J. Renewable Sustainable Energy* **2012**, *4*, 033114.
[117] X. Hu, Y. Huai, Z. Lin, J. Suo, Z. Deng, *J. Electrochem. Soc.* **2007**, *154*, A1026.
[118] X. B. Hu, Z. J. Lin, L. Liu, Y. J. Huai, Z. H. Deng, *J. Serb. Chem. Soc.* **2010**, *75*, 1259.
[119] K. Naoi, *Meet. Abstr.* **2012**, *MA2012–02*, 519.
[120] L. Hu, H. Wu, F. LaMantia, Y. Yang, Y. Cui, *ACS Nano* **2010**, *4*, 5843.
[121] L. Hu, J. W. Choi, Y. Yang, S. Jeong, F. LaMantia, L.-F. Cui, Y. Cui, *Proc. Natl. Acad. Sci.USA* **2009**, *106*, 21490.
[122] N. Aliahmad, M. Agarwal, S. Shrestha, K. Varahramyan, *Nanotechnol., IEEE Trans.* **2013**, *12*, 408.
[123] J. Liu, K. Song, P. A. vanAken, J. Maier, Y. Yu, *Nano Lett.* **2014**, *14*, 2597.
[124] S. Chen, Y. Xin, Y. Zhou, Y. Ma, H. Zhou, L. Qi, *Energy Environ. Sci.* **2014**, *7*, 1924.
[125] S.-H. Kim, K.-H. Choi, S.-J. Cho, J.-S. Park, K. Y. Cho, C. K. Lee, S. B. Lee, J. K. Shim, S.-Y. Lee, *J. Mater. Chem. A* **2014**, *2*, 10854.
[126] K.-H. Choi, S.-J. Cho, S.-H. Kim, Y. H. Kwon, J. Y. Kim, S.-Y. Lee, *Adv. Funct. Mater.* **2014**, *24*, 44.
[127] S. Xu, Y. Zhang, J. Cho, J. Lee, X. Huang, L. Jia, J. A. Fan, Y. Su, J. Su, H. Zhang, H. Cheng, B. Lu, C. Yu, C. Chuang, T. I. Kim, T. Song, K. Shigeta, S. Kang, C. Dagdeviren, I. Petrov, P. V. Braun, Y. Huang, U. Paik, J. A. Rogers, *Nat. Commun.* **2013**, *4*.
[128] G. Zheng, Y. Cui, E. Karabulut, L. Wågberg, H. Zhu, L. Hu, *MRS Bull.* **2013**, *38*, 320.
[129] A. M. Gaikwad, B. V. Khau, G. Davies, B. Hertzberg, D. A. Steingart, A. C. Arias, *Adv. Energy Mater.* **2015**, *5*, 1401389.
[130] J. Guo, J. Liu, *RSC Adv.* **2014**, *4*, 12950.
[131] P. Svens, R. Eriksson, J. Hansson, M. Behm, T. Gustafsson, G. Lindbergh, *J. Power Sources* **2014**, *270*, 131.
[132] J. Wang, M. W. Verbrugge, P. Liu, *J. Electrochem. Soc.* **2010**, *157*, A185.
[133] Q. Cheng, Z. Song, T. Ma, B. B. Smith, R. Tang, H. Yu, H. Jiang, C. K. Chan, *Nano Lett.* **2013**, *13*, 4969.
[134] T. Ohzuku, K. Ariyoshi, *Chem. Lett.* **2006**, *35*, 848.
[135] K. Ariyoshi, T. Ohzuku, *J. Power Sources* **2007**, *174*, 1258.
[136] I. Belharouak, G. M. Koenig Jr, K. Amine, *J. Power Sources* **2011**, *196*, 10344.
[137] O. K. Park, Y. Cho, S. Lee, H.-C. Yoo, H.-K. Song, J. Cho, *Energy Environ. Sci.* **2011**, *4*, 1621.
[138] I. Belharouak, Y.-K. Sun, W. Lu, K. Amine, *J. Electrochem. Soc.* **2007**, *154*, A1083.
[139] K. Amine, I. Belharouak, Z. Chen, T. Tran, H. Yumoto, N. Ota, S.-T. Myung, Y.-K. Sun, *Adv. Mater.* **2010**, *22*, 3052.
[140] N. Takami, H. Inagaki, Y. Tatebayashi, H. Saruwatari, K. Honda, S. Egusa, *J. Power Sources* **2013**, *244*, 469.
[141] G. G. Amatucci, N. Pereira, T. Zheng, J.-M. Tarascon, *J. Electrochem. Soc.* **2001**, *148*, A171.
[142] G. Amatucci, A. Du Pasquier, A. Blyr, T. Zheng, J. M. Tarascon, *Electrochim. Acta* **1999**, *45*, 255.
[143] C. M. Ionica-Bousquet, D. Muñoz-Rojas, W. J. Casteel, R. M. Pearlstein, G. GirishKumar, G. P. Pez, M. R. Palacín, *J. Power Sources* **2010**, *195*, 1479.
[144] A. Du Pasquier, C. C. Huang, T. Spitler, *J. Power Sources* **2009**, *186*, 508.
[145] L. J. Xi, H. K. Wang, S. L. Yang, R. G. Ma, Z. G. Lu, C. W. Cao, K. L. Leung, J. Q. Deng, A. L. Rogach, C. Y. Chung, *J. Power Sources* **2013**, *242*, 222.
[146] W. Lu, I. Belharouak, J. Liu, K. Amine, *J. Power Sources* **2007**, *174*, 673.
[147] W. Cui, Y.-B. He, Z.-Y. Tang, Q.-H. Yang, Q. Xu, F.-Y. Su, L. Ma, *J. Solid State Electrochem.* **2012**, *16*, 265.
[148] J. Jiang, J. Chen, J. R. Dahn, *J. Electrochem. Soc.* **2004**, *151*, A2082.
[149] D. Peramunage, K. M. Abraham, *J. Electrochem. Soc.* **1998**, *145*, 2609.
[150] D. Peramunage, K. M. Abraham, *J. Electrochem. Soc.* **1998**, *145*, 2615.
[151] J. Christensen, V. Srinivasan, J. Newman, *J. Electrochem. Soc.* **2006**, *153*, A560.

[152] P. Reale, S. Panero, B. Scrosati, *J. Electrochem. Soc.* **2005**, *152*, A1949.
[153] P. Reale, S. Panero, B. Scrosati, J. Garche, M. Wohlfahrt-Mehrens, M. Wachtler, *J. Electrochem. Soc.* **2004**, *151*, A2138.
[154] P. Reale, A. Fernicola, B. Scrosati, *J. Power Sources* **2009**, *194*, 182.
[155] Z. Wang, Z. Wang, W. Peng, H. Guo, X. Li, *Ceram. Int.* **2014**, *40*, 10053.
[156] M. Thunman, K. Marquardt, R. Hahn, D. Kober, O. Goerke, H. Schubert, *ECS Trans.* **2012**, *41*, 147.
[157] X. Wang, B. Liu, X. Hou, Q. Wang, W. Li, D. Chen, G. Shen, *Nano Res.* **2014**, *7*, 1073.
[158] I. Belharouak, G. M. Koenig, T. Tan, H. Yumoto, N. Ota, K. Amine, *J. Electrochem. Soc.* **2012**, *159*, A1165.
[159] Y. Zhao, Q. Zhou, L. Liu, J. Xu, M. Yan, Z. Jiang, *Electrochim. Acta* **2006**, *51*, 2639.
[160] K. Wu, J. Yang, Y. Zhang, C. Wang, D. Wang, *J. Appl. Electrochem.* **2012**, *42*, 989.
[161] K. Wu, J. Yang, Y. Liu, Y. Zhang, C. Wang, J. Xu, F. Ning, D. Wang, *J. Power Sources* **2013**, *237*, 285.
[162] N. Yabuuchi, T. Ohzuku, *J. Power Sources* **2005**, *146*, 636.
[163] W. Lu, J. Liu, Y. K. Sun, K. Amine, *J. Power Sources* **2007**, *167*, 212.
[164] X. Guo, H. F. Xiang, T. P. Zhou, W. H. Li, X. W. Wang, J. X. Zhou, Y. Yu, *Electrochim. Acta* **2013**, *109*, 33.
[165] K. Chen, Z. Yu, S. Deng, Q. Wu, J. Zou, X. Zeng, *J. Power Sources* **2015**, *278*, 411.
[166] M. Imazaki, K. Ariyoshi, T. Ohzuku, *J. Electrochem. Soc.* **2009**, *156*, A780.
[167] M. Imazaki, L. Wang, T. Kawai, K. Ariyoshi, T. Ohzuku, *Electrochim. Acta* **2011**, *56*, 4576.
[168] K. Ariyoshi, E. Iwata, M. Kuniyoshi, H. Wakabayashi, T. Ohzuku, *Electrochem. Solid-State Lett.* **2006**, *9*, A557.
[169] L. Wang, K. Nakura, M. Imazaki, N. Kakizaki, K. Ariyoshi, T. Ohzuku, *J. Electrochem. Soc.* **2012**, *159*, A1710.
[170] Y.-B. He, B. Li, M. Liu, C. Zhang, W. Lv, C. Yang, J. Li, H. Du, B. Zhang, Q.-H. Yang, J.-K. Kim, F. Kang, *Sci. Rep.* **2012**, *2*, 913.
[171] R. Bernhard, S. Meini, H. A. Gasteiger, *J. Electrochem. Soc.* **2014**, *161*, A497.
[172] S. Jayaraman, V. Aravindan, P. Suresh Kumar, W. C. Ling, S. Ramakrishna, S. Madhavi, *Chem. Commun.* **2013**, *49*, 6677.
[173] C. Julien, K. Zaghib, A. Mauger, H. Groult, *Adv. Chem. Eng. Sci.* **2012**, *2*, 321.
[174] J. Morales, R. Trócoli, S. Franger, J. Santos-Peña, *Electrochim. Acta* **2010**, *55*, 3075.
[175] S. Franger, C. Bourbon, F. LeCras, *J. Electrochem. Soc.* **2004**, *151*, A1024.
[176] J. S. Wang, P. Liu, S. Soukiazian, H. Tataria, M. Dontigny, A. Guerfi, K. Zaghib, M. W. Verbrugge, *J. Power Sources* **2014**, *256*, 288.
[177] A. K. Padhi, K. S. Nanjundaswamy, J. B. Goodenough, *J. Electrochem. Soc.* **1997**, *144*, 1188.
[178] W. H. Jang, M. C. Kim, S. N. Lee, J. Y. Ahn, V. Aravindan, Y.-S. Lee, *J. Alloys Compd.* **2014**.
[179] S. Lee, S. Cho, J. Heo, V. Aravindan, H. Kim, Y. Lee, *J. Alloys Compd.* **2009**, *488*, 380.
[180] S. Lee, I. Jang, H. Lim, V. Aravindan, H. Kim, Y. Lee, *J. Alloys Compd.* **2010**, *491*, 668.
[181] H. Lim, I. Jang, S. Lee, K. Karthikeyan, V. Aravindan, Y. Lee, *J. Alloys Compd.* **2010**, *495*, 181.
[182] C. G. Son, H. M. Yang, G. W. Lee, A. R. Cho, V. Aravindan, H. S. Kim, W. S. Kim, Y. S. Lee, *J. Alloys Compd.* **2011**, *509*, 1279.
[183] L. Q. Sun, R. H. Cui, A. F. Jalbout, M. J. Li, X. M. Pan, R. S. Wang, H. M. Xie, *J. Power Sources* **2009**, *189*, 522.
[184] W. Wang, D. Choi, Z. Yang, *Metall. Mater. Trans. A* **2013**, *44*, 21.
[185] A. Jaiswal, C. R. Horne, O. Chang, W. Zhang, W. Kong, E. Wang, T. Chern, M. M. Doeff, *J. Electrochem. Soc.* **2009**, *156*, A1041.
[186] C.-C. Yang, H.-C. Hu, S. J. Lin, W.-C. Chien, *J. Power Sources* **2014**, *258*, 424.
[187] W. Jin, L. Linlin, W. Chui Ling, M. Srinivasan, *Nanotechnology* **2012**, *23*, 495401.
[188] Y.-H. Lee, J.-S. Kim, J. Noh, I. Lee, H. J. Kim, S. Choi, J. Seo, S. Jeon, T.-S. Kim, J.-Y. Lee, J. W. Choi, *Nano Lett.* **2013**, *13*, 5753.
[189] J.-S. Kim, Y.-H. Lee, I. Lee, T.-S. Kim, M.-H. Ryou, J. W. Choi, *J. Mater. Chem. A* **2014**, *2*, 10862.
[190] L. Hu, F. LaMantia, H. Wu, X. Xie, J. McDonough, M. Pasta, Y. Cui, *Adv. Energy. Mater.* **2011**, *1*, 1012.
[191] L. Jabbour, R. Bongiovanni, D. Chaussy, C. Gerbaldi, D. Beneventi, *Cellulose* **2013**, *20*, 1523.
[192] Y. Lei, Z.-H. Huang, W. Shen, F. Kang, Y. Zheng, *Electrochim. Acta* **2013**, *107*, 413.
[193] N. Li, Z. Chen, W. Ren, F. Li, H.-M. Cheng, *Proc. Natl. Acad. Sci. USA* **2012**, *109*, 17360.
[194] K. Zaghib, M. Dontigny, P. Perret, A. Guerfi, M. Ramanathan, J. Prakash, A. Mauger, C. M. Julien, *J. Power Sources* **2014**, *248*, 1050.
[195] K. Zaghib, M. Dontigny, A. Guerfi, P. Charest, I. Rodrigues, A. Mauger, C. M. Julien, *J. Power Sources* **2011**, *196*, 3949.
[196] H. Srour, H. Rouault, C. C. Santini, *J. Electrochem. Soc.* **2013**, *160*, A781.
[197] G. T. Kim, S. S. Jeong, M. Joost, E. Rocca, M. Winter, S. Passerini, A. Balducci, *J. Power Sources* **2011**, *196*, 2187.
[198] A. Moretti, S. Jeong, G. A. Giffin, S. Jeremias, S. Passerini, *J. Power Sources* **2014**, *269*, 645.
[199] A. Swiderska-Mocek, *Electrochim. Acta* **2014**, *139*, 337.
[200] K. Zaghib, M. Dontigny, A. Guerfi, J. Trottier, J. Hamel-Paquet, V. Gariepy, K. Galoutov, P. Hovington, A. Mauger, H. Groult, C. M. Julien, *J. Power Sources* **2012**, *216*, 192.
[201] L. M. Moshuchak, M. Bulinski, W. M. Lamanna, R. L. Wang, J. R. Dahn, *Electrochem. Commun.* **2007**, *9*, 1497.
[202] M. Wakihara, Y. Kadoma, N. Kumagai, H. Mita, R. Araki, K. Ozawa, Y. Ozawa, *J. Solid State Electrochem.* **2012**, *16*, 847.
[203] S. Choi, T.-H. Kim, J.-I. Lee, J. Kim, H.-K. Song, S. Park, *ChemSusChem* **2014**, *7*, 3483.
[204] S. K. Martha, O. Haik, V. Borgel, E. Zinigrad, I. Exnar, T. Drezen, J. H. Miners, D. Aurbach, *J. Electrochem. Soc.* **2011**, *158*, A790.
[205] V. Ramar, K. Saravanan, S. R. Gajjela, S. Hariharan, P. Balaya, *Electrochim. Acta* **2013**, *105*, 496.
[206] S. K. Martha, J. Grinblat, O. Haik, E. Zinigrad, T. Drezen, J. H. Miners, I. Exnar, A. Kay, B. Markovsky, D. Aurbach, *Angew. Chem. Int. Ed.* **2009**, *48*, 8559.
[207] V. Borgel, G. Gershinsky, T. Hu, M. G. Theivanayagam, D. Aurbach, *J. Electrochem. Soc.* **2013**, *160*, A650.
[208] C.-C. Yang, H.-J. Hwu, S. J. Lin, W.-C. Chien, J.-Y. Shih, *Electrochim. Acta* **2014**, *125*, 637.
[209] Q.-Q. Zou, G.-N. Zhu, Y.-Y. Xia, *J. Power Sources* **2012**, *206*, 222.
[210] R. Sharabi, E. Markevich, V. Borgel, G. Salitra, G. Gershinsky, D. Aurbach, G. Semrau, M. A. Schmidt, N. Schall, C. Stinner, *J. Power Sources* **2012**, *203*, 109.
[211] E. Markevich, R. Sharabi, H. Gottlieb, V. Borgel, K. Fridman, G. Salitra, D. Aurbach, G. Semrau, M. A. Schmidt, N. Schall, C. Bruenig, *Electrochem. Commun.* **2012**, *15*, 22.
[212] J. Ni, W. Liu, J. Liu, L. Gao, J. Chen, *Electrochem. Commun.* **2013**, *35*, 1.
[213] C. Du, Z. Tang, J. Wu, H. Tang, X. Zhang, *Electrochim. Acta* **2014**, *125*, 58.
[214] S. Amaresh, G. J. Kim, K. Karthikeyan, V. Aravindan, K. Y. Chung, B. W. Cho, Y. S. Lee, *Phys. Chem. Chem. Phys.* **2012**, *14*, 11904.
[215] S. Okada, M. Ueno, Y. Uebou, J.-i. Yamaki, *J. Power Sources* **2005**, *146*, 565.
[216] I. C. Jang, H. Lim, S. Lee, K. Karthikeyan, V. Aravindan, K. Kang, W. Yoon, W. Cho, Y. Lee, *J. Alloys Compd.* **2010**, *497*, 321.

[217] S. M. G. Yang, V. Aravindan, W. I. Cho, D. R. Chang, H. S. Kim, Y. S. Lee, *J. Electrochem. Soc.* **2012**, *159*, A1013.
[218] I. C. Jang, C. G. Son, S. M. G. Yang, J. W. Lee, A. R. Cho, V. Aravindan, G. J. Park, K. S. Kang, W. S. Kim, W. I. Cho, Y. S. Lee, *J. Mater. Chem.* **2011**, *21*, 6510.
[219] K. Amine, H. Yasuda, M. Yamachi, *Electrochem. Solid-State Lett.* **2000**, *3*, 178.
[220] X. Wu, Z. Gong, S. Tan, Y. Yang, *J. Power Sources* **2012**, *220*, 122.
[221] S. Panero, D. Satolli, M. Salomon, B. Scrosati, *Electrochem. Commun.* **2000**, *2*, 810.
[222] X. Huang, M. Lin, Q. Tong, X. Li, Y. Ruan, Y. Yang, *J. Power Sources* **2012**, *202*, 352.
[223] J. Barker, R. K. B. Gover, P. Burns, A. J. Bryan, *Electrochem. Solid-State Lett.* **2007**, *10*, A130.
[224] T. Ohzuku, A. Ueda, N. Yamamoto, Y. Iwakoshi, *J. Power Sources* **1995**, *54*, 99.
[225] W.-f. Mao, N.-n. Zhang, Z.-y. Tang, Y.-q. Feng, C.-x. Ma, *J. Alloys Compd.* **2014**, *588*, 25.
[226] J. Barker, R. K. B. Gover, P. Burns, A. J. Bryan, *J. Electrochem. Soc.* **2007**, *154*, A882.
[227] W. K. Pang, N. Sharma, V. K. Peterson, J.-J. Shiu, S.-h. Wu, *J. Power Sources* **2014**, *246*, 464.
[228] M. C. Kim, K.-W. Nam, E. Hu, X.-Q. Yang, H. Kim, K. Kang, V. Aravindan, W.-S. Kim, Y.-S. Lee, *ChemSusChem* **2014**, *7*, 829.
[229] M. C. Kim, S. H. Kim, V. Aravindan, W. S. Kim, S. Y. Lee, Y. S. Lee, *J. Electrochem. Soc.* **2013**, *160*, A1003.
[230] R. Santhanam, B. Rambabu, *J. Power Sources* **2010**, *195*, 5442.
[231] W. H. Jang, M. C. Kim, S. H. Kim, V. Aravindan, W. S. Kim, Y.-S. Lee, *Electrochim. Acta.*
[232] W. H. Jang, M. C. Kim, S. N. Lee, J. Y. Ahn, V. Aravindan, Y. S. Lee, *J. Alloys Compd.* **2014**, *612*, 51.
[233] N. Arun, A. Jain, V. Aravindan, S. Jayaraman, W. Chui Ling, M. P. Srinivasan, S. Madhavi, *Nano Energy* **2015**, *12*, 69.
[234] N. Arun, V. Aravindan, W. C. Ling, S. Madhavi, *J. Power Sources* **2015**, *280*, 240.
[235] K. Ariyoshi, S. Yamamoto, T. Ohzuku, *J. Power Sources* **2003**, *119–121*, 959.
[236] K. Ariyoshi, R. Yamato, Y. Makimura, T. Amazutsumi, Y. Maeda, T. Ohzuku, *Electrochem.* **2008**, *76*, 46.
[237] T. Amazutsumi, K. Ariyoshi, K. Okumura, T. Ohzuku, *Electrochem.* **2007**, *75*, 867.
[238] T. Ohzuku, K. Ariyoshi, S. Yamamoto, Y. Makimura, *Chem. Lett.* **2001**, *30*, 1270.
[239] K. Ariyoshi, Y. Maeda, T. Kawai, T. Ohzuku, *J. Electrochem. Soc.* **2011**, *158*, A281.
[240] S. Patoux, L. Sannier, H. Lignier, Y. Reynier, C. Bourbon, S. Jouanneau, F. LeCras, S. Martinet, *Electrochim. Acta* **2008**, *53*, 4137.
[241] S. Patoux, L. Daniel, C. Bourbon, H. Lignier, C. Pagano, F. LeCras, S. Jouanneau, S. Martinet, *J. Power Sources* **2009**, *189*, 344.
[242] A. Kraytsberg, Y. Ein-Eli, *Adv. Energy Mater.* **2012**, *2*, 922.
[243] H. M. Wu, I. Belharouak, H. Deng, A. Abouimrane, Y.-K. Sun, K. Amine, *J. Electrochem. Soc.* **2009**, *156*, A1047.
[244] H. F. Xiang, X. Zhang, Q. Y. Jin, C. P. Zhang, C. H. Chen, X. W. Ge, *J. Power Sources* **2008**, *183*, 355.
[245] S. R. Li, C. H. Chen, J. R. Dahn, *J. Electrochem. Soc.* **2013**, *160*, A2166.
[246] S. R. Li, N. N. Sinha, C. H. Chen, K. Xu, J. R. Dahn, *J. Electrochem. Soc.* **2013**, *160*, A2014.
[247] H. F. Xiang, Q. Y. Jin, R. Wang, C. H. Chen, X. W. Ge, *J. Power Sources* **2008**, *179*, 351.
[248] H. G. Jung, M. W. Jang, J. Hassoun, Y. K. Sun, B. Scrosati, *Nat. Commun.* **2011**, *2*.
[249] J.-H. Kim, N. P. W. Pieczonka, Y.-K. Sun, B. R. Powell, *J. Power Sources* **2014**, *262*, 62.
[250] Y.-L. Ding, B. M. Goh, H. Zhang, K. P. Loh, L. Lu, *J. Power Sources* **2013**, *236*, 1.
[251] D. I. Choi, H. Lee, D. J. Lee, K.-W. Nam, J.-S. Kim, R. A. Huggins, J.-K. Park, J. W. Choi, *J. Mater. Chem. A* **2013**, *1*, 5320.
[252] S. R. Li, C. H. Chen, X. Xia, J. R. Dahn, *J. Electrochem. Soc.* **2013**, *160*, A1524.
[253] R. Dedryvère, D. Foix, S. Franger, S. Patoux, L. Daniel, D. Gonbeau, *J. Phys. Chem. C* **2010**, *114*, 10999.
[254] K. Nakura, Y. Ohsugi, M. Imazaki, K. Ariyoshi, T. Ohzuku, *J. Electrochem. Soc.* **2011**, *158*, A1243.
[255] T. Ohzuku, R. Yamato, T. Kawai, K. Ariyoshi, *J. Solid State Electrochem.* **2008**, *12*, 979.
[256] J. Demeaux, E. DeVito, M. LeDigabel, H. Galiano, B. Claude-Montigny, D. Lemordant, *Phys. Chem. Chem. Phys.* **2014**, *16*, 5201.
[257] K. M. Colbow, J. R. Dahn, R. R. Haering, *J. Power Sources* **1989**, *26*, 397.
[258] A. Kuhn, C. Baehtz, F. García-Alvarado, *J. Power Sources* **2007**, *174*, 421.
[259] A. Kuhn, M. Martín, F. García-Alvarado, *J. Solid State Chem.* **2010**, *183*, 20.
[260] J. Yang, J. Zhao, Y. Chen, Y. Li, *Ionics* **2010**, *16*, 425.
[261] L. Persi, F. Croce, B. Scrosati, *Electrochem. Commun.* **2002**, *4*, 92.
[262] M. Manickam, M. Takata, *J. Power Sources* **2003**, *114*, 298.
[263] V. Aravindan, W. C. Ling, S. Madhavi, *ChemPhysChem* **2012**, *13*, 3263.
[264] V. Aravindan, W. Chuiling, S. Madhavi, *J. Mater. Chem.* **2012**, *22*, 16026.
[265] T. Ohzuku, K. Tatsumi, N. Matoba, K. Sawai, *J. Electrochem. Soc.* **2000**, *147*, 3592.
[266] X. Feng, C. Shen, N. Ding, C. Chen, *J. Mater. Chem.* **2012**, *22*, 20861.
[267] J. Yang, B. Yan, J. Ye, X. Li, Y. Liu, H. You, *Phys. Chem. Chem. Phys.* **2014**, *16*, 2882.
[268] F. García-Alvarado, M. Martín-Gil, A. Kuhn, *Mater. Res. Soc. Symp. – Proc.* Vol. *756*, **2003**, pp. 255–260.
[269] A. Kuhn, M. Martín, F. García-Alvarado, *Zeitschrift Anorgan. Allgem. Chem.* **2008**, *634*, 880.
[270] F. G. B. Ooms, E. M. Kelder, J. Schoonman, M. Wagemaker, F. M. Mulder, *Solid State Ionics* **2002**, *152–153*, 143.
[271] C. V. Rao, B. Rambabu, *Solid State Ionics* **2010**, *181*, 839.
[272] J.-T. Han, J. B. Goodenough, *Chem. Mater.* **2011**, *23*, 3404.
[273] X. Lu, Z. Jian, Z. Fang, L. Gu, Y.-S. Hu, W. Chen, Z. Wang, L. Chen, *Energy Environ. Sci.* **2011**, *4*, 2638.
[274] B. Guo, X. Yu, X.-G. Sun, M. Chi, Z.-A. Qiao, J. Liu, Y.-S. Hu, X.-Q. Yang, J. B. Goodenough, S. Dai, *Energy Environ. Sci.* **2014**, *7*, 2220.
[275] K. Tang, X. Mu, P. A. vanAken, Y. Yu, J. Maier, *Adv. Energy Mater.* **2013**, *3*, 49.
[276] J.-T. Han, Y.-H. Huang, J. B. Goodenough, *Chem. Mater.* **2011**, *23*, 2027.
[277] S. Jayaraman, V. Aravindan, P. Suresh Kumar, W. Chui Ling, S. Ramakrishna, S. Madhavi, *ACS Appl. Mater. Interfaces* **2014**, *6*, 8660.
[278] L. Fei, Y. Xu, X. Wu, Y. Li, P. Xie, S. Deng, S. Smirnov, H. Luo, *Nanoscale* **2013**, *5*, 11102.
[279] C. Jo, Y. Kim, J. Hwang, J. Shim, J. Chun, J. Lee, *Chem. Mater.* **2014**, *26*, 3508.
[280] V. Aravindan, J. Sundaramurthy, A. Jain, P. S. Kumar, W. C. Ling, S. Ramakrishna, M. P. Srinivasan, S. Madhavi, *ChemSusChem* **2014**, *7*, 1858.
[281] Q. Cheng, J. Liang, Y. Zhu, L. Si, C. Guo, Y. Qian, *J. Mater. Chem. A* **2014**, *2*, 17258.
[282] B. Guo, X. Yu, X.-G. Sun, M. Chi, Z.-A. Qiao, J. Liu, Y.-S. Hu, X.-Q. Yang, J. B. Goodenough, S. Dai, *Energy Environ. Sci.* **2014**.

[283] Z. Chen, I. Belharouak, Y. K. Sun, K. Amine, *Adv. Funct. Mater.* **2013**, *23*, 959.
[284] I. Koseva, J. P. Chaminade, P. Gravereau, S. Pechev, P. Peshev, J. Etourneau, *J. Alloys Compd.* **2005**, *389*, 47.
[285] D. Dambournet, I. Belharouak, K. Amine, *Inorg. Chem.* **2010**, *49*, 2822.
[286] I. Belharouak, K. Amine, *Electrochem. Commun.* **2003**, *5*, 435.
[287] D. Dambournet, I. Belharouak, J. Ma, K. Amine, *J. Power Sources* **2011**, *196*, 2871.
[288] J. Liu, Y. Li, X. Wang, Y. Gao, N. Wu, B. Wu, *J. Alloys Compd.* **2013**, *581*, 236.
[289] J. Liu, X. Sun, Y. Li, X. Wang, Y. Gao, K. Wu, N. Wu, B. Wu, *J. Power Sources* **2014**, *245*, 371.
[290] E. Quartarone, P. Mustarelli, *Chem. Soc. Rev.* **2011**, *40*, 2525.
[291] M. Tatsumisago, M. Nagao, A. Hayashi, *J. Asian Cerm. Soc.* **2013**, *1*, 17.
[292] H. Xie, K.-S. Park, J. Song, J. B. Goodenough, *Electrochem. Commun.* **2012**, *19*, 135.
[293] E. J. Cussen, T. W. S. Yip, *J. Solid State Chem.* **2007**, *180*, 1832.
[294] R. Satish, V. Aravindan, W. C. Ling, J. B. Goodenough, S. Madhavi, *Adv. Energy. Mater.* **2014**, *4*, 1301715.
[295] V. Aravindan, W. C. Ling, S. Hartung, N. Bucher, S. Madhavi, *Chem. Asian J.* **2014**, *9*, 878.
[296] J.-Y. Luo, W.-J. Cui, P. He, Y.-Y. Xia, *Nat. Chem.* **2010**, *2*, 760.
[297] N. Arun, V. Aravindan, W. C. Ling, S. Madhavi, *J. Alloys Compd.* **2014**, *603*, 48.
[298] J. Y. Luo, Y. Y. Xia, *J. Power Sources* **2009**, *186*, 224.
[299] J.-Y. Luo, J.-L. Liu, P. He, Y.-Y. Xia, *Electrochim. Acta* **2008**, *53*, 8128.
[300] V. Aravindan, W. Chuiling, M. V. Reddy, G. V. S. Rao, B. V. R. Chowdari, S. Madhavi, *Phys. Chem. Chem. Phys.* **2012**, *14*, 5808.
[301] A. Aatiq, M. Menetrier, L. Croguennec, E. Suard, C. Delmas, *J. Mater. Chem.* **2002**, *12*, 2971.
[302] V. Aravindan, W. Chuiling, S. Madhavi, *RSC Adv.* **2012**, *2*, 7534.
[303] J. O. Besenhard, M. Winter, *ChemPhysChem* **2002**, *3*, 155.
[304] Z. Gong, Y. Yang, *Energy Environ. Sci.* **2011**, *4*, 3223.
[305] C. Masquelier, L. Croguennec, *Chem. Rev.* **2013**, *113*, 6552.
[306] J. B. Goodenough, Y. Kim, *Chem. Mater.* **2009**, *22*, 587.
[307] J. N. Son, S. H. Kim, M. C. Kim, G. J. Kim, V. Aravindan, Y. G. Lee, Y. S. Lee, *Electrochim. Acta* **2013**, *97*, 210.
[308] J. N. Son, S. H. Kim, M. C. Kim, K. J. Kim, V. Aravindan, W. I. Cho, Y. S. Lee, *J Appl Electrochem* **2013**, *43*, 583.
[309] A. R. Cho, J. N. Son, V. Aravindan, H. Kim, K. S. Kang, W. S. Yoon, W. S. Kim, Y. S. Lee, *J. Mater. Chem.* **2012**, *22*, 6556.
[310] J. N. Son, G. J. Kim, M. C. Kim, S. H. Kim, V. Aravindan, Y. G. Lee, Y. S. Lee, *J. Electrochem. Soc.* **2013**, *160*, A87.
[311] X. H. Rui, N. Yesibolati, S. R. Li, C. C. Yuan, C. H. Chen, *Solid State Ionics* **2011**, *187*, 58.
[312] G. Delaizir, V. Viallet, A. Aboulaich, R. Bouchet, L. Tortet, V. Seznec, M. Morcrette, J.-M. Tarascon, P. Rozier, M. Dollé, *Adv. Funct. Mater.* **2012**, *22*, 2140.
[313] S. Patoux, C. Wurm, M. Morcrette, G. Rousse, C. Masquelier, *J. Power Sources* **2003**, *119–121*, 278.
[314] A. Aboulaich, R. Bouchet, G. Delaizir, V. Seznec, L. Tortet, M. Morcrette, P. Rozier, J.-M. Tarascon, V. Viallet, M. Dollé, *Adv. Energy Mater.* **2011**, *1*, 179.
[315] W.-f. Mao, H.-q. Tang, Z.-y. Tang, J. Yan, Q. Xu, *ECS Electrochem. Lett.* **2013**, *2*, A69.
[316] E. Kobayashi, L. S. Plashnitsa, T. Doi, S. Okada, J.-i. Yamaki, *Electrochem. Commun.* **2010**, *12*, 894.
[317] L. S. Plashnitsa, E. Kobayashi, Y. Noguchi, S. Okada, J.-i. Yamaki, *J. Electrochem. Soc.* **2010**, *157*, A536.
[318] Z. Jian, W. Han, Y. Liang, Y. Lan, Z. Fang, Y.-S. Hu, Y. Yao, *J. Mater. Chem. A* **2014**, *2*, 20231.
[319] J. Barker, R. K. B. Gover, P. Burns, A. J. Bryan, *Electrochem. Solid-State Lett.* **2007**, *10*, 130.
[320] J. Barker, R. K. B. Gover, P. Burns, A. Bryan, M. Y. Saidi, J. L. Swoyer, *J. Power Sources* **2005**, *146*, 516.
[321] J. Barker, M. Y. Saidi, J. L. Swoyer, *J. Electrochem. Soc.* **2004**, *151*, A1670.
[322] J. Barker, M. Y. Saidi, J. L. Swoyer, *J. Electrochem. Soc.* **2003**, *150*, A1394.
[323] R. Ma, L. Shao, K. Wu, M. Shui, D. Wang, J. Pan, N. Long, Y. Ren, J. Shu, *ACS Appl. Mater. Interfaces* **2013**, *5*, 8615.
[324] J. Barker, R. K. B. Gover, P. Burns, A. Bryan, *Electrochem. Solid-State Lett.* **2005**, *8*, A285.
[325] J.-M. Ateba Mba, C. Masquelier, E. Suard, L. Croguennec, *Chem. Mater.* **2012**, *24*, 1223.
[326] J. Wang, X. Li, Z. Wang, B. Huang, Z. Wang, H. Guo, *J. Power Sources* **2014**, *251*, 325.
[327] L. S. Plashnitsa, E. Kobayashi, S. Okada, J.-i. Yamaki, *Electrochim. Acta* **2011**, *56*, 1344.
[328] F. Zhou, X. Zhao, J. R. Dahn, *Electrochem. Commun.* **2009**, *11*, 589.
[329] M. S. Whittingham, *Science* **1976**, *192*, 1126.
[330] M. S. Whittingham, F. R. Gamble Jr, *Mater. Res. Bull.* **1975**, *10*, 363.
[331] M. S. Whittingham, *J. Electrochem. Soc.* **1976**, *123*, 315.
[332] Z.-L. Tao, L.-N. Xu, X.-L. Gou, J. Chen, H.-T. Yuan, *Chem. Commun.* **2004**, 2080.
[333] H.-S. Ryu, J.-S. Kim, J.-S. Park, J.-W. Park, K.-W. Kim, J.-H. Ahn, T.-H. Nam, G. Wang, H.-J. Ahn, *J. Electrochem. Soc.* **2013**, *160*, A338.
[334] P. Fragnaud, R. Brec, E. Prouzet, P. Deniard, *Mater. Res. Bull.* **1993**, *28*, 337.
[335] J. B. Goodenough, Y. Kim, *Chem. Mater.* **2009**, *22*, 587.
[336] E. J. Plichta, W. K. Behl, D. Vujic, W. H. S. Chang, D. M. Schleich, *J. Electrochem. Soc.* **1992**, *139*, 1509.
[337] E. J. Plichta, W. K. Behl, *J. Electrochem. Soc.* **1993**, *140*, 46.
[338] F. Croce, S. Passerini, B. Scrosati, E. Plichta, W. Behl, M. Salomon, D. Schleich, *J. Power Sources* **1993**, *44*, 481.
[339] F. Croce, S. Passerini, B. Scrosati, *J. Electrochem. Soc.* **1994**, *141*, 1405.
[340] P. Poizot, S. Laruelle, S. Grugeon, L. Dupont, J. M. Tarascon, *Nature* **2000**, *407*, 496.
[341] Y. Sharma, N. Sharma, G. V. Subba Rao, B. V. R. Chowdari, *Solid State Ionics* **2008**, *179*, 587.
[342] J. Hassoun, F. Croce, I. Hong, B. Scrosati, *Electrochem. Commun.* **2011**, *13*, 228.
[343] D. Shanmukaraj, S. Grugeon, S. Laruelle, G. Douglade, J.-M. Tarascon, M. Armand, *Electrochem. Commun.* **2010**, *12*, 1344.
[344] J. Q. Zhao, Y. Wang, *J. Mater. Chem. A* **2014**, *2*, 14947.
[345] A. Banerjee, V. Aravindan, S. Bhatnagar, D. Mhamane, S. Madhavi, S. Ogale, *Nano Energy* **2013**, *2*, 890.
[346] S. Okada, J.-i. Yamaki, *J. Ind. Eng. Chem.* **2004**, *10*, 1104.
[347] D. Maiti, V. Aravindan, S. Madhavi, P. Sujatha Devi, *J. Power Sources* **2015**, *276*, 291.
[348] K. Cao, L. Jiao, H. Liu, Y. Liu, Y. Wang, Z. Guo, H. Yuan, *Adv. Energy. Mater.* **2015**, *5*, 1401421.
[349] M. Zheng, D. Qiu, B. Zhao, L. Ma, X. Wang, Z. Lin, L. Pan, Y. Zheng, Y. Shi, *RSC Adv.* **2013**, *3*, 699.
[350] S. Hariharan, V. Ramar, S. P. Joshi, P. Balaya, *RSC Adv.* **2013**, *3*, 6386.
[351] O. Vargas, Á. Caballero, J. Morales, *Electrochim. Acta* **2014**, *130*, 551.
[352] M. Biswal, A. Suryawanshi, V. Thakare, S. Jouen, B. Hannoyer, V. Aravindan, S. Madhavi, S. Ogale, *J. Mater. Chem. A* **2013**, *1*, 13932.
[353] L. Ji, Z. Tan, T. R. Kuykendall, S. Aloni, S. Xun, E. Lin, V. Battaglia, Y. Zhang, *Phys. Chem. Chem. Phys.* **2011**, *13*, 7170.

[354] X. Fan, J. Shao, X. Xiao, L. Chen, X. Wang, S. Li, H. Ge, *J. Mater. Chem. A* **2014**, *2*, 14641.
[355] H. Ming, J. Ming, S.-M. Oh, S. Tian, Q. Zhou, H. Huang, Y.-K. Sun, J. Zheng, *ACS Appl. Mater. Interfaces* **2014**, *6*, 15499.
[356] J. Ming, W. J. Kwak, S. J. Youn, H. Ming, J. Hassoun, Y.-K. Sun, *Energy Technol.* **2014**, *2*, 778.
[357] R. Sahay, P. Suresh Kumar, V. Aravindan, J. Sundaramurthy, W. Chui Ling, S. G. Mhaisalkar, S. Ramakrishna, S. Madhavi, *J. Phys. Chem. C* **2012**, *116*, 18087.
[358] A. Debart, L. Dupont, P. Poizot, J. B. Leriche, J. M. Tarascon, *J. Electrochem. Soc.* **2001**, *148*, A1266.
[359] S. Grugeon, S. Laruelle, R. Herrera-Urbina, L. Dupont, P. Poizot, J.-M. Tarascon, *J. Electrochem. Soc.* **2001**, *148*, A285.
[360] A. Banerjee, U. Singh, V. Aravindan, M. Srinivasan, S. Ogale, *Nano Energy* **2013**, *2*, 1158.
[361] R. Verrelli, J. Hassoun, A. Farkas, T. Jacob, B. Scrosati, *J. Mater. Chem. A* **2013**, *1*, 15329.
[362] R. Verrelli, B. Scrosati, Y.-K. Sun, J. Hassoun, *ACS Appl. Mater. Interfaces* **2014**, *6*, 5206.
[363] W. Zhang, G. Ma, H. Gu, Z. Yang, H. Cheng, *J. Power Sources* **2015**, *273*, 561.
[364] Y. Deng, L. Wan, Y. Xie, X. Qin, G. Chen, *RSC Adv.* **2014**, *4*, 23914.
[365] C. Chae, H. Park, D. Kim, J. Kim, E.-S. Oh, J. K. Lee, *J. Power Sources* **2013**, *244*, 214.
[366] G.-L. Xu, Y.-F. Xu, J.-C. Fang, F. Fu, H. Sun, L. Huang, S. Yang, S.-G. Sun, *ACS Appl. Mater. Interfaces* **2013**, *5*, 6316.
[367] X. Fang, X. Lu, X. Guo, Y. Mao, Y.-S. Hu, J. Wang, Z. Wang, F. Wu, H. Liu, L. Chen, *Electrochem. Commun.* **2010**, *12*, 1520.
[368] Y. Wang, Y. Wang, D. Jia, Z. Peng, Y. Xia, G. Zheng, *Nano Lett.* **2014**, *14*, 1080.
[369] P. Poizot, S. Laruelle, S. Grugeon, L. Dupont, J. M. Tarascon, *J. Power Sources* **2001**, *97–98*, 235.
[370] F. Badway, I. Plitz, S. Grugeon, S. Laruelle, M. Dollé, A. S. Gozdz, J.-M. Tarascon, *Electrochem. Solid-State Lett.* **2002**, *5*, A115.
[371] D. Bresser, E. Paillard, P. Niehoff, S. Krueger, F. Mueller, M. Winter, S. Passerini, *ChemPhysChem* **2014**, *15*, 2177.
[372] J. B. Goodenough, Y. Kim, *Chem. Mater.* **2010**, *22*, 587.
[373] Y. Kim, J. B. Goodenough, *J. Phys. Chem. C* **2008**, *112*, 15060.
[374] X. Wang, Q. Xiang, B. Liu, L. Wang, T. Luo, D. Chen, G. Shen, *Sci. Rep.* **2013**, *3*, 10.1038srep02007.
[375] T. Stephenson, Z. Li, B. Olsen, D. Mitlin, *Energy Environ. Sci.* **2014**, *7*, 209.
[376] M. A. Py, R. R. Haering, *Can. J. Phys.* **1983**, *61*, 76.
[377] H. Hwang, H. Kim, J. Cho, *Nano Lett.* **2011**, *11*, 4826.
[378] H. Yu, C. Zhu, K. Zhang, Y. Chen, C. Li, P. Gao, P. Yang, Q. Ouyang, *J. Mater. Chem. A* **2014**, *2*, 4551.
[379] A. N. Dey, *J. Electrochem. Soc.* **1971**, *118*, 1547.
[380] D. Larcher, S. Beattie, M. Morcrette, K. Edstrom, J.-C. Jumas, J.-M. Tarascon, *J. Mater. Chem.* **2007**, *17*, 3759.
[381] A. D. W. Todd, P. P. Ferguson, M. D. Fleischauer, J. R. Dahn, *Int. J. Energy Res.* **2010**, *34*, 535.
[382] W.-J. Zhang, *J. Power Sources* **2011**, *196*, 13.
[383] C.-M. Park, J.-H. Kim, H. Kim, H.-J. Sohn, *Chem. Soc. Rev.* **2010**, *39*, 3115.
[384] M. N. Obrovac, L. Christensen, D. B. Le, J. R. Dahn, *J. Electrochem. Soc.* **2007**, *154*, A849.
[385] S. Goriparti, E. Miele, F. DeAngelis, E. Di Fabrizio, R. Proietti Zaccaria, C. Capiglia, *J. Power Sources* **2014**, *257*, 421.
[386] Z. Li, J. Huang, B. Yann Liaw, V. Metzler, J. Zhang, *J. Power Sources* **2014**, *254*, 168.
[387] N.-S. Choi, Y. Yao, Y. Cui, J. Cho, *J. Mater. Chem.* **2011**, *21*, 9825.
[388] H. Wu, Y. Cui, *Nano Today* **2012**, *7*, 414.
[389] M. R. Zamfir, H. T. Nguyen, E. Moyen, Y. H. Lee, D. Pribat, *J. Mater. Chem. A* **2013**, *1*, 9566.
[390] D. Deng, M. G. Kim, J. Y. Lee, J. Cho, *Energy Environ. Sci.* **2009**, *2*, 818.
[391] X.-L. Wu, Y.-G. Guo, L.-J. Wan, *Chem. Asian J.* **2013**, *8*, 1948.
[392] J. R. Szczech, S. Jin, *Energy Environ. Sci.* **2011**, *4*, 56.
[393] T. Song, L. Hu, U. Paik, *J. Phys. Chem. Lett.* **2014**, *5*, 720.
[394] B. Liang, Y. Liu, Y. Xu, *J. Power Sources* **2014**, *267*, 469.
[395] Y. Idota, T. Kubota, A. Matsufuji, Y. Maekawa, T. Miyasaka, *Science* **1997**, *276*, 1395.
[396] R. A. Huggins, *J. Power Sources* **1999**, *81–82*, 13.
[397] C.-Y. Chou, H. Kim, G. S. Hwang, *J. Phys. Chem. C* **2011**, *115*, 20018.
[398] R. A. Huggins, *Solid State Ionics* **2002**, *152–153*, 61.
[399] Z. Chen, V. Chevrier, L. Christensen, J. R. Dahn, *Electrochem. Solid-State Lett.* **2004**, *7*, A310.
[400] L. Y. Beaulieu, K. C. Hewitt, R. L. Turner, A. Bonakdarpour, A. A. Abdo, L. Christensen, K. W. Eberman, L. J. Krause, J. R. Dahn, *J. Electrochem. Soc.* **2003**, *150*, A149.
[401] C. K. Chan, H. Peng, G. Liu, K. McIlwrath, X. F. Zhang, R. A. Huggins, Y. Cui, *Nat Nano* **2008**, *3*, 31.
[402] C. J. Wen, R. A. Huggins, *J. Solid State Chem.* **1981**, *37*, 271.
[403] L. Baggetto, D. Danilov, P. H. L. Notten, *Adv. Mater.* **2011**, *23*, 1563.
[404] C. K. Chan, R. Ruffo, S. S. Hong, Y. Cui, *J. Power Sources* **2009**, *189*, 1132.
[405] J. Li, J. R. Dahn, *J. Electrochem. Soc.* **2007**, *154*, A156.
[406] H. Li, L. Shi, W. Lu, X. Huang, L. Chen, *J. Electrochem. Soc.* **2001**, *148*, A915.
[407] N. Liu, Z. Lu, J. Zhao, M. T. McDowell, H.-W. Lee, W. Zhao, Y. Cui, *Nat. Nanotechnol.* **2014**, *9*, 187.
[408] J.-G. Ren, Q.-H. Wu, G. Hong, W.-J. Zhang, H. Wu, K. Amine, J. Yang, S.-T. Lee*Energy Technol.* **2013**, *1*, 77.
[409] K.-L. Lee, J.-Y. Jung, S.-W. Lee, H.-S. Moon, J.-W. Park, *J. Power Sources* **2004**, *130*, 241.
[410] V. Baranchugov, E. Markevich, E. Pollak, G. Salitra, D. Aurbach, *Electrochem. Commun.* **2007**, *9*, 796.
[411] H. Yang, P. Fu, H. Zhang, Y. Song, Z. Zhou, M. Wu, L. Huang, G. Xu, *J. Power Sources* **2007**, *174*, 533.
[412] J. Yin, M. Wada, K. Yamamoto, Y. Kitano, S. Tanase, T. Sakai, *J. Electrochem. Soc.* **2006**, *153*, A472.
[413] H. Jung, M. Park, S. H. Han, H. Lim, S.-K. Joo, *Solid State Commun.* **2003**, *125*, 387.
[414] G. B. Cho, M. G. Song, S. H. Bae, J. K. Kim, Y. J. Choi, H. J. Ahn, J. H. Ahn, K. K. Cho, K. W. Kim, *J. Power Sources* **2009**, *189*, 738.
[415] R. Elazari, G. Salitra, G. Gershinsky, A. Garsuch, A. Panchenko, D. Aurbach, *J. Electrochem. Soc.* **2012**, *159*, A1440.
[416] E. Markevich, K. Fridman, R. Sharabi, R. Elazari, G. Salitra, H. E. Gottlieb, G. Gershinsky, A. Garsuch, G. Semrau, M. A. Schmidt, D. Aurbach, *J. Electrochem. Soc.* **2013**, *160*, A1824.
[417] K. Fridman, R. Sharabi, R. Elazari, G. Gershinsky, E. Markevich, G. Salitra, D. Aurbach, A. Garsuch, J. Lampert, *Electrochem. Commun.* **2013**, *33*, 31.
[418] K. Fridman, R. Sharabi, E. Markevich, R. Elazari, G. Salitra, G. Gershinsky, D. Aurbach, J. Lampert, M. Schulz-Dobrick, *ECS Electrochem. Lett.* **2013**, *2*, A84.
[419] K. Hanai, Y. Liu, N. Imanishi, A. Hirano, M. Matsumura, T. Ichikawa, Y. Takeda, *J. Power Sources* **2005**, *146*, 156.
[420] M.-H. Park, M. G. Kim, J. Joo, K. Kim, J. Kim, S. Ahn, Y. Cui, J. Cho, *Nano Lett.* **2009**, *9*, 3844.
[421] L.-F. Cui, Y. Yang, C.-M. Hsu, Y. Cui, *Nano Lett.* **2009**, *9*, 3370.
[422] B. Liu, X. Wang, H. Chen, Z. Wang, ChenDi, Y.-B. Cheng, C. Zhou, G. Shen, *Sci. Rep.* **2013**, *3*, 1622.
[423] M. W. Forney, R. A. DiLeo, A. Raisanen, M. J. Ganter, J. W. Staub, R. E. Rogers, R. D. Ridgley, B. J. Landi, *J. Power Sources* **2013**, *228*, 270.

[424] S. Song, S. W. Kim, D. J. Lee, Y.-G. Lee, K. M. Kim, C.-H. Kim, J.-K. Park, Y. M. Lee, K. Y. Cho, *ACS Appl. Mater. Interfaces* **2014**, *6*, 11544.
[425] C. Chae, H.-J. Noh, J. K. Lee, B. Scrosati, Y.-K. Sun, *Adv. Funct. Mater.* **2014**, *24*, 3036.
[426] M. Ko, S. Chae, S. Jeong, P. Oh, J. Cho, *ACS Nano* **2014**, *8*, 8591.
[427] L. Ji, H. Zheng, A. Ismach, Z. Tan, S. Xun, E. Lin, V. Battaglia, V. Srinivasan, Y. Zhang, *Nano Energy* **2012**, *1*, 164.
[428] S. Sim, P. Oh, S. Park, J. Cho, *Adv. Mater.* **2013**, *25*, 4498.
[429] J.-I. Lee, E.-H. Lee, J.-H. Park, S. Park, S.-Y. Lee, *Adv. Energy Mater.* **2014**, *4*, na.
[430] S. Choi, T. Bok, J. Ryu, J.-I. Lee, J. Cho, S. Park, *Nano Energy* **2015**, *12*, 161.
[431] R. Kataoka, T. Mukai, A. Yoshizawa, T. Sakai, *J. Electrochem. Soc.* **2013**, *160*, A1684.
[432] D. Tan, B. Liu, D. Chen, G. Shen, *RSC Adv.* **2014**, *4*, 18391.
[433] M.-H. Park, M. Noh, S. Lee, M. Ko, S. Chae, S. Sim, S. Choi, H. Kim, H. Nam, S. Park, J. Cho, *Nano Lett.* **2014**, *14*, 4083.
[434] M.-S. Jung, J.-H. Seo, M.-W. Moon, J. W. Choi, Y.-C. Joo, I.-S. Choi, *Adv. Energy. Mater.* **2015**, *5*, 1400611.
[435] A. Vlad, A. L. M. Reddy, A. Ajayan, N. Singh, J.-F. Gohy, S. Melinte, P. M. Ajayan, *Proc. Natl. Acad. Sci. USA* **2012, 109, 15168**.
[436] C.-M. Hwang, J.-W. Park, *J. Power Sources* **2011**, *196*, 6772.
[437] M. Yamada, A. Inaba, A. Ueda, K. Matsumoto, T. Iwasaki, T. Ohzuku, *J. Electrochem. Soc.* **2012**, *159*, A1630.
[438] I. W. Seong, K. T. Kim, W. Y. Yoon, *J. Power Sources* **2009**, *189*, 511.
[439] Z. Zeng, B. Wu, L. Xiao, X. Jiang, Y. Chen, X. Ai, H. Yang, Y. Cao, *J. Power Sources* **2015**, *279*, 6.
[440] M. Yamada, A. Ueda, K. Matsumoto, T. Ohzuku, *J. Electrochem. Soc.* **2011**, *158*, A417.
[441] M. Yamada, K. Uchitomi, A. Ueda, K. Matsumoto, T. Ohzuku, *J. Power Sources* **2013**, *225*, 221.
[442] J. K. Lee, W. Y. Yoon, B. K. Kim, *J. Electrochem. Soc.* **2013**, *160*, A1348.
[443] T. Kajita, R. Yuge, K. Nakahara, J. Iriyama, H. Takahashi, R. Kasahara, T. Numata, S. Serizawa, K. Utsugi, *J. Electrochem. Soc.* **2014**, *161*, A708.
[444] B. Liu, A. Abouimrane, Y. Ren, M. Balasubramanian, D. Wang, Z. Z. Fang, K. Amine, *Chem. Mater.* **2012**, *24*, 4653.
[445] B. Liu, A. Abouimrane, Y. Ren, J. Neuefeind, Z. Z. Fang, K. Amine, *J. Electrochem. Soc.* **2013**, *160*, A882.
[446] http:www.sony.netSonyInfoNewsPress20050205–006E, accessed: 20/03/2015.
[447] J. Y. Huang, L. Zhong, C. M. Wang, J. P. Sullivan, W. Xu, L. Q. Zhang, S. X. Mao, N. S. Hudak, X. H. Liu, A. Subramanian, H. Fan, L. Qi, A. Kushima, J. Li, *Science* **2010**, *330*, 1515.
[448] V. Aravindan, K. B. Jinesh, R. R. Prabhakar, V. S. Kale, S. Madhavi, *Nano Energy* **2013**, *2*, 720.
[449] V. Aravindan, J. Sundaramurthy, E. N. Kumar, P. S. Kumar, W. C. Ling, R. vonHagen, S. Mathur, S. Ramakrishna, S. Madhavi, *Electrochim. Acta* **2014**, *121*, 109.
[450] G. Derrien, J. Hassoun, S. Panero, B. Scrosati, *Adv. Mater.* **2007**, *19*, 2336.
[451] J. Hassoun, S. Panero, P. Reale, B. Scrosati, *Int. J. Electrochem. Sci.* **2006**, *1*, 110.
[452] J. Hassoun, S. Panero, P. Reale, B. Scrosati, *Adv. Mater.* **2009**, *21*, 4807.
[453] F. Croce, M. L. Focarete, J. Hassoun, I. Meschini, B. Scrosati, *Energy Environ. Sci.* **2011**, *4*, 921.
[454] G. A. Elia, S. Panero, A. Savoini, B. Scrosati, J. Hassoun, *Electrochim. Acta* **2013**, *90*, 690.
[455] G. A. Elia, F. Nobili, R. Tossici, R. Marassi, A. Savoini, S. Panero, J. Hassoun, *J. Power Sources* **2015**, *275*, 227.
[456] J. Hassoun, K.-S. Lee, Y.-K. Sun, B. Scrosati, *J. Am. Chem. Soc.* **2011**, *133*, 3139.
[457] J. N. Son, G. J. Kim, M. C. Kim, S. H. Kim, V. Aravindan, Y. G. Lee, Y. S. Lee, *J. Electrochem. Soc.* **2013**, *160*, A87.
[458] D. Di Lecce, S. Brutti, S. Panero, J. Hassoun, *Mater. Lett.* **2015**, *139*, 329.
[459] G. A. Elia, J. Wang, D. Bresser, J. Li, B. Scrosati, S. Passerini, J. Hassoun, *ACS Appl. Mater. Interfaces* **2014**, *6*, 12956.
[460] S. Brutti, J. Hassoun, B. Scrosati, C.-Y. Lin, H. Wu, H.-W. Hsieh, *J. Power Sources* **2012**, *217*, 72.
[461] J. Hassoun, M. Wachtler, M. Wohlfahrt-Mehrens, B. Scrosati, *J. Power Sources* **2011**, *196*, 349.
[462] J. Hassoun, D.-J. Lee, Y.-K. Sun, B. Scrosati, *Solid State Ionics* **2011**, *202*, 36.
[463] J. Hassoun, A. Fernicola, M. A. Navarra, S. Panero, B. Scrosati, *J. Power Sources* **2010**, *195*, 574.
[464] W. Ni, J. Cheng, L. Shi, X. Li, B. Wang, Q. Guan, L. Huang, G. Gu, H. Li, *J. Mater. Chem. A* **2014**, *2*, 19122.
[465] M. G. Kim, S. Sim, J. Cho, *Adv. Mater.* **2010**, *22*, 5154.
[466] M. Yao, K. Okuno, T. Iwaki, T. Awazu, T. Sakai, *J. Power Sources* **2010**, *195*, 2077.
[467] Z. Chen, K. Xie, X. Hong, *Electrochim. Acta* **2013**, *108*, 674.
[468] Y. H. Kwon, S.-W. Woo, H.-R. Jung, H. K. Yu, K. Kim, B. H. Oh, S. Ahn, S.-Y. Lee, S.-W. Song, J. Cho, H.-C. Shin, J. Y. Kim, *Adv. Mater.* **2012**, *24*, 5192.
[469] X. Hou, B. Liu, X. Wang, Z. Wang, Q. Wang, D. Chen, G. Shen, *Nanoscale* **2013**, *5*, 7831.
[470] X. Hou, X. Wang, B. Liu, Q. Wang, Z. Wang, D. Chen, G. Shen, *ChemElectroChem* **2014**, *1*, 108.
[471] L. Baggetto, P. H. L. Notten, *J. Electrochem. Soc.* **2009**, *156*, A169.
[472] J. Graetz, C. C. Ahn, R. Yazami, B. Fultz, *J. Electrochem. Soc.* **2004**, *151*, A698.
[473] C. S. Fuller, J. C. Severiens, *Phys. Rev.* **1954**, *96*, 21.
[474] M.-H. Park, Y. Cho, K. Kim, J. Kim, M. Liu, J. Cho, *Angew. Chem. Int. Ed.* **2011**, *50*, 9647.
[475] F.-W. Yuan, H.-J. Yang, H.-Y. Tuan, *ACS Nano* **2012**, *6*, 9932.
[476] F.-W. Yuan, H.-Y. Tuan, *Chem. Mater.* **2014**, *26*, 2172.
[477] D. Lv, M. L. Gordin, R. Yi, T. Xu, J. Song, Y.-B. Jiang, D. Choi, D. Wang, *Adv. Funct. Mater.* **2014**, *24*, 1059.
[478] X.-L. Wang, W.-Q. Han, H. Chen, J. Bai, T. A. Tyson, X.-Q. Yu, X.-J. Wang, X.-Q. Yang, *J. Am. Chem. Soc.* **2011**, *133*, 20692.
[479] W. Li, X. Wang, B. Liu, S. Luo, Z. Liu, X. Hou, Q. Xiang, D. Chen, G. Shen, *Chem. Eur. J.* **2013**, *19*, 8650.
[480] W. Li, X. Wang, B. Liu, J. Xu, B. Liang, T. Luo, S. Luo, D. Chen, G. Shen, *Nanoscale* **2013**, *5*, 10291.
[481] Y. Sharma, N. Sharma, G. V. S. Rao, B. V. R. Chowdari, *Electrochim. Acta* **2008**, *53*, 2380.
[482] D. Bresser, E. Paillard, R. Kloepsch, S. Krueger, M. Fiedler, R. Schmitz, D. Baither, M. Winter, S. Passerini, *Adv. Energy Mater.* **2013**, *3*, 513.
[483] J. Xie, W. Song, G. Cao, T. Zhu, X. Zhao, S. Zhang, *RSC Adv.* **2014**, *4*, 7703.
[484] A. Varzi, D. Bresser, J. vonZamory, F. Müller, S. Passerini, *Adv. Energy Mater.* **2014**, *4*, 1400054.
[485] F. M. Courtel, H. Duncan, Y. Abu-Lebdeh, I. J. Davidson, *J. Mater. Chem.* **2011**, *21*, 10206.
[486] Y. Sharma, N. Sharma, G. V. Subba Rao, B. V. R. Chowdari, *Adv. Funct. Mater.* **2007**, *17*, 2855.
[487] B. Liu, J. Zhang, X. Wang, G. Chen, D. Chen, C. Zhou, G. Shen, *Nano Lett.* **2012**, *12*, 3005.
[488] B. Liu, X. Wang, B. Liu, Q. Wang, D. Tan, W. Song, X. Hou, D. Chen, G. Shen, *Nano Res.* **2013**, *6*, 525.